Università degli Studi di Palermo

Ph.D. course in Chemical, Environmental, Biomedical, Hydraulic
And Materials Engineering
S.S.D. ICAR/02

Monitoring of marine litter through remote sensing and hydrodynamic Lagrangian models

Ph.D candidate
Dr. Laura Corbari

Ph.D. Coordinator
Prof. Giorgio Domenico Maria Micale

Tutor
Prof. Giuseppe Ciraolo

Co-Tutors
Dr. Fulvio Capodici

Dr. Maria Cristina Mangano

Prof. Konstantinos Topouzelis

External reviewers
Dr. Oscar Alvarez

Dr. Adam Gauci

XXXVI Cycle
Graduation Year – 2024

Abstract

Marine pollution is a growing global issue. Following the proof of the significant impacts of marine debris on the ecosystem worldwide, in the last decades, the scientific community has focused the efforts on monitoring and detection to assess more effective management strategies. The first efforts were focused on the quantification and characterisation of pollutants, mostly performing *in-situ* campaigns both in the beach and sea environments. Up to now, the characterisation of the debris fractions has shown that the most commonly portion is represented by plastic items. These polymers are characterised by long residence times and the predisposition to be degraded in smaller items, causing even greater impact on several marine fauna species and, consequently, on humans. Recently, due to the difficulties to perform intensive *in-situ* sampling campaigns especially over large areas, the growing of new observation technologies has driven the scientific community to develop remote sensing techniques for marine litter detection. Several applications carried out using unmanned aerial vehicles and satellite data highlighted that there is a lack of knowledge about the spectral response of marine litter and plastic items. Additionally, their detection could be also more difficult by considering their temporal evolution due to degradation processes in the marine environment.

The issue concerns marine pollution is even worse considering that once at the sea marine litter debris could be drifted by the sea currents to areas which can be very far from the source points. Thus, there is high uncertainty about the areas which can be more impacted by these kinds of pollution both at the sea (accumulation areas) and at the coast (beaching). In this framework, the existing monitoring actions (i.e. *in-situ* or remote detection)

could be not enough to study and thus deal with the marine litter pollution problem.

In this context, this thesis has been designed to test, and then to provide new insights into the marine litter issue through an integrated approach which include the *in-situ* monitoring campaigns, the application of remote sensing techniques following a bottom-up approach, the setup of numerical Lagrangian models to determine areas were these kinds of pollutions could be severe (accumulation and beaching areas). A monitoring campaign conducted in two urban beaches, with different management, allowed to quantify and characterise the pollution status of those areas. Results show the need to manage the beaches, organising frequently beach cleaning activities.

Some of the samples collected during the monitoring, have been spectrally characterised via a Laboratory experiment, and the wavelengths/bands useful for the detection as well as the best sensors to use, were identified. Some bands in the visible, red-edge, and in some infrared bands, appear effective for the beach litter detection. WorldView-3 resulted the sensor more useful for this purpose among the nowadays operating satellite platforms.

Furthermore, the interconnection between sea and beach environments was studied applying Lagrangian hydrodynamic models able to identify accumulation and beaching area. Outcomes of the models have confirmed as the marine litter is a transboundary issue that only a joint action of the countries can mitigate.

Finally, the potentiality of hyperspectral satellite data was tested analysing PRISMA images evaluating the capability to detect an artificial floating target deployed at the Aegean Sea. Results showed that satellite

hyperspectral images represent a useful tool for marine litter detection, although their spatial resolution limits their applicability.

Keywords: marine litter, beach litter, *in-situ* monitoring activities, spectral signatures, remote sensing detection, hydrodynamic models

Contents

List of Figures

The maps represented in this research work are always north-oriented.

List of Tables

List of Symbols

Symbol	Reference	Dimension	Description
α	Eq. 4.2	(°)	SAM score
B_{PCA}	-	[-]	Bands from the PCA analysis
B_{PI}	-	[-]	Bands similar at centre wavelength of Planetscope's bands
B_{SWIR}	-	[-]	Bands of the SWIR range
B_{VNIR}	-	[-]	Bands of the VIS-NIR range
C	-	[-]	Couples of Plastic and seawater fractions cover
d_*	Eq. 4.10	[-]	Dimensionless particle diameter
$dX(t)$	Eq. 4.3, 4.4, 4.5	[L]	x-shift
$dX'(t)$	Eq. 4.3, 4.4, 4.5	[L]	Random component
$dX_{adv}(t)$	Eq. 4.3, 4.4, 4.5	[L]	Advective displacement
$dX_{diff}(t)$	Eq. 4.3, 4.4, 4.5	[L]	Turbulent diffusion
$dY(t)$	Eq. 4.3, 4.4, 4.5	[L]	y-shift
$dY'(t)$	Eq. 4.3, 4.4, 4.5	[L]	Random component
$dY_{adv}(t)$	Eq. 4.3, 4.4, 4.5	[L]	Advective displacement
$dY_{diff}(t)$	Eq. 4.3, 4.4, 4.5	[L]	Turbulent diffusion
$dZ(t)$	Eq. 4.3, 4.4, 4.5	[L]	z-shift
$dZ'(t)$	Eq. 4.3, 4.4, 4.5	[L]	Random component
$dZ_{diff}(t)$	Eq. 4.3, 4.4, 4.5	[L]	Turbulent diffusion
$dZ_{sink}(t)$	Eq. 4.5	[L]	Sinking displacement
$d(r,ri)$	Eq. 4.13	[L]	Distance between the point r and the r_i

Symbol	Reference	Dimension	Description
Δt	Eq. 4.6, 4.7, 4.8	[t]	Finite time-step
Δt_i	Eq. 4.6, 4.7, 4.8, 4.9	[t]	Internal time step
E	Eq. 4.1	(W/m^2)	Irradiance
$f_{p,i}$	Eq. 4.14	[-]	Plastic fractions cover of the i-th intersected pixel
$f_{w,i}$	Eq. 4.14	[-]	Seawater fractions cover the of i-th intersected pixel
g	Eq. 4.11	[M^0 L^1 T^{-2}]	Gravity acceleration
k_h	Eq. 4.9	[L^2 T^{-1}]	Horizontal dispersion coefficient
k_v	-	[L^2 T^{-1}]	Vertical dispersion coefficient
L	Eq. 4.11	[L]	Length of the particles
M	Eq. 4.1	(W/m^2)	Exitance
μR_w	-	[-]	Mean spectral signature of the mixed pixel
μR_{mix}	-	[-]	Spectral signatures of the mixed i-th pixel (plastic target and water)
N	Eq. 4.2	[-]	Number of the spectral bands
P	Eq. 4.13		Coefficient
π	Eq. 4.11	[-]	Pi-greco
R	Eq. 4.9, 4.10, 4.11	[L]	Random number
R	Eq. 4.9	[L]	Standard deviation
$R_{mix,i}(\lambda)$	Eq. 4.14	[-]	Spectral signatures of the mixed i-th pixel (plastic target and water)
$R_{p,i}(\lambda)$	Eq. 4.14	[-]	Spectral signatures of the plastic's target
$R_{w,i}(\lambda)$	Eq. 4.14	[-]	Spectral signatures of the pure seawater
r_i	Eq. 4.2	[-]	Spectra
P	Eq. 4.1	[-]	Reflectance
ρ_p	Eq. 4.11	[ML^{-3}]	Particle density
ρ_w	Eq. 4.11	[ML^{-3}]	Water density
SSH	(-)	[L]	Sea surface height above geoid
T	(-)	[-]	Threshold

Symbol	Reference	Dimension	Description
t_i	Eq. 4.2	[-]	Spectra
U	Eq. 4.3, 4.4, 4.5, 4.6, 4.7, 4.8, 4.9, Copernicus data	$[L\ T^{-1}]$	Eastward Sea water velocity
u_i	Eq. 4.12	$[L\ T^{-1}]$	Velocities falling within a search radius
V	Eq. 4.3, 4.4, 4.5, 4.6, 4.7, 4.8,	$[L\ T^{-1}]$	Northward Sea water velocity
v'	Eq. 4.12		Velocities
v	Eq. 4.11	$[L^2\ T^{-1}]$	Water kinematic viscosity
W	Eq. 4.3, 4.4, 4.5, 4.6, 4.7, 4.8	$[L\ T^{-1}]$	Current velocities
$w_i(r)$	Eq. 4.12, 4.13		Weighting factors
$w_s(t)$	Eq. 4.5, Eq. 4.10		Settling velocity
x	Eq. 4.3, 4.4, 4.5	[-]	X axis
x_n	Eq. 4.6, 4.9	[L]	Original location of the particle
x_{n+1}	Eq. 4.6, 4.9	[L]	New location of the particle
y	Eq. 4.3, 4.4, 4.5	[-]	Y axis
y_n	Eq. 4.7	[L]	Original location of the particle
y_{n+1}	Eq. 4.7	[L]	New location of the particle
z	Eq. 4.3, 4.4, 4.5	[-]	Z axis
z_n	Eq. 4.8	[L]	Original location of the particle
z_{n+1}	Eq. 4.8	[L]	New location of the particle

List of Acronyms

Acronym	Description
ARPA	Agenzia Regionale per la Protezione ambientale
ASI	Agenzia Spaziale Italiana
CMS	Copernicus Marine service
CNR	Consiglio Nazionale delle Ricerche
EVA	Ethylene vinyl acetate
GESAMP	Guidelines or the monitoring and assessment of plastic litter and microplastics in the ocean
GLT	Geographic Lookup Table
GPS	Global Positioning System
HDPE	High-density polyethylene
HFR	High Frequency Radar
I-1	N. 1 beach in Isola delle Femmine
I-2	N. 2 beach in Isola delle Femmine
I-3	N. 3 beach in Isola delle Femmine
JRC	Joint Research Centre
MATLAB$^{®}$	MATrix LABoratory
M-D1	N. 1 beach in Mondello (Daily management)
M-D2	N. 2 beach in Mondello (Daily management)
M-D3	N. 3 beach in Mondello (Daily management)
M-L1	N. 1 beach in Mondello (Low-cost management)
M-L2	N. 2 beach in Mondello (Low-cost management)
MPA	Marine Protected Area
M-S1	N. 1 beach in Mondello (Seasonal management)
M-S2	N. 2 beach in Mondello (Seasonal management)
M-S3	N. 3 beach in Mondello (Seasonal management)
PCA	Principal component analysis
PET	Polyethylene terephthalate
PLP	Plastic Litter Project
PP	Polypropylene
PRISMA	PRecursore IperSpettrale della Missione Applicativa
PS	Polystyrene
SAM	Spectral angle mapper
SWIR	Short Wave Infra-Red

Acronym	Description
TrackMPD	Track Marine Plastic Debris
UAS	Unmanned Aircraft System
UAV	Unmanned Aerial Vehicle
VIS	Visible
VNIR	Visible and near-infrared
NEMO	Nucleus for European Modelling of the Ocean
NIR	Near Infra-Red

Chapter 1

Introduction

Marine litter is defined by the European Commission as "*any persistent, manufactured or processed solid material discarded, disposed of or abandoned in the marine and coastal environment*" (European Commission, Joint Research Centre 2015). This definition includes the beach litter. Marine and beach litter are extremely interconnected because one can affect the other. Indeed, debris left in coastal areas can be sources of marine litter (becoming sources and discharge points) and *vice versa*.

Marine litter is raising global concern due to the negative impacts firstly observable on the marine ecosystems and then on human health and socio-economic activities.

Organisms may encounter and then be affected by marine pollutants in different ways: through entanglement, ingestion, chemical transfer. Those can cause considerable suffering and often the death of the exposed fauna (Gall and Thompson 2015). Human welfare is also affected by marine pollution at different scales. Economic losses at both individual, enterprises and communities levels were registered in different productive sectors like tourism, fisheries, aquaculture, navigation and energy (Werner et al. 2016).

Marine and beach litter are composed by a heterogeneity of materials. The most common are plastics, wood, metals, glass, rubber, clothing, and paper. Plastic items are usually the most abundant elements, as resulting from an increasing production in the last decades. An incrementing of more 20 Mt (millions of tons) of plastics has been recorded between the 2019 and 2021, reaching a total mass of 390.7 Mt produced in 2021 worldwide. Despite the European Community is trying to reduce the production and dispersion of plastic items amending several laws, in 2021 a total of 52.7 Mt plastic items were manufactured (Plastic, the fact 2021). Most plastic objects

produced, once became waste, are used to produce energy while a small portion is recycled or dispatched to landfill. Unfortunately, part of the plastic waste is deliberately dispersed in the environment. In order to facilitate the monitoring and data comparison on collected plastic items, the scientific community has suggested to classify plastic items by categories based on their sizes: mega- (> 1 m diameter), macro- (between 2.5 cm and <1 m), meso- (between 5 mm and <2.5 cm), micro- (between 0.1 μm and <5 mm) and nano- (<0.1 μm) plastic (Kroon et al. 2018). The impacts of these fractions to the marine environment are different. Specifically, mega- and macro-plastics often cause the entanglement of marine species such as turtles, seals, whales, and some species of marine birds (Kühn, Bravo Rebolledo, and van Franeker 2015). Instead, microplastics could be ingested by various marine species (Gola et al. 2021) causing the introduction of plastic polymers into the food chain (Gruber et al. 2023). Another reason of concern is connected with the release of chemical compounds, like additives, into the sediment and tissues of organisms, having a dangerous impact on the organisms and human health (Browne et al. 2013).

The research interest on marine litter globally grew from 1960s, with a peak recorded at the beginning of this century (Ryan 2015; Thompson et al. 2004). Several impacts on the environment have been already underlined between the 1970s and 1980s. The first activities that allowed to monitor, quantify/characterise the beach and marine litter were the *in-situ* campaigns, operated by trained operators, regulated by different sampling guides/manuals (one of the first was written in 1992; Ribic 1992). Considering the variety of habitats in the coastal environment (sandy and rocky beaches) and the sea depths to be sampled (deep sediment and/or water column) different monitoring protocols, specific for each aera, have been developed. These manuals are also differentiated according to the fraction being studied: for examples, macrolitter items can be sampled

directly using clamps; instead, microlitter (in sandy beaches) can be sampled by collecting sand samples inside standard sampling surface (i.e. quadrats) which are then sieved isolating the debris. Mega- and macro-litter at sea can be detected by sighting surveys that allow to collect information regarding the distribution and the amount of floating litter. Finally, micro-litter which usually float in the water column, are usually quantified by using different kind of nets (e.g. Manta net or Neuston net).

In-situ beach/marine litter surveys are time-consuming, expensive, and require a high number of operators (COBSEA & CSIRO 2022) regardless the sampling protocols applied. Furthermore, the surveyed areas are often very limited which contrasts with the boundless nature of this kind of pollution which is rapidly spread by the sea currents circulation.

In this context, recently, the scientific community is trying to overcome some of the *in-situ* monitoring limitations by implementing new approaches, like the application of hydrodynamic models and the use of remote sensing technologies. Hydrodynamic models represent useful tools to track and predict the particles position allowing to detect accumulation and beaching areas. Instead, remote sensing methods, such as the use of images collected by drones and satellites, allow to detect and quantify marine litter more quickly and over a larger area compared to the *in-situ* campaigns. Despite remote sensing tools have several benefits, some limitations were underlined in the literature, like the lack of knowledge on plastic spectral signatures and the low spatial resolutions of sensors (especially when using satellite data) that allow only the detection of areas characterised by high litter accumulations.

This thesis considers all these factors and analyse the opportunity to study the marine/beach litter through the application of a multi-disciplinary approach.

Beach litter was studied jointly *in-situ* monitoring activities and remote sensing techniques. Italian beaches are characterised by various management practices that can be broadly categorised into two types: beaches where access is regulated by beach resorts (entrance allowed under paid subscription), and free access beaches.

In particular, sampling campaigns have been conducted focusing on examine the different quantities and categories of macro-litter (in terms of material, shape, dimensions, etc.) collected on beaches with the final aim to detect patterns to be correlated with the respective beach management practices – when existing – and with the existing human activities or marine protected areas more in general. The study areas were selected to achieve these goals. Furthermore, once the litter was categorised according to different materials and objects, the most abundant were identified. Additionally, a specific analysis was performed considering only plastic items.

A selection of the debris, collected during the *in-situ* campaign, based on the samples most commonly found on the beaches and those with peculiar characteristic in terms of colour, shape, etc. was spectrally characterised via an indoor experiment to achieve the following main goals: *i*) build a spectral library refereed to harvested marine-debris; *ii*) provide data and information to develop a standardise protocol for spectral data acquisition; indeed, the absence of it is cause of uncertain concerning the methodologies to adapt for the laboratory measurements; *iii*) evaluate distinguishability of the samples from the sand background via the application of an appropriated index *iv*) identify which are the most useful wavelength bands and the more promising remote sensing platforms (already available) for marine litter detection and plan future remote sensing detection tools; *v*) evaluate the possibly to identify the polymers of which the plastic debris are composed.

Beaches and marine litter are deeply connected, indeed the waste released on the beach can reach the sea and/or the debris released directly into the sea can end up on the beach. This interconnection was studied through the application of Lagrangian Hydrodynamic models, considering the coastal area as source of macroplastics, and examining the establishment of sea surface accumulation and beaching areas. The identification of these areas represents an important information for marine litter detection and mitigation.

It is known that beach litter is easier to detect and quantify compared to marine litter. Indeed, debris at sea is exposed to wave motion, wind action, and it can float or sink in the water column thus making its detection a more complex (or impossible) task. Considering all these negative factors, the marine litter detection was explored focusing on an experimental setup carried out within the Plastic Litter Project (PLP) 2021. A floating plastic target has been deployed on the sea surface in the coastal area of the Aegean Sea and considering it as a plastic accumulation area, it was tested the capability to detect plastic item using the PRecursore IperSpettrale della Missione Applicativa (PRISMA) hyperspectral satellite images, jointly with the *in-situ* data.

A synthetic description of each chapter is reported in following:

- Chapter 1: introduces the marine litter issue and defines the main goals of this thesis.
- Chapter 2: provides the state of art concerning beach and marine litter with a particular focus on topic related to the main goals of the thesis research.
- Chapter 3: defines the case studies conceived and designed to achieve the main goals.
- Chapter 4: provides a detailed description of the materials and methods adopted for each case study.

- Chapter 5: reports the scientific evidence gathered by the analyses carried out.

- Chapter 6: collates the discussions relative to the results achieved.

- Chapter 7: synthetises the main conclusions and presents some of the potential future developments of the present research.

Chapter 2

State of art: beach and marine litter

2.1 Beach litter

2.1.1 Beach litter: sampling campaigns

The increasing quantity of litter in the environment, especially in the marine environment, is a cause for concern. Different sources can be identified as cause of marine litter. Approximately 80% of marine litter originates from terrestrial sources and is composed mostly of plastic items (Allsopp et al. 2016; Bergmann et al. 2015). Often the litter encountered on the beaches is discharged by tourists, especially during the summer season. In some touristic area, during the summer season, more than 75% of the annual waste production is generated (Galgani et al. 2013). Litter can also be introduced in the beaches by the action of marine currents, which can lead to its stranding (Solbakken, Kleiven, and Haarr 2022). The proximity with major rivers or municipalities characterised by ineffective urban waste collection systems can highly influence the presence of litter on the beaches (Fazey and Ryan 2016).

The estimation of beach litter quantities is not easy to get, mostly because different phenomena are involved such as the action of currents and waves, the time of permanence on the beaches, the discharge rate by citizen and the presence of local cleanup activities (Portman and Brennan 2017; Nachite et al. 2019).

A wide knowledge baseline already exists on the variety of impacts caused by beach litter affecting both the ecological and economic systems. Despite over the years, several protocols have been drafted with the aim to

guide the sampling campaigns, often data on occurrence of marine litter are collected without referring to existing rigorous scientific protocols of data collection. As a result, it is sometimes difficult to compare data across temporal and spatial scale, with difficulties emerging when dealing to local complex patterns of occurrence.

To both investigate the existing state of art of beach litter analysis and the different protocols useful for the monitoring sampling campaigns on global scale, a preliminary scoping review exercise was performed. The search was performed by using a complex search string:

(("beach") AND ("litter" OR "*plastic*" OR "plastic debris") AND ("sand*") AND ("monitor*" OR "protocol*"))*

The wildcard asterisk (*) following a search word has been used allowing the search engine to consider, and accept, the word variation in the search; quotation marks around word indicate the exact word allowed in the search results. The search string was set to identify the different existing protocols for the monitoring of beach litter, particularly dealing with sandy beach and focusing on plastic debris. It was searched at TITLE-ABS-KEY level on Scopus scientific literature database. The search was conducted in 2021, before the sampling activities to have a clearly known about the issue and the protocols that must be adhered to. Furthermore, it was performed without applying temporal and spatial restriction. A total of 197 scientific articles were retrieved from the research, but after a first screening, only 106 of them were considered suitable for the purpose of the review (or rather reflecting the key items of our main research questions). Most of the collated scientific articles have been published from 2015 showing a steady increasing trend, testifying how much actual the issue of beach litter is, and an associated increased scientific interest. The review highlighted the following main protocols drafted to analyse the issues of beach litter in the

most rigorous and replicable possible manner: UNEP (2009), OSPAR (2010), MSFD TSG-ML (2013), NOAA (2013-2015), GESAMP (2019).

The listed protocols differ each other's mainly in terms of type of litter monitored, morphologies of the beaches etc.; consequently, it is often useful to consult several of them and integrate the information from each to be able to cover a wider range of data collection.

Interestingly, the analysis of the scoping literature review highlights that many monitoring studies do not adhere to standard (from official protocols) sampling procedures. For meso- and macro-fractions, approximately half of the surveys follow standard sampling procedures, while only a quarter do so for sample processing. This represents a relevant issue because the non-adoption of protocols prevents from data comparisons (Cesarano et al. 2023).

2.1.2 Beach litter: detection through remote sensing techniques

The *in-situ* campaigns for beach litter monitoring are time consuming and difficult to manage especially over large areas (due to the high number of operators to be employed) and during warm seasons. Thus, a more efficient monitoring can be achieved through remote sensing applications. Recently, several surveys were realised using the Unmanned Aerial Vehicles (UAV) (Manfreda et al. 2018) which have numerous benefits, such as the much less human effort required in the field and its feasibility for detecting and mapping litter on different environments like as beaches, dunes, rivers, and sea or lake waters (Andriolo et al. 2022). In Escobar-Sánchez et al. (2021) the possibility to complement the OSPAR protocol by drone-based monitoring was evaluated. Four different beaches located in the Southern Baltic Sea (three in Germany and one in Lithuania), were

mapped acquiring aerial images under different weather conditions. The data collected were classified by using both unsupervised and supervised techniques. Only litter characterised by a size > 2.5 cm was detectable as several of the smaller items were misclassified. Furthermore, only an estimation of the abundance and distribution of the debris was provided due to the high variety of shapes, sizes, colours, and materials of the plastic items. Several studies (e.g. Egorov et al. 2015) underlined the need to know the spectral signatures of marine litter (also in wet or submerged conditions) to train adequately the supervised classification algorithms. A lack of knowledge regarding these data is evident and needs to be filled (Knaeps et al. 2021). Indeed, despite the spectral signatures of dry virgin polymers are already known and often used in the industry of material recovery to identify the plastic items by others waste (Serranti and Bonifazi 2019) and to distinguish the nature of polymers (Masoumi, Safavi, and Khani 2012), spectra of marine plastic debris both in dry and wet conditions are not available, driving the scientific community to fill this gap.

In Garaba and Dierssen (2018) the reflectance of marine-harvested macro- and micro- plastics were acquired outdoor using the PANalytical Boulder ASD FieldSpec 4 spectroradiometer (in the range from 350 to 2500 nm, at 1 nm of spectral resolution). Spectra of debris commonly found in the beach environment (macroplastics) were collected and compared with the spectra of the virgin microplastics to evaluate the similarities. The spectra acquired were published online with the aim to create a spectra library, available to the scientific community.

In Acuña-Ruz et al., (2018) monitoring campaigns have been conducted in the beach environment with the aim to collect samples and spectrally characterise them in the sun-range wavelengths. The experimental setup of this application is not in-depth explained, not allowing the replicability of

the measurements. However, thermal infrared data of the same samples were acquired, describing in depth the experimental setup (Garaba, Acuña-Ruz, and Mattar 2020).

In the framework of the Hyperspectral Remote Sensing Of Marine Plastics (HYPER) project (Knaeps et al. 2021), the spectra of marine-harvested and virgin plastics in different conditions were acquired both in dry (using the ASD FieldSpec 4 spectroradiometer) and in wet conditions (using the SEV SR-3501 hyperspectral spectroradiometer). The dry experiment was carried out in a dark laboratory room by illuminating the samples with two halogen tungsten lamps.

Following the acquisition of the spectral data, one of the main scientific question regards the methodology and the algorithms to implement in order to identify the main spectral differences between the different kind of polymers dispersed in the environment (Samokhin et al. 2015). For example, in Garaba and Dierssen (2018) it was used the spectral contrast angle (Wan, Vidavsky, and Gross 2002), instead in other studies (Van Der Meer, 2006) the performance of other indexes like as the spectral angle mapper (SAM) or the vector distance (Euclidean distance measure, ED) was evaluated.

Finally, one of the main scientific gap concerning the marine spectral data regards the absence of a standardised protocol that causes a non-homogeneity of the dataset (often acquired with different techniques or with different instruments).

2.2 Marine litter

2.2.1 Tracking models

The use of a numerical model is essential to figure out where and how marine litter, once at the sea, can be accumulated in a specific sea area and/or reach coastal zones. Indeed, tracking marine litter is fundamental as its

detection using remote sensing is quite difficult and *in-situ* campaigns, which are expensive both economically and in terms of staff employed, provide only point-based information.

In this framework, the use of the hydrodynamic tracking models represent an important instrument to evaluate the trajectories of marine litter, identify possible accumulation areas at sea and beaching zones thus addressing remote sensing detection and *in-situ* operations. Indeed, knowing the particles' accumulation area, it is possible to focus on a specific domain using the suitable remote sensing data. Additionally, hydrodynamic tracking models allow to simulate different discharging scenarios, in terms of quantity, initial discharge points, and discharging temporal dynamic; thus, providing spatio-temporal distributions of litter.

From the literature review Lagrangian and Eulerian schemes, often jointly employed, are the most used in fluid-dynamics (Batchelor 2000, Bigdeli et al. 2022). These approaches allow to model the advection-dispersion-reaction process of the pollutants once they are in the sea environment (e.g. van Sebille et al. 2018). The main difference between Lagrangian and Eulerian models lies in the distinct approach used to build the equations with respect the considered coordinate system (Guerrini, Mari, and Casagrandi 2021). Punctual elements following an instantaneous flow, such as the litter particles, can be tracked by the Lagrangian models. These models allow to track particles' positions (in time and space) individually, also quantifying their concentrations, by adopting a movable coordinate system and considering particles as discrete (Zhang and Chen 2007). On the other hand, the description of the motion of substances at a fixed locations, like the nodes of a computational grid, is usually done using an Eulerian scheme (Guerrini, Mari, and Casagrandi 2021). With this approach, the particles position is known at fixed points (computational nodes) in

continuum (Van Utenhove 2019). Eulerian models were applied to different case studies (Nordam et al. 2023). For example, to track suspended particles in water, like as nanoparticles in rivers (Saharia et al. 2019) or microplastics in the oceans (Mountford and Morales Maqueda 2019). However, Eulerian approaches are frequently applied to simulate vortex flow fields (Azarpira, Zarrati, and Farrokhzad 2021). Examples of ocean circulation models using the Eulerian scheme are ROMS (Shchepetkin and McWilliams 2005) and NEMO ('NEMO Ocean Engine' 2024). Lagrangian approaches are frequently applied to track the movement of the particles in the ocean (van Sebille et al. 2018) that are moved by the sea currents considering also a random further displacement of them due to turbulent diffusion phenomena. Several Lagrangian models were employed to simulate the fate of plastic items (Delandmeter and van Sebille 2019; de la Fuente et al. 2021, Liubartseva et al. 2018) but also the transport of dissolved gases (Wimalaratne et al. 2015). The possibility to consider each particle independently by the others, is one of the main advantages of the Lagrangian approach as, in principle, it is possible to assume specific properties for each particle or groups of particles which are to be tracked (Nordam et al. 2023).

The Lagrangian "Track Marine Plastic Debris" (TrackMPD) model, explained in Jalón-Rojas, Wang, and Fredj (2019) simulates plastic particles transport tacking into account the geometric characteristics of the items, such as the size, shape, density, and the physical process like advection, beaching, deposition, diffusion, sinking and washing-off. The model also counts the influence of different kind of phenomena, such as biofouling and degradation which play an important role in the fate and transport of the particles; indeed, both these phenomena can affect the status and the behaviour of the particles themselves. When released, plastic debris have usually regular shapes (e.g., beads or spherules) that, after their exposition

to degradation actions can be altered creating various shapes, often characterised by smoother boundaries (Khatmullina and Isachenko 2017). These changes have direct effects on the transport of the particles. Thus, in this framework, the residence time in the sea environment can play a role in the motion of plastic particles (Doyle et al. 2011). Also, the biofouling plays an important role in plastic transport. Biofilm developed by the microorganisms causes an increase of plastics' weight which can in some cases lead to the sink of the particles (Li, Zhang, and Tang 2020).

In this work, two different Lagrangian models were applied: the TrackMPD (developed by Jalón-Rojas et al., 2019) and the "Simple tracking model" (STM) developed by the remote sensing group of the *Diparimento di Ingegneria - Università degli Studi di Palermo* (Italy).

TrackMPD is specifically tailored to track plastic litter; it takes into account several phenomena that influence the position of the particles like as beaching, washing-off etc. Considering these phenomena, the model can require high computation time.

STM was developed to address the need to rapidly track a huge number of particles, aiming to assess the tendency of the sea current fields to accumulate/spread floating debris. The model is based only on the advection phenomenon tracking virtual points (no mass, no volume). The minor complexity of the STM model makes it a valid tool in case of ecological disasters as it can provide real time outcomes.

Due to the different simulated phenomena, the two models could differ significantly. This necessitates a comparison of the simulations results obtained using TrackMPD and STM.

Both models are developed in MATLAB® and, specifically, the TrackMPD is based on the Particle Tracking and Analysis Toolbox (PaTATO, Fredj et al. 2016). Both are compatible with sea currents data from different sources

and need to know the coordinates of the discharge points. This implies that unless the study is focus on a specific case study, it is necessary to assume the release points. To this aim, were investigated the main sources of marine litter. It is demonstrated that rivers are one of the main sources of plastic debris in the oceans (Martínez-Vicente et al. 2019; Lebreton et al. 2017; Van Emmerik et al. 2022). Additionally, Xia et al. (2020) underlined the strong correlation between rainfall and microplastic concentration at sea. Thus, one possibility is to build a discharge scenario using data provided by the hydrological service (specific for each region). Indeed, the discharge scenario could be based on the rivers' mouths position (discharge sources) and their runoff volumes (magnitude and temporal distribution). A different source of information could be the interactive map of the Ocean cleanup organisation, available in the company's website (*https://theoceancleanup.com/*). The Ocean cleanup is a non-profit organisation, founded in 2013, focused on rid the plastic pollutants dispersed in the ocean and it is involved in important projects whose goals are the cleaning of the ocean through the develop of new technologies. The data, produced by a model and reported in the available maps, indicate the plastics' presence at the coast which are discharged by the rivers.

Despite several data are available in the scientific literature as input for hydrodynamic models, an integrated approach with the data acquisition on site is a useful methodology to apply/validate the models.

2.2.2 Detection of floating plastic litter on sea surface using remote sensing

Detection of marine litter through remote sensing is crucial to identify areas where plastic pollution represents an hotspot and to determine activities that could be undertaken to address the problem.

One of the main problems connected with the marine plastic detection is the presence of various plastic elements (in terms of shape, size, and colour) and their spatial variabilities along the water column (Papatheodorou et al. 2012). Several approaches have been explored in the studies of marine plastic detection through remote sensing. In many instances, drones equipped with RGB cameras, were employed for applications related to plastic detection (e.g., Papakonstantinou et al. 2021) jointly with the use of deep learning algorithms. Despite the economic benefits of the use of these cameras, as pointed out by Freitas, Silva, and Silva 2021, their effectiveness in marine plastic detection is hindered by challenges related to spatial resolution and surface water reflections.

Notable successes in the localisation, identification, and quantification of debris in coastal areas have been demonstrated through the utilisation of very-high spatial resolution images collected by Unmanned Aerial Vehicles (UAV) (Merlino et al. 2020). Also, Fallati et al. (2019) applied deep-learning algorithms to UAV data, successfully detecting plastic objects on the shoreline. The main limitations of using aerial surveys for marine litter detection are related to different operational challenges such as the need of specialised operators, the presence of restricted areas (not flyable zones) and the high cost of frequent flight scheduling (Unger et al. 2021).

These issues are resolved using satellite images which, however, have some limitations in both temporal and geometric resolutions. In Biermann et al. (2020) a method for detection of plastic litter using Sentinel-2 images was developed using the Floating Debris Index (FDI). The problem of not knowing the spectral signature of plastic materials in the sea is addressed through the use of non-linear unmixing techniques. Topouzelis et al. (2020) applied this methodology to Sentinel-2 images, obtaining a plastic spectral signature similar to that retrieved by using UAV data. Benefits of the use of

non-linear unmixing were confirmed also in Papageorgiou et al. 2022, where this technique was applied to Sentinel-2 images for detecting artificial targets in the sea of Lesvos Island (Greece). However, due to the low spectral resolutions of Sentinel-2 the authors highlighted the need to test the detection capabilities of hyperspectral data. In this framework, laboratory measurements (Corbari et al. 2020) and hyperspectral UAV surveys (Balsi et al. 2021) demonstrated the advantages of use hyperspectral data for detection of marine litter. The main limitations of these data are related to the low spatial resolution inherent in this type of sensor if mounted on satellite platforms. Some authors suggested the use of pan-sharpening technique to enhance the spatial resolution of hyperspectral band (Kremezi et al. 2021). In different studies (e.g., Freitas, Silva, and Silva 2021), various plastic targets were deployed on the sea surface, and hyperspectral images were collected through manned and unmanned aerial platforms. Machine learning algorithms, specifically Random Forest (RF) and Support Vector Machines (SVM), were applied to classify the targets, revealing promising results in terms of detection.

To assess the most effective techniques for marine litter detection, it is important to understand how pollutants interact with the marine environment and how their spectral behaviours change. A bottom-up approach is certainly useful to know the spectral signatures of the litter discharged on the sea environment confirmed by two laboratory experiments (Corbari et al. 2020; Garaba and Dierssen 2018) focused on the spectral characterisation of plastic litter.

Due to the difficulties to detect debris dispersed in the marine environment, ad-hoc experiments were carried out in the framework of the series of projects called "Plastic Litter Project", conducted by the University of the Aegean and financed by ESA. These projects allow to advance the

study of plastic litter detection through the implementation of remote sensing. In particular, the main goals of the PLP projects were:

- To expand the spectral signature database to incorporate floating marine litter.
- To evaluate the capability and limitation of the Sentinel-2 and Unmanned Aircraft System (UAS) for detecting marine plastic.

Over the years (from 2018 to 2023), various types of targets (in terms of material, shape, etc.), have been deployed at sea, particularly in the Gulf of Gera (Lesvos Island, Greece), and detected using satellite and drone imagery. Sentinel-2 images were used and shown promising results in terms of detection of targets.

Chapter 3

Study areas

The study areas selected in this research activity were chosen to address the main scientific questions. In this Chapter these areas are described, focusing both on beach and marine litter.

3.1 Beach litter

The choice of the study areas in which perform the beach litter monitoring campaigns was guided by the necessity to achieve the main goals of this activity. Two study areas located along the north-west Sicilian coasts (Italy), were selected: Mondello and Isola delle Femmine (Figure 3.1).
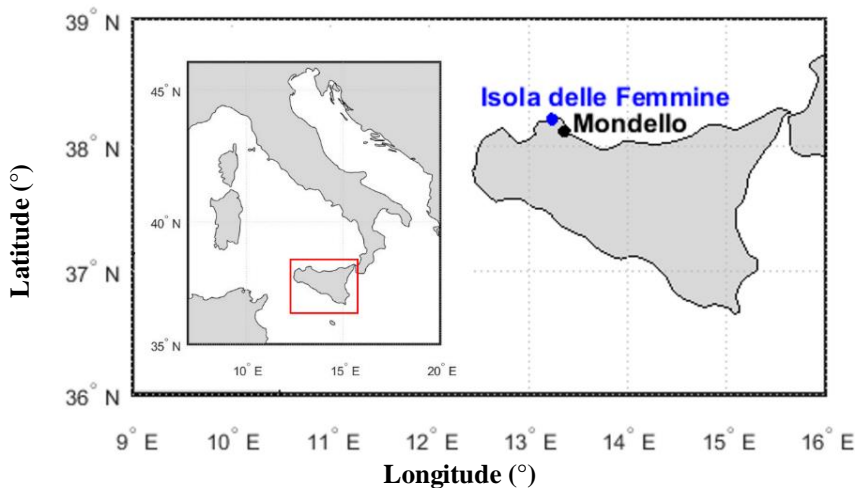
Figure 3.1– *In-situ* sampling area. The study area of Mondello is represented by the black dot and the one of Isola delle Femmine by the blue dot.

Both areas are characterised by flat sandy beaches and by the presence of bathing lidos and free access zone. To correlate beach management with quantity/kind of litter, in Mondello were sampled areas with different

management; instead, in Isola delle Femmine free access beaches were chosen.

These two beaches shared several characteristics (e.g. sand based, high tourist pressure each summer season, due to their proximity to Palermo city) as well as management distinctions, such as the presence of cleaning activities and a variety of in use patterns.

In the following the sampling areas are described more in details.

3.1.1 Mondello beach

Mondello beach (38.20° N, 13.32° E) is located in a small bay close to the municipality of Palermo and is targeted by both citizens and tourists. The population of Mondello is around 4200 inhabitants, but its increases significantly on summer season (City Facts, 2020).

This beach is a typical example of coastal area characterised by management measures in which the entrances and permanence – human pressure – is regulated by a variety of existing entrance subscription options (where it is possible to stay only by paying the expected cost for the rental of umbrellas, deckchairs or sunbeds, and even small rooms). Indeed, the majority of this coastal area is managed by a private company "Mondello Italo Belga" and a section is free access for the citizen. The company managed different kind of bathing establishment that differ in the type of subscription that citizens can pay for: seasonal, daily and low-cost. These differ in the frequency with which citizens can access on the beaches, respectively: for the entire summer season, daily or for a few hours.

The areas covered by the sampling activities for the different sectors, are reported in Figure 3.2.

Figure 3.2 – Mondello sites sampled with different management: Seasonal (M-S1, M-S2, M-S3), Daily (M-D1, M-D2, M-D3), Low-cost (M-L1, M-L2).

The beach resorts in which the surveys were conducted are characterised by different length and width, and consequently different size square. In each site, only the shoreline immediately close to the sea was used as free access zones.

All the beaches are maintained by the managers that offer a daily cleaning up (regulated by regional law e.g. by means of a beach cleaning machine at the beginning of the summer and every day during the summer season by operators using a net with 0.5 - 1 cm mesh), lifeguards and services as bar and restaurants are provided of waste bins.

All the sampling activities were carried out during the summer of 2021, in the very early morning (to avoid the presence of many bathers). Table 3.1 reports the collection date jointly with the square meters extension of each beach.

Table 3.1 – Geometric characteristics of sampled sites in Mondello and collection date.

		Beach - code	Collection date	Square (m^2)
Type of beaches	**Daily D**	M-D1	5th July 2021	4754
		M-D2	2nd August 2021	4559
		M-D3	20th September 2021	3738
	Seasonal S	M-S1	26th July 2021	3040
		M-S2	13th September 2021	5262
		M-S3	27th September 2021	4305
	Low-cost L	M-L1	26th July 2021	1794
		M-L2	20th September 2021	4115
				Total 31567

3.1.2 Isola delle Femmine

Isola delle Femmine beach (38.20°N, 13.24°E) is located 20 km faraway from Palermo city. The population census in Isola delle Femmine is around 7000 inhabitants (City Facts, 2022). The beach is mostly targeted during the year by local citizens (that conduct fishing activities) with an increase of users during the summer season when it is targeted by both tourists and citizen from the neighboring municipality (main from Palermo city).

Isola delle Femmine is partially located inside the Marine Protected Area (MPA) of "Capo Gallo – Isola delle Femmine" that covers a sea area of 2.173 ha and a coastal area of 16 km (from Palermo to Isola delle Femmine). The MPA is divided in three main zones, depending on the different protection levels:

- The A zone (77 ha) is characterised by the maximum level of protection. In this area bathing is forbidden.
- The B zone (242 ha) in which bathing is allowed but the anchoring of the boats is allowed only through the buoys provided by the managing body.

- The C zone (1854 ha), in which human activities like swimming, diving, and fishing (small scales ones) are allowed.

The MPA was established in 2002 and different studies focused on the importance of this area in terms of biodiversity. Crosti et al. (2020) studied the conservation status of the area and underlined that more than 44 protected species are hosted in the Capo Gallo MPA.

Figure 3.3 reports the MPA zones.
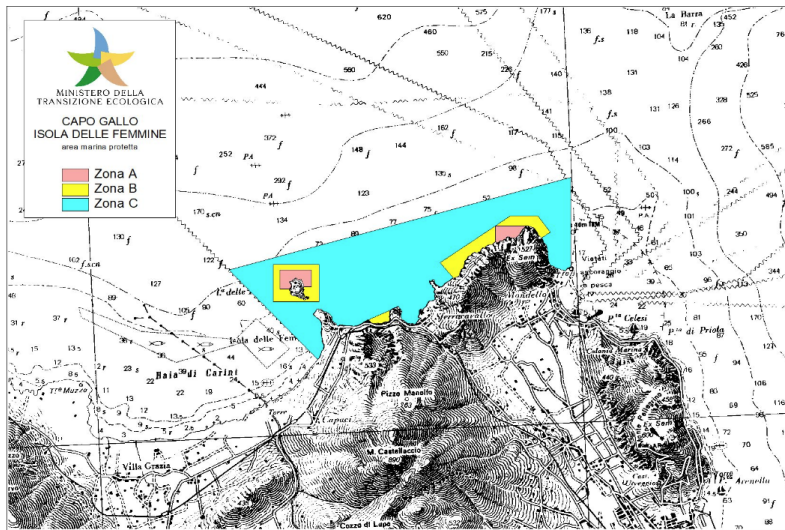
Figure 3.3 – Marine protected area (MPA) of Capo Gallo - Isola delle Femmine. (Source: *https://www.mase.gov.it/pagina/area-marina-protetta-capo-gallo-isola-delle-femmine*).

Despite some of the areas in Isola delle Femmine beach are managed through the establishment of private lidos, the sampling activities were performed in portions characterised by free access for users. The sampled areas are reported in Figure 3.4.

Figure 3.4 – Isola delle Femmine sampled sites.

All the monitored areas are sandy beaches apart from the so called I-1 that is characterised by the presence of a few rocks close to the sea. Importantly, it should be noted that only I-1 beach portion falls within this designated C zone of the MPA.

In all selected beaches there are no scheduled beach cleaning activities (organised by private companies or by the municipality) but only during the summer season and on a voluntary basis, a group of citizens removes macro-litter on the beach surface. In addition, all the beach portions sampled in Isola delle Femmine are interested by the presence of a small fishing and touristic port.

Table 3.2 reports the sampling date and the square meters of each sampled beach. All the sampling activities were carried out in the early morning, as was done for the case study of Mondello.

Table 3.2 – Geometric characteristics of sampled sites in Isola delle Femmine beach and collection date.

Beach - code	Collection date		Square (m²)
I-1	28th July 2021	8th September 2021	1374
I-2	4th August 2021	22th September 2021	2592
I-3	1nd September 2021	15th September 2021	3365
			Total 7331

3.2 Marine litter: tracking and detection

The transport of marine litter particles dispersed on the sea surface was studied through the application of two hydrodynamic Lagrangian models. Three different areas were chosen to this purpose: the Tyrrhenian Sea, the Strait of Sicily and the West Africa Coastal areas. The simulations conducted in each domain differ in methodology, source points, and outcomes' analysis. Detailed descriptions are reported in the Material and Methods section.

On the other hands, the marine plastic detection through the use of hyperspectral PRISMA satellite sensor was focused on the large plastic target deployed on the sea surface in the Aegean marine area.

In the following, a general overview of the Mediterranean basin main circulation patterns will be described with a focus on Tyrrhenian Sea and the Strait of Sicily study areas. Then the West Africa Coastal study areas are described. Finally, for the remote sensing plastic detection activity, the Aegeas Sea study area is described.

3.2.1 TrackMPD – STM models application areas: Mediterranean basin

Mediterranean basin is one of the most populated area with the 10% of the global coastal population (Jones, O'Neill, and Gao 2020). The considerable production and dispersion of the plastic elements and the

morphology of this area cause long waters' residence time (Lacombe H, Gascard JC, Gonella J, Bethoux JP, 1981). In the last decades, different campaigns were carried out in the Mediterranean basin to quantify the presence of plastic pollutants. A monitoring campaign was conducted by Cózar et al. (2015) in May 2013, sampling the sea surface water in 28 sites of the Mediterranean sea using neuston nets. Around 3900 plastic items were found out in the nets and five different shapes have been identified: fragment, film, foam, fishing thread, pellet/granule. The quantifications from the monitoring campaigns are comparable with the accumulation zone of floating plastic debris predicted at global scale using a global surface circulation model (Cózar et al. 2015). The concentrations of the global plastic waste are reported in Figure 3.5. In this map, the dark and grey areas represent the modelled accumulation zones, considering the five subtropical gyres, while the white oceanic areas represent the non-accumulation zones. This research clearly highlighted the presence of a hotspot of concentration in the cross-border area between the Sicilian coast and Malta island.
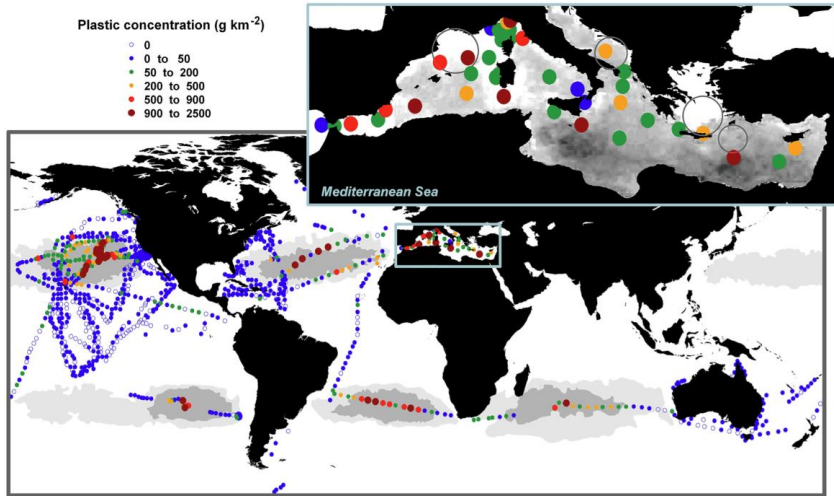
Figure 3.5 – Concentrations of plastic elements on sea water surface in the Mediterranean Sea compared with the quantity on global ocean. (Source: Cózar et al. 2015).

Within the international experimental bottom trawl surveys (MEDITS), on August 2019, a sampling campaign was accomplished on board the commercial stern trawler (Pegaso S.B. - UE 7826) in the South of Sicily (Monique et al. 2022) allowing to quantify the microplastics items ingested by the shark *Scyliorhinus canicula*. The study reported that 80.3% of the shark's stomachs present plastic items including both macroplastics and microplastics, confirming the presence of a hotspot of accumulation on the South of Sicily cross-border area.

With more than 8500 species of macroscopic marine organisms - between 4% / 18% of the world marine species - the Mediterranean basin represents a global hotspot of biodiversity (Bianchi and Morri 2000). The study of marine litter's impacts is of crucial relevance into the basin, as marine litter represent another layer of human disturbance that is exerted on the marine ecosystems on the area, which detrimental effects may have an additive and synergistic effects on the already recorded negative effects due to overfishing (Bennema and Rijnsdorp 2015; Consoli et al. 2016), marine

traffic (La Loggia et al. 2011), oil and gas extraction (Mangano and Sarà 2017). Specifically, due to the structure of semi-enclosed basin, then the peculiar water circulation, the study of the particles of marine litter cannot disregard the sea currents that occur in the area (Figure 3.6) that have then integrated into the models used (see the list of currents in Table 3.3 and Table 3.4).
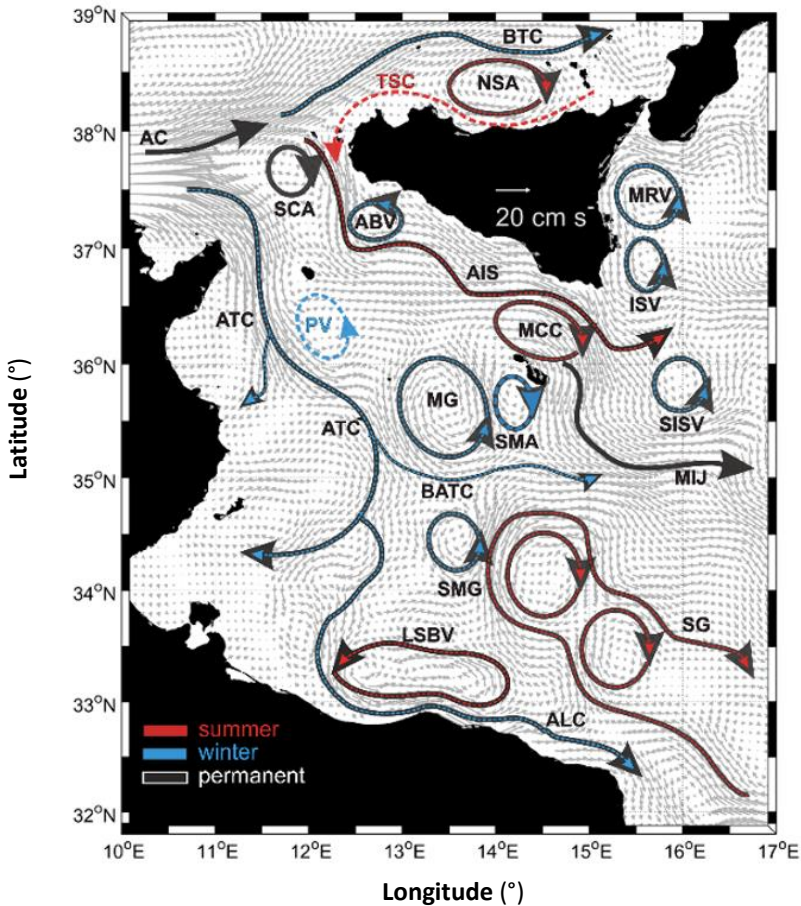
Figure 3.6 – Mean surface circulation in the Sicily Channel and Southern Tyrrhenian Sea. The Black arrows represent permanent sub-basin and mesoscale structures; dashed red/blue lines are referring to the seasonal summer/winter structures, respectively. These last are superimposed on the black arrows when the structures are permanent but most intense in summer/winter. (Source: Menna et al. 2019).

Table 3.3 – Main Sea currents in the Sicily-Malta Channel.

Sea currents	
Acronyms	**Description**
AC	Algerian Current
AIS	Atlantic Ionian Stream
ALC	Atlantic Libyan Current
ATC	Atlantic Tunisian Current
ATC	Atlantic Tunisian Current
MIJ	Mid-Ionian Jet
BTC	Bifurcation Tyrrhenian Current
BATC	Bifurcation Atlantic Tunisian Current
TSC	Tyrrhenian Sicilian Current
TSC	Tyrrhenian Sicilian Current

Table 3.4 – Main Gyres and Eddies in the Sicily-Malta Channel.

Gyres and Eddies	
Acronyms	**Description**
ABV	Adventure Bank Vortex
ISV	Ionian Shelf break Vortex
LSBV	Libyan Shelf Break Vortex
MG	Medina Gyre
MCC	Maltese Channel Crest
MRV	Messina Rice Vortex
NSA	Northern Sicily Anticyclone
PV	Pantelleria Vortex
SCA	Sicily Channel Anticyclone
SG	Sidra Gyre
SISV	Southern Ionian Shelf break Vortex
SMG	Southern Medina Gyre
SMA	Southern Maltese Anticyclone

As is it possible to see in Figure 3.6, most of the sea currents are permanent but influenced by the season variability. Only TSC and the PV are seasonal occurring in summer and winter, respectively. The sea currents

undergo an intensification caused by the wind stress: this is evident especially for BTC, ATC, BATC, and ALC. In opposite AIS, SG, and the MCC, are stronger in summer, when the wind stress is feeble. The presence of different gyres and eddies in the area suggests the possibly accumulation of debris.

South Tyrrhenian Sea

The model application on the South Tyrrhenian Sea (10.8°W, 16°E; 35.8°S, 43°N) was conducted considering as "sources", or rather main discharging points, the two studied beaches of Mondello and Isola delle Femmine, sampled during the *in-situ* monitoring campaign specifically conducted during the summer season in 2021 (Figure 3.7).
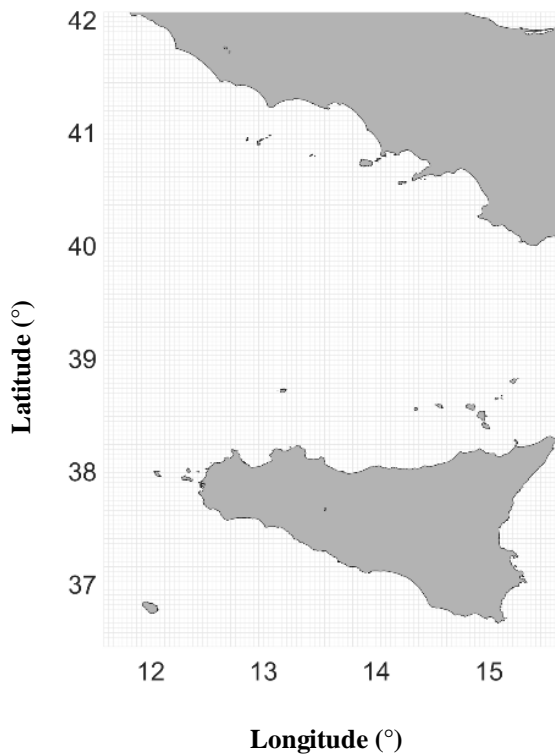
Figure 3.7 – Study area for the South Tyrrhenian Sea application.

Strait of Sicily

The Strait of Sicily (11.5° W, 16.5° E; 35° S, 37.8°N) was considered as study area (Figure 3.8) for the importance in the plastic/litter pollution processes considering that large Sicilian Rivers (Imera Meridionale, Platani, Verdura, Belice, etc.) have their outlet in this region.
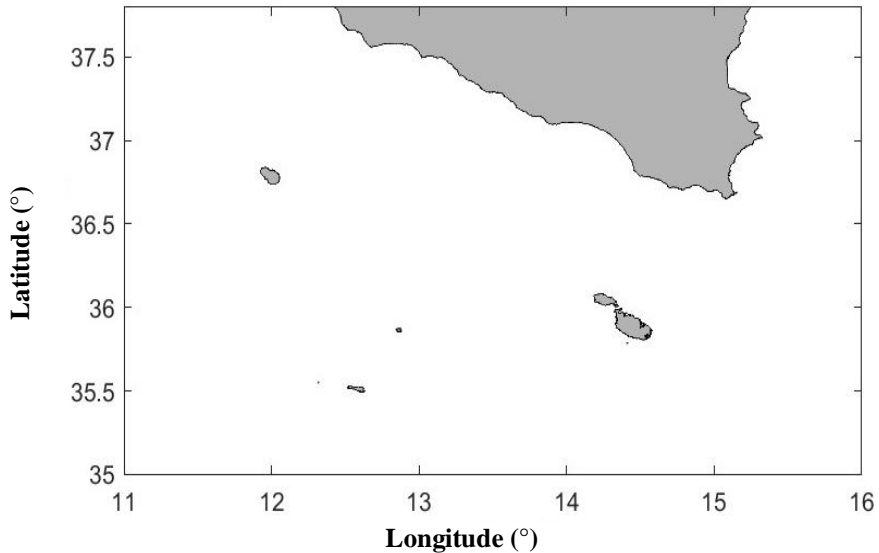
Figure 3.8 – Study area for the Strait of Sicily application.

Morphologically, this area is narrow and shallow. It is characterised by an important hydrodynamical processes, including meandering sea currents, mesoscale eddies, filaments, and recurrent wind-driven upwelling events (e.g. Basilone et al. 2013; Capodici et al. 2018). The presence of this oceanographic components allows to maintain an high level of local biodiversity (e.g. Béranger et al. 2004). The relevance of this area prompted to the implementation of a dedicated HFR (High Frequency Radar) systems network within the CALYPSO project (Drago et al., 2015). Three HFR systems were deployed in the area in 2013 reaching a total of seven HFR in 2021. CALYPSO permits to monitor the sea surface currents for oil spill dispersion and emergency management. Sea surface current maps provide

from this network allowed characterising the surface circulation patterns in the region (e.g., Cosoli et al. 2015) with a very high temporal and spatial resolution. For the data validation several Lagrangian drifters were deployed in December 2012 and June, September and October 2013 (Capodici et al. 2019). Other validation campaigns were realised also recently.

Although the CALYPSO data are reliable, these data were not used in this thesis work as not adequate to be considered as input of Lagrangian models: HFR data are indeed collected over a limited area and are characterised by moderate/high data gaps in time and space due to failures and/or radio frequency interferences. For the above-mentioned reasons, the CMS data were used to force the tracking models.

3.2.2 TrackMPD model application areas: Liberia/Gulf of Guinea

The coastal area between Liberia and the Gulf of Guinea was studied within the GDA AID Marine Environment & Blue Economy project. The aim of this project, funded by the European Space Agency, in collaboration with the Asian Development Bank and World Bank, is to assist International Funding Institutions teams in the framework of the marine environment and Blue Economy by implementing innovative Earth Observation services. The study is part of two Use Cases for the World Bank's PROBLUE and West Africa Coastal Areas (WACA) programs, which focus on the west Africa coastal area.

The Gulf of Guinea represents an important source of natural resources (Banchani 2016; Osaretin 2011) sustaining the economy of the encircled countries (Annan and Wan 2022). These countries like Cameroon, Equatorial Guinea, Gabon, Ghana, Ivory Coast, Nigeria are still in the early phase of development and their infrastructures expansion depends also on

energy resources available in the Guinea's area. (Brownfield, M.E. and Charpentier, R.R. 2006). Focusing on marine economy, it was analysed the plastic particles circulation on the sea surface using the TrackMPD model, considering as sources the most important rivers in the Liberian region. The Liberian Hydrological Services provides the streamflow's data with daily, monthly, and annual temporal resolution (*https://lhsliberia.com/hydrology-for-the-curious/rivers/*).

Preliminarily, the main oceanic circulations of the study area were analysed. In Djakouré et al. (2014) the main oceanic currents and wind stress directions are schematise as reported in Figure 3.9.
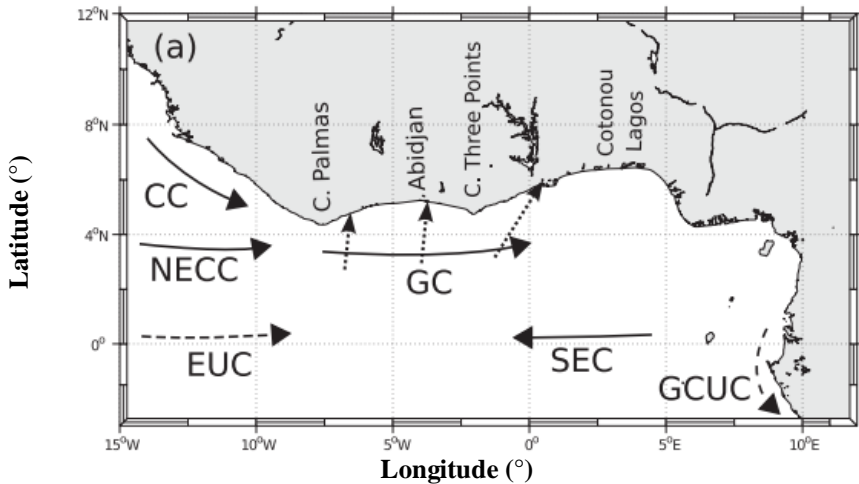
Figure 3.9 – Scheme of the main oceanic currents in the Gulf of Guinea. The solid lines represent the major surface currents (GC = Guinea Current, NECC = North Equatorial CounterCurrent, CC = Canary Current, SEC = South Equatorial Current, EUC = Equatorial UnderCurrent, GCUC = Gabon-Congo UnderCurrent); instead, the black dotted arrows the wind stress directions.

The major oceanic currents (Ingham,1970 and Bourle`s, 2003) are: Guinea Current (GC); North Equatorial CounterCurrent (NECC); Canary Current (CC); South Equatorial Current (SEC); Equatorial UnderCurrent (EUC); Gabon-Congo UnderCurrent (GCUC). The analyses of the sea

current patterns showed that a debris accumulation is possible especially in the north-east area, where the morphology facilitates the build-up.

The study area (-17°W, 12°E; -5°S, 7° N) includes the coastal zone between the Liberian region and the Gulf of Guinea (Figure 3.10). The sources of discharge were assumed to be located at the estuarine of the five main rivers flowing in Liberia (Figure 3.10).
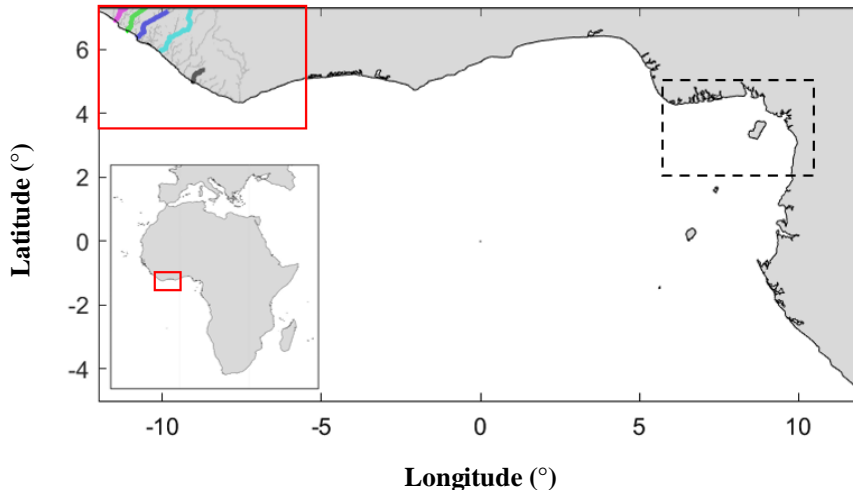
Figure 3.10 – Study area for the Liberia/Gulf of Guinea application: red box represents the input zone. The colored lines represent rivers considered as a source of pollution. The dashed black box represents the area where the outputs of the model will be displayed.

The dashed black box indicates the area of which the outcomes of the model have been reported.

3.2.3 Detection of floating target: Aegean Sea study Area

The study area for the marine litter detection through satellite data is in the Gulf of Gera (Lesvos Island, Greece) where two artificial targets were deployed within the PLP 2021 project (Figure 3.11). The Gulf is a semi-enclosed water body with a surface area of approximately 43 km^2, connected

to the sea through a 200-800 m wide and 6.5 km long channel (Tamvaki and Tsirtsis 2005).

Figure 3.11 – Study area for remote sensing application. (Source: https://plp.aegean.gr/plastic-litter-project-2021/).

One target was made of plastic and deployed the 6th June 2021; the second, was crafted from wood and deployed the 17th June 2021.

Unmanned aerial vehicle (UAV) surveys were scheduled every five days to monitor the two targets.

Chapter 4

Materials and Methods

In this section the main tools and methodologies, applied to achieve the research's goals are reported. Beach and marine litter topics are separately described.

4.1 Materials

4.1.1 Beach litter

4.1.1.1 Sampling campaign

As mentioned, the sampling campaign was realised to collect macro-, meso- and micro-plastics. As suggested by the protocols adapted, different tools have been used to collect each fraction. Common to all surveys, regardless of the collected material, was the essential presence of a team of trained operators.

In this section, the materials used to collect the macro-, meso-, and microplastics are described.

Macroplastics

The macroplastics sampling was done considering the "*Guidelines for the monitoring and assessment of plastic litter in the ocean*" (GESAMP 2019) protocol. The materials needed were:

- Meters to define the survey area.
- GPS to take coordinates of start and end of section.
- Adequate number of clamps to collect waste.
- Gloves for operators.
- Bags for laying the collected waste.

- Scale for weighing the waste collected.
- The master list of Categories of Litter Items, drawn up by the "Joint Research Centre" (JRC), papers and pens to classify the waste collected.

Mesoplastics

The mesoplastics sampling was done considering the GESAMP protocol (2019). The materials needed to collect this plastic debris fraction were:

- 1-meter square quadrat.
- A steel shovel.
- A 5 mm stainless steel sieve.
- Glass containers to store the sand.

Microplastics

All the materials used to sample the meso-plastics were used to collect the microplastics fraction, except the 5 mm stainless steel sieve that was replaced with a 1 mm one, cause of the smaller dimension of this debris.

4.1.1.2 Laboratory experiment

With the aim to acquire the spectral signatures of the marine samples, two different experimental setups were carried out. The samples were placed within a black and white box and the spectral reflectance of each sample was measured using the FieldSpec 4 Hi-Res spectroradiometer by ASD (Analytical Spectral Devices). This instrument measures the spectral signatures across the entire solar-reflected spectrum (i.e. from 300 to 2500 nm) by means a 1.5 m long optical fiber with a field of view of 25°. Because the samples have limited dimensions (some of them were characterised by a surface smaller than 1 cm^2) an 8° optic was employed to ensure a centred measurement over the sample. The instrument is composed of three

spectroradiometers, one operating in the visible range (VNIR, 350-1000 nm) with a spectral resolution of 3 nm and the other two in different infrared ranges named shortwave 1 (SWIR-1, 1001-1800 nm) and shortwave 2 (SWIR-2, 1801-2500 nm) having spectral resolution of 8 nm. The instrument is controlled via a personal computer in which the collected spectra are stored. The samples positioned inside the boxes were illuminated using two ASD pro - Illuminator Reflectance Lamp Halogen equipped with Single-Ended Quartz JC14.5V-50WC lamps characterised by an irradiance curve which approximate that of the sun.

The boxes used have very similar volumes ($60 \times 70 \times 60$ cm and $60 \times 60 \times 60$ cm for the black and the white boxes respectively) but different purposes: the black box absorbs the illumination while the white one reflect more than 90% of the light radiation. The shape and the paint used for the boxes were chosen to emphasise these differences. The top of the white box has a 'cupola' shape, to enhance the light diffusion, instead the one of the black box is horizontal. The paints used to build the two boxes were properly selected after several tests performed over small wood samples, which were spectral characterised. The most absorbing and reflecting paints were used for the black and white box respectively. The height and width of the boxes are designed to properly place the lamps and samples for performing the analysis accordingly to the two different planned illumination geometry (please refer to the 4.2.1.2 section, Figure 4.12). To avoid influences due to external lights and of the operator, two curtains (matching the colour of the box) allowed to completely close the boxes during the measures. These were made with a fabric previously spectrally characterised to confirm their matching with the white and black, above-mentioned, paints. Figure 4.1 reports the schematisation of the experimental setup conducted using the white box with the electronic instruments used: the spectroradiometer (with

the optical fiber), the personal computer and the lamps. It is shown also the tripod in which the samples were placed for the measurements. The experiment carried out using the black box differs for the lamps' orientation (see Figure 4.12, panel *a*). Pictures of the experiments are reported in Annex 1.
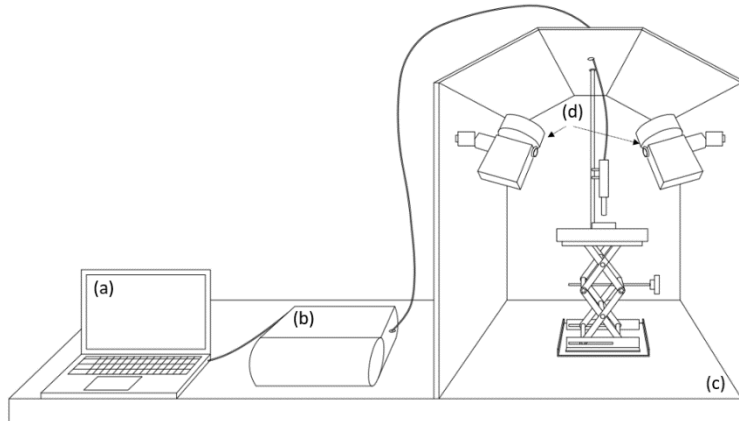
Figure 4.1 – Experimental setup: a) personal computer, b) spectroradiometer, c) box (white and black), d) lamps.

To perform the measures, the samples were placed on a black panel $(21 \times 15 \times 1\ cm)$ (Figure 4.2, panel *a*) realised by covering a wood board with a black opaque fabric (the same used to close the black box). In order to compute the reflectance of the samples (refer to the Section 4.2.1.2), a reference radiance measures were taken over a barium sulphate panel $(20 \times 20 \times 1\ cm)$ (Figure 4.2, panel *b*).

(a)   *(b)*

Figure 4.2 – Black *(a)* and white *(b)* panels used to place the samples to acquire the radiance.

The transparent plastic samples were excluded from the analysis; the others were categorised (basing on their colours and sizes), numbered and finally spectrally characterised. Totally, 136 samples were examined and some of them are shown in Figure 4.3 (refer to the Annex 1 for pictures of all other samples).
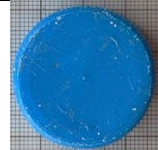
Samples				
Id	1	5	6	12
Samples				
Id	31	131	178	221

Figure 4.3 – Some of the samples collected during the monitoring campaign and of which the spectral signatures were acquired.

From Figure 4.3 it is clear the wide and high variety of the collected samples in terms of colour, dimensions, and shape. This is due to the high heterogeneity of beach litter composition, in which bottle, cups, children's toys are present; also, some of the items were fragmented making difficult to determine the original object.

With the aim of detect the polymers composition of the samples the following virgin polymers were used (Figure 4.4): ethylene vinyl acetate (EVA), high-density polyethylene (HDPE), polyethylene terephthalate (PET), polypropylene (PP), and polystyrene (PS).

(a)   *(b)*   *(c)*

(d)   *(e)*
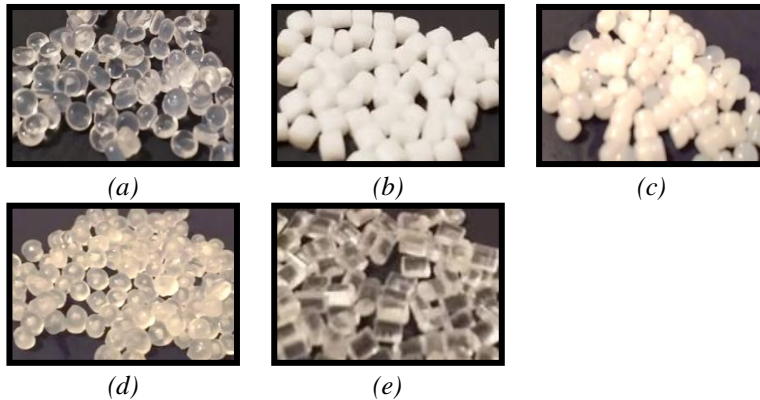
Figure 4.4 - Spectrally characterised virgin polymers: ethylene vinyl acetate (EVA) *(a)*, polyethylene terephthalate (PET) *(b)*, high density polyethylene (HDPE) *(c)*, polypropylene (PP) *(d)* and polystyrene (PS) *(e)*.

4.1.2   Marine litter

4.1.2.1 TrackMPD and STM models: general overview

Different input files are required to work with TrackMPD model. These are following reported:

- The sea currents.
- The bathymetry.
- The sea surface height above geoid (SSH).
- The initial particles' position.
- The study area.

For the case studies analysed in this thesis work, TrackMPD was adapted to use the sea currents data in the Network Common Data Form (netCDF) format provided by Copernicus Marine Service

(*https://data.marine.copernicus.eu/products*). In particular, the Eastward (U) and the Northward (V) Sea surface water velocities were downloaded from the Copernicus Marine Services in which different temporal and spatial resolution are available, depending on the geographical area considered. The bathymetry and the sea surface height above geoid of the study areas were downloaded jointly with the sea surface current data. Other input data as the initial particles' position and the study area (the computation domain) were properly setup following the recommendations provided by the authors. The initial particles' position file (in *.txt* format) is composed by three columns reporting the longitude, latitude, and depth. The study area is defined by the coast coordinates reported in a *.dat* or *.txt* file containing two columns representing the longitude and the latitude of the coastline.

Regarding the STM model, as it is a simplified Lagrangian model (comparing with the TrackMPD) two only inputs data are required: the input discharge points and the sea surface currents; whereas the coastline is automatically computed for the sea current data domain by exploiting the MATLAB® m_map (*https://www.eoas.ubc.ca/~rich/map.html*) feature named 'm_gshhs'.

All the simulations were conducted on a system characterised by: an Intel® Core™ i9-13900K processor with 24 cores up to 5.8 GHz; 32 GB DDR4 RAM at 4400 MHz; an NVIDIA RTX A2000 video card with 16 GB dedicated memory.

Follows a description of the different dataset used for the case studies analysed in this thesis.

4.1.2.1.1 Mediterranean basin

South Tyrrhenian Sea

A realistic discharging scenario was tested in the western Mediterranean Sea (Tyrrhenian Sea) applying the TrackMPD model. As discharging points were considered Mondello and Isola delle Femmine in which the *in-situ* monitoring were carried out. Different macroplastics quantities were released, proportionally with the marine debris collected during the *in-situ* campaign (Table 4.1).

Table 4.1 – Plastic items/m^2 found in the beaches of Mondello and Isola delle Femmine.

Beach - code	Plastic items/m^2
M-D1	0.005
M-D2	0.004
M-D3	0.006
M-S1	0.005
M-S2	0.006
M-S3	0.005
M-L1	0.401
M-L2	0.003
I-1	0.401
I-2	0.287
I-3	0.159

The simulation was run using the required fields of the physical variables (see Section 4.2.2.1.1) available through the *Mediterranean Sea Physics Analysis and Forecast. E.U. Copernicus Marine Service Information (CMS). Marine Data Store (MDS). DOI: 10.25423/CMCC/MEDSEA_ANALYSISFORECAST_PHY_006_013_EAS8* (Accessed on 06-02-2024). The product is an outcome of the Mediterranean Forecasting System (Med-Physics) which coupling the hydrodynamic model Nucleus for European Modelling of the Ocean (NEMO v4.2) and the

WaveWatch-III providing the sea surface currents (computed considering e.g. tidal waves, the air-surface fluxes etc.) and wave component respectively. This dataset has a spatial resolution of 0.042° x 0.042° (4-5 km c.a.) and 141 vertical levels (from 1.02 m to 5646.2754 m); different time resolutions are available such as 15 minutes, hourly, daily and monthly mean. Simulations have been computed considering sea surface currents at daily temporal resolution.

Strait of Sicily

For the Strait of Sicily study area, two different applications were carried out. For the first one (therefore called as "coastal release application") both TrackMPD and STM models were applied, considering a continuous particles discharge from the Sicilian coastal area (hereinafter this application is indicated as "STM – coastal release application" or "TrackMPD – coastal release application"). Instead, for the second one (therefore called "STM – grid release application") only the STM model was used, and the discharge points were considered those in the centre pixel of a regular grid covering the whole domain. For this last application the TrackMPD was not tested as the very high number of the discharging points per day to be simulated.

The hydrodynamic models application carried out in this area benefitted of data gathered by the sampling campaigns conducted by "Agenzia Regionale per la Protezione ambientale" (ARPA) and "Consiglio Nazionale delle Ricerche" (CNR) in August 2018 and 2019. TrackMPD and STM models were run considering macroplastics which are one of the main sources of the smaller elements (precursors).

For the coastal release application in the Strait of Sicily the number of discharged points was chosen based on the estimations of the quantity of plastics discharge at the coast, available in the *https://theoceancleanup.com/sources/* website, described in 2.1.1. This

website delivers an assessment of the quantity of plastics discharge from the most important worlds' rivers as an interactive map (Figure 4.5).

Figure 4.5 – River plastic emissions to the world's oceans (Source: *https://theoceancleanup.com/sources/*).

The information displayed in Figure 4.5 have been published in Meijer et al. (2021) in which the probability that plastic waste reach the rivers and thereafter, the oceans is calculated yearly by a model application that takes into account the most recent field data on microplastic, the land use, wind, precipitation, and rivers' class and size. The results of the model are calibrated and compared with field data points. The quantity of macroplastics coming from the rivers was considered proportional to the size of the rivers itself.

For the grid release application, the particles were discharged on the basis of a regular grid.

The simulations (coastal and grid release applications) were run using the *Mediterranean Sea Physics Reanalysis. E.U. Copernicus Marine Service Information (CMS). Marine Data Store (MDS). DOI: 10.25423/CMCC/MEDSEA_MULTIYEAR_PHY_006_004_E3R1* current data (Accessed on 21-09-2023). The details of the product are reported in this section ("South Tyrrhenian Sea" paragraph).

The simulations, realised for the 2018 and 2019, were compared with the data from the campaign conducted by ARPA and CNR. This campaign had the goal to collect the microplastics particles floating on the sea water surface, using a Manta net in fixed transects. In Figure 4.6 are reported the five transects repeated during the monitoring campaign.
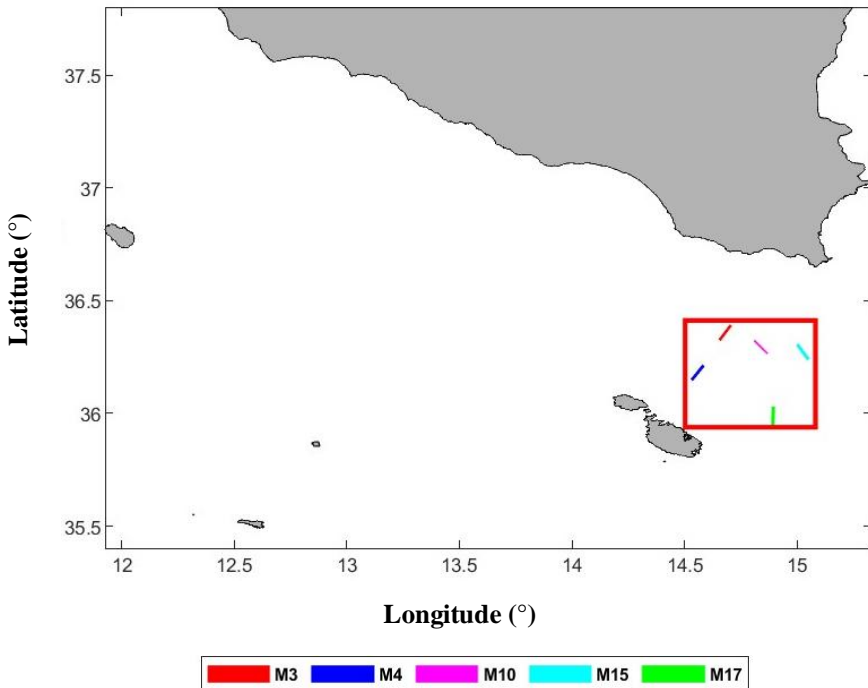
Figure 4.6 – Study area for the Strait of Sicily. The red area represents the area where the transects (colored lines) were made and where the models were compared with *in-situ* data.

The Manta net is characterise by a rectangular aperture (16 cm high and 61 cm wide) connected with a 3 m long net with a 335 μm mesh (Eriksen et al. 2018). A schematic drawing is reported in Figure 4.7.
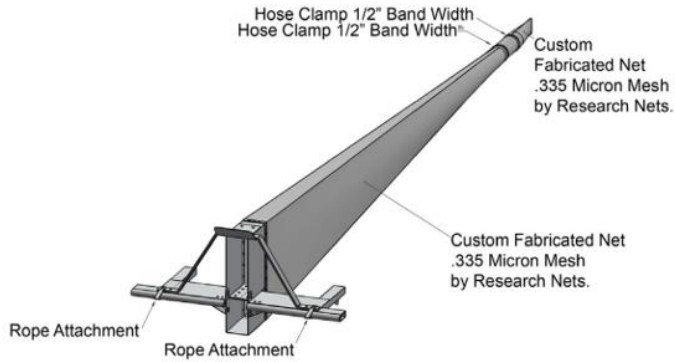
Figure 4.7 – Schematic drawing of the AVANI trawl, Manta trawl. (Source: Eriksen et al. 2018).

The *in-situ* campaign was conducted in different days for each transects. Table 4.2 reports the coordinates of the transects and the timetable of the sampling.

Table 4.2 – Transects coordinates and timetable of the *in-situ* campaign conducted by ARPA and CNR in the Strait of Sicily.

Year	day*	Time (UTC)	Station**	LON	LAT
	12	20:45	M3	14.68	36.35
	13	00:16	M4	14.56	36.18
2018	12	17:11	M10	14.84	36.29
	11	21:07	M15	15.03	36.27
	12	00:20	M17	14.89	35.99
	11	21:20	M3	14.68	36.35
	11	20:02	M4	14.56	36.18
	11	06:21	M10	14.84	36.29
2019	10	04:47	M15	15.03	36.27
	10	23:50	M17	14.89	35.99
	12	00:59	A1	14.10	36.40

* all the samplings were carried out in August
**central point of the transept

Microplastics collected were analysed and categorised in laboratory by ARPA which counted and classified the samples basing on their shape and size (Table 4.3).

Table 4.3 – Number of items per m^3 sampled in each transects of the *in-situ* campaign conducted by ARPA and CNR during the two years campaigns.

Year	Transect	Fragments	Filaments	Sheets	Foams	Total
		(items/m^3)				
2018	M3	0.34	0.02	0.10	0.00	0.45
	M4	0.59	0.03	0.39	0	1.01
	M10	0.39	0.02	0.12	0.02	0.54
	M15	0.97	0	0.01	0	0.99
	M17	0.93	0.02	0.29	0.02	1.27
2019	M3	0.22	0.04	0.01	0.02	0.28
	M4	0.3	0.01	0.06	0.01	0.38
	M10	0.07	0.06	0.03	0.01	0.17
	M15	0.35	0.08	0.01	0.02	0.46
	M17	0.57	0.01	0.12	0	0.7

An example of the elements sampled is reported in Figure 4.8.
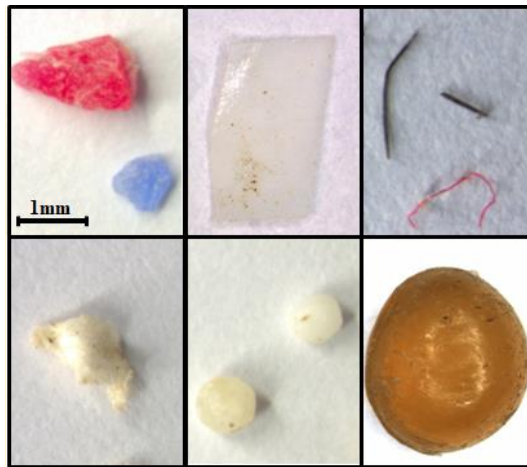
Figure 4.8 – Samples collected during the *in-situ* campaign: examples of fragments (top left), sheets (top center), filaments (top right), foam (bottom left), granules (bottom center), and pellets (bottom right).

As it is evident, there is a high heterogeneity in terms of shapes, colours and sizes highlighting that the detection of these debris at sea is very complex thus strengthen the need of analyse the problem from a hydrodynamic point of view.

4.1.2.1.2   Liberia/Gulf of Guinea

For the Liberia/Gulf of Guinea case study, the simulation was performed for the whole 2021.

Considering, as mentioned in 2.1.1, the high correlation between the rivers and the presence of marine plastic litter (especially during rainfalls), the estuaries of the five main rivers in the Liberian region were considered as continuous plastic discharge points. The selection of these five rivers was based on the rainfall data provided by the Liberian Hydrological service (*https://lhsliberia.com/water-data/*). Figure 4.9 reports an example of data available from the Liberian Hydrological services and the main rivers are represented using green dots.
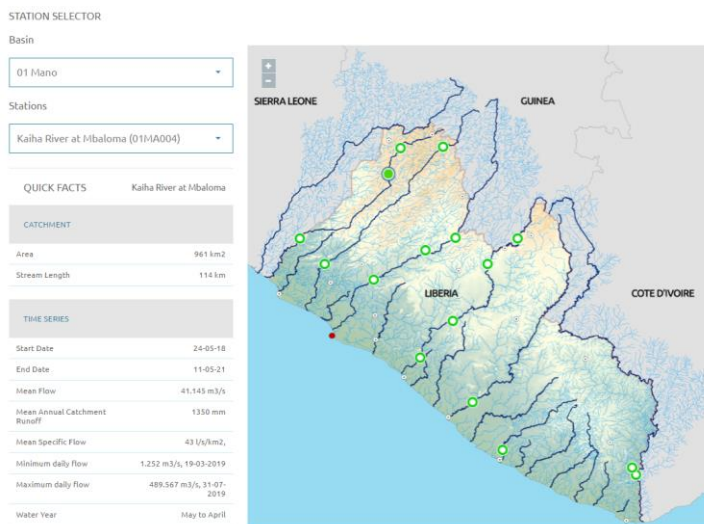
Figure 4.9 – Data availability from the Liberian Hydrological services (*https://lhsliberia.com/water-data/*).

U, *V*, SSH and the bathymetry layers were downloaded from E.U. Copernicus Marine Service Information (*https://doi.org/10.48670/moi-00016*). The *Global Ocean Physics Analysis and Forecast E.U. Copernicus Marine Service Information (CMEMS). Marine Data Store (MDS). DOI: 10.48670/moi-00016* (Accessed on 25-02-2023) was used. The global ocean analysis and forecast model, GLO12v4, uses the version 3.6 of the NEMO ocean model. This dataset has a spatial resolution of 0.083° × 0.083° (10 km c.a.) and 50 vertical levels (from 0 m to 5500 m); different time resolutions are available such as hourly, daily and monthly means. The simulation was performed using the sea surface currents "GLOBAL_ANALYSISFORECAST_PHY_001_024" at daily temporal resolution with the aim to track the pathways of the daily constant discharge of macroplastics from the rivers.

Finally, the domain area was realised in QGIS environment by thicken the geometry nodes of the "ne_10m_coastline" form the *Natural Earth* website (*https://www.naturalearthdata.com*) and converting these coordinates into a text file as required by TrackMPD.

4.1.2.2 Aegean Gulf: detection of floating target on sea surface

Within the PLP 2021 project two artificial targets were deployed: one made by wood, useful to simulate natural debris, and a plastic target. The wooden target, boasting a diameter of 28 meters, was assembled using planks of the same material, connected by 4 m long and 22 cm wide ropes. Nine groups of planks were arranged with 30 cm gaps between each, creating a structured configuration. The plastic target was crafted from high-density polyethylene (HDPE); it was made employing 23 rows of 1.2 m wide of white wide HDPE mesh, interconnected by a 4 mm nylon rope. A

28 m diameter HDPE pipe was used to link these mesh rows, resulting in a total coverage area of approximately 600 m^2. Additionally, to partially elevate the HDPE mesh from the sea surface, 4 l HDPE containers were affixed at 2.5 m intervals along the sheet. A picture of the targets is shown in Figure 4.10.

(a)   *(b)*
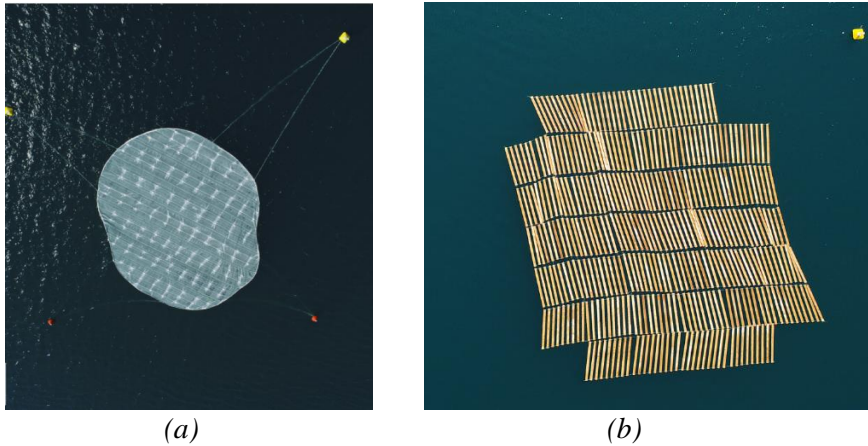
Figure 4.10 – Targets of PLP2021 deployed on the sea surface: Plastic target *(a)*; wooden target *(b)*. (Source: *https://plp.aegean.gr/*).

The focus of the research was the detection of the plastic target using the hyperspectral images acquired by the PRISMA satellite. PRISMA has an orbit repeat cycle of 29 days with a relook capability of 7 days. The sensor has ~ 250 bands in the spectral range of 400 - 2500 nm with a spectral resolution of 12 nm and 30 m of spatial resolution. A panchromatic band acquires images at 5 m spatial resolution. The PRISMA data are provided by the Agenzia Spaziale Italiana, ASI (*https://www.asi.it/en/earth-science/prisma/*) at different processing levels: 1A (in radiance radiometrically corrected and calibrated at the Top-of-Atmosphere), 2B (Geolocated at Bottom-of-Atmosphere, Radiance values), 2C (Geolocated at Bottom-of-Atmosphere, Reflectance values) and 2D (Geocoded version of the level 2C products). The PRISMA Level 1A images were used in this part of the research work. As it was preferred the ACOLITE atmospheric

processor instead of the standard one (applied by ASI), and it was done a fine geolocalisation of the images using a PlanetScope multispectral image and UAV images. The PlanetScope image was acquired the 17th July 2021. PlanetScope is a multispectral satellite data (4 bands, red-green-blue and near-infrared) characterised by 3 m of spatial resolution and daily acquiring capability. The UAV images are RGB data collected by a standard camera at ~3 cm of spatial resolution. Table 4.4 shows both PRISMA and UAV images used for this application.

Table 4.4 – Selected pairs of images (in bold the dataset reported in the thesis).

PRISMA	UAV
June 29th	July 1st
July 16th	**July 16th**
July 22nd	July 21st
August 14th	August 20th

Only the UAV image of the 16th July 2021 was contextually acquired to the PRISMA data, thus, results hereinafter shown will refer to this date (selected as an example).

4.2 Methods

4.2.1 Beach litter

In this section, the methodology for the collection of macro-, meso-, and microplastics is described first, followed by the approach used for the spectroradiometric analysis of the collected samples.

Meso- and micro-plastics were sampled but not analysed in the laboratory within this thesis work. For this reason, the methodology will be focus only on the sampling activities.

4.2.1.1 *In-situ* sampling: definition of areas and quantification/characterisation of macroplastics

The literature review conducted (see Section 2.1.1) allows to select the appropriate sampling protocols and to fix a rigorous and salient scientific methodology during the sampling thus providing a harmonised set of outcomes, exploitable from various stakeholders into future monitoring plans. In particular, the information available in MSFD TSG-ML (2013) and GESAMP (2019) protocols have been merged. Both incorporate important information from previous protocols, such as OSPAR. The MSFD TSG-ML was used for the selection of the study areas; meanwhile, GESAMP has proven useful for defining the sampling protocol for meso- and microplastics. The categorisation of the debris in terms of material, shape, dimensions, etc. was realised using the Joint List of Litter Categories (J-code list), proposed by the Joint Research Centre, Institute for Environment and Sustainability, Marine Strategy Framework Directive TSG-ML (European Commission MSFD) in 2013, and assigning different codes to the various litter collected. In the following a description of the methodology applied in the monitoring campaign is reported.

The beaches monitored were chosen according to the protocol. They respected the following criteria:

- Minimum length of 100 m.
- Low/moderate slope varying between 15° and 45°.
- Free access to the sea, i.e. absence of breakwaters or jetties that can screen the pollutants.
- Accessible to the survey team throughout the entire year.
- Absence of other waste collection activities. In case this is not verified, it is necessary to know the timing and methods of cleaning conducted by third parties.

The activities were conducted without impacting endangered or protected species such as marine turtles, seabirds or coastal birds, marine mammals, or vegetation.

In addition to the geometric characteristics of the beaches, explained before, these have to be selected considering also the kind of beach litter that can be found out:

- Beaches close to urban area, subject to terrestrial inputs.
- Beaches along rural area in which is possible to identify background pollution.
- Beaches near large rivers to assess their influence in the establishment of beach litter.

The selected beaches satisfy the first requirement.

The protocol also suggests the period in which sample the area, like as:

- Winter: mid-December to mid-January.
- Spring: April.
- Summer: mid-June to mid-July.
- Autumn: mid-September to mid-October.

To evaluate the seasonal variation, four surveys should be conducted during each season.

The replicability of the analyses at the same site over time, is guaranteed by memorising the GPS coordinate, as indicated in the "Marine Litter Beach Documentation and Characterization Module" of the OSPAR Marine Litter Beach questionnaire (OSPAR, 2010).

The criteria followed to characterise the sampling area (in terms of length, distance from sea etc.) are described in Figure 4.11.
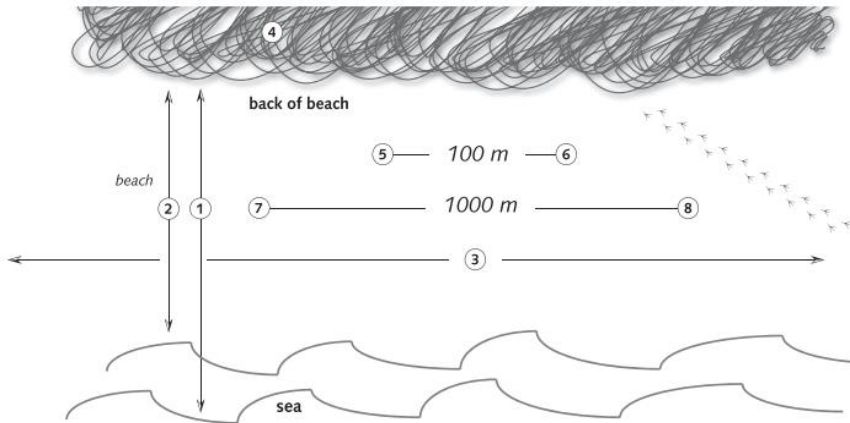
Figure 4.11 – Criteria to adopt for the definition of sampling area: 1) distance from mean low water spring tide, 2) distance from mean high water spring tide, 3) total length of beach, 4) description of zone beyond intertidal, 5) and 6) GPS coordinates of 100 m sampling unit, 7) and 8) GPS coordinates of 1000 m sampling unit. The 1000m transect has been discontinued. (Source: OSPAR 2010).

The sampling campaign was conducted during the 2021 summer season (in the framework of the project SenHAR - Campagne di sensibilizzazione per una armonizzazione Italo-Maltese per un buono stato dell'ambiente" INTERREG Italy-Malta V-A Operational Program call n. 02/2019), in which micro-, meso-, and macro-litter were collected.

One of the goals of this work was to evaluate the connection between the different beaches management and presence/absence of MPA *vs* the quantity/kind of beach litter. Consequently, the length of the beaches was not 100 m but was constrained by the length of the different beach resort or by the extension of MPA area.

The macroplastics collected were analysed by dividing them in n. items per square meters to standardise the values and compare the results. As suggested by the protocols (GESAMP, 2019; NOAA, 2013), only items larger than 2.5 cm were collected and considered as macrolitter. To collect the macroplastics the operators wore gloves and picked up the visible litter using the clamps and stored them in the bags. The bags were weighted, to

have an idea about the kilograms of debris found out in each beach. In Mondello, the operators of the beach resorts were cleaning every day the beaches. The items collected by them were jointly with the debris collected by the researchers.

Once the debris have been collected, they were categorised in different materials and items according with the "Master List of Categories of Litter Items" by Marine Strategy Framework Directive Technical Group on Marine Litter (MSFD TSG-ML, 2013). This activity was done by two operators that worked together: one identified the macro debris, in terms of material, shape etc and the other searched the items in the list and assigned a J-code to it. The analyses were performed in November 2021 and the J-code were updated considering the new list "The Joint List of Litter Categories for Macrolitter Monitoring" (Joint Research Centre – JRC, 2021). Eight material categories were considered: artificial polymers/plastic, rubber, clothes/textile, paper/cardboard, processed/worked wood, metal, glass/ceramics and chemicals. A more specific analysis could be done considering the different objects within the categories such as for the plastics fraction the elements J9 "plastic bottles and containers of cleaning products", J7 "plastic drink bottles ≤ 0.5 l" etc.

As mentioned before, the number of litter found on each beach was divided per the square meters of the beach. Different analyses were performed to answer the scientific questions. In particular, the mean of all items per square meters were calculated for each beach, obtaining from Figure 5.1 to Figure 5.3. To quantify the presence of each material on every beach, the average number of items per square meters for each material was calculated (Figure 5.4, Figure 5.5). A more thorough analysis, considering various object categories within the materials category, allowed to pinpoint the top five most recurring 'J-code' elements (Figure 5.6, Figure 5.7). Further

assessment facilitated the identification of the top five plastic elements at each site (Figure 5.8, Figure 5.9).

4.2.1.2 Laboratory Experiments

Experimental setups

To evaluate the influence of the illumination geometry on the spectral behaviour, the spectral signatures of samples were acquired through two novel and *ad-hoc* laboratory set up. The realisation of these experimental setups was necessary because of the absence of a standardised protocol to adapt for the laboratory measurements.

One set of measures was carried out using a black box (quasi-totally adsorbing the light inside) where two lamps were rotated downward thus illuminating directing the samples (Figure 4.12, *a*). The second set of measures was realised using a white box (quasi-totally reflecting the light inside) where the two lamps were rotated upward, thus illuminating the samples with diffuse light (Figure 4.12, *b*).
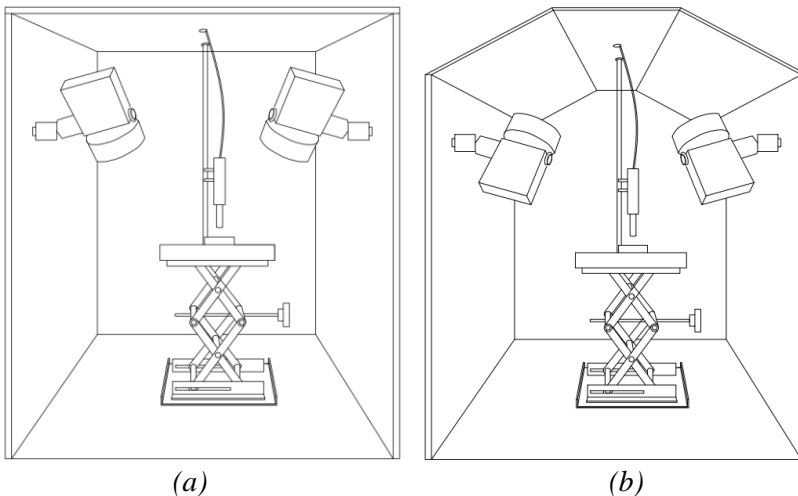

(a)   *(b)*

Figure 4.12 – Schematisation of black *(a)* and white *(b)* box used for the indoor experiment.

As mentioned in 4.1.1.2, and evident in Figure 4.12, also the shape of the white box was properly designed to optimise the diffusion of the light inside the box itself.

Spectral signatures collection

The spectral signature is the reflectance of a material along the wavelengths. The reflectance, ρ, (Eq. 4.1) is defined as the ratio between the density of radiant flux reflected from the target surface, hereinafter named exitance, M (W/m^2), divided by the density of radiant flux incident on the same surface, hereinafter named irradiance, E (W/m^2).

$$\rho = \frac{M}{E} \ (-) \qquad \qquad \text{Eq. 4.1}$$

The spectroradiometer allows to acquire the signal through the optical fiber. This is composed by several small fibers having different diameters (the smaller diameter conveys the signal in the visible, while the others convey the signal in the near infrared). The spectroradiometer allows to acquire not the exitance but the radiant flux per unit area and solid angle, hereinafter named radiance, L [$W \cdot m^{-2} \cdot sr^{-1}$] (in a plane perpendicular to the given direction). Assuming a Lambertian behaviour for the examined surface (i.e. the reflected radiance is the same in all directions) values of M could be computed by multiplying L with π (representing, in radiant, the whole hemisphere).

In this framework, the reflectance of the litter collected was evaluated by dividing the radiance of the samples (i.e. M/ π) with the radiance of the barium sulphate white panel (i.e. E/ π). The barium sulphate white panel is a quasi-perfect Lambertian surface reflecting almost 100% of the incident light, while this assumption can note be verified for the marine sample. This

implies that the two different illumination geometries could led for the same sample to different reflectance curves.

Although the software allows to speed up the acquisition phase by collecting in-reflectance measures of the objects, it was preferred to take in-radiance measurements of the samples and of the white panel, and then compute the reflectance of samples during the data processing phase. Indeed, in-reflectance measurements are taken by collecting one 'white reference' radiance measure which is assumed constant and automatically used by the ASD software to perform a measurement cycle (sequence of reflectance measurements of different samples). With in-radiance measurement method a number (equal to those of the samples to be spectrally characterised) of white reference radiance are measured during the measurement cycle; thus, allowing to verify that the illumination conditions remained constant (or not) throughout each sampling cycle (the whole spectral laboratory experiment was carried out in different measurement sessions/cycles per day, for a total of approximately 20 days). Before starting a new measurement cycle, the optimisation of the instrument was performed through the so called "dark current" procedure which allow to measure and correct the instrument noise floor.

Before acquiring the spectra, it was verified that the 8° optic was pointed to the samples. Furthermore, to make the measurement for each sample comparable each other, the distance between the instrument and the samples was still maintained constant (6 cm) by adjusting the distance between the optical fiber and the sample by placing this latter over a tripod with a geared elevator.

Also, spectra of sand samples (of the two study areas) and of some virgin polymers (EVA, HDPE, PET, PS, and PP) were collected for further analyses.

Analysis of the spectra and role played by the illumination geometry

The spectral signatures of the litter were plotted and analysed. The comparison between the two boxes was conducted computing the average of the spectral signature of each sample, *s*, obtaining $\rho\mu_{s,white}$ and $\rho\mu_{s,black}$ for the white and black box respectively.

Finally, the samples represented in the scatterplot by points far from the 1:1 line were furtherly investigated as these are those for which their signatures were strongly affected by the two different illumination conditions.

The use of the SAM index as a tool for detectability of the litter

All the spectra collected in the laboratory were further analysed via the calculation of a spectral similarity/dissimilarity index named Spectral Angle Mapper (SAM) (Kruse et al. 1993; Garcia-Allende et al. 2008). All the analyses hereinafter described were performed using both the measures acquired in the white and in the black box. The SAM index, α, is computed as follows:

$$\alpha = cos^{-1}\left(\frac{\sum_{i=1}^{n} t_i r_i}{\sqrt{\sum_{i=1}^{n} t_i^2}\sqrt{\sum_{i=1}^{n} r_i^2}}\right) \qquad\qquad \text{Eq. 4.2}$$

in which *n* is the number of the spectral bands, t_i and r_i are the two spectra to be compared. The SAM index is the spectral angle between two signatures; it is evaluated in radians thus it ranges between 0 and $\pi/2$. A small SAM value corresponds to a small angle between the two signatures which thus exhibit a very high similarity and *vice versa*. Therefore, when SAM value is low, the two objects being compared are similar and difficult to be distinguished one each other.

Through the SAM index the following scientific questions were addressed.

Litter on sand detectability using spectral signatures and role played by the illumination geometry

The SAM was evaluated between the spectral signature of the collected litter and that of the sand resulting in graphs showing the SAM index values (for both the white and the black box acquisition); a comparison between the index calculated considering the two configurations was realised through a scatterplot.

Best spectral bands suitable for litter detection on sandy beaches

The SAM was evaluated between the spectral signature of the collected litter and that of the sand (reference) by employing a moving window of 21 nm.

Assessment of the polymers' composition of plastic litter through analysis of the spectral signature

One of the main difficulties encountered during the *in-situ* sampling campaign and the laboratory analyses is related to the impossibility of identifying, without use a specific instrument, the polymers composing the collected samples. For the chemical characterisation, an attempt was made by assessing the SAM between the spectra of the plastic litter and those of some virgin polymers (as already reported in the Section 4.1.1.2, Figure 4.4).

Detectability performance of different virgin polymers from sand

To this aim, the SAM index was evaluated between the spectral signatures of the virgin polymers and that one of sand. Results are shown in a bar graph (for both white and black box acquisitions).

Best currently operating satellite sensors to detect litter on sandy beaches

To this aim, among the currently operating sensors only those characterised by a geometric resolution equal or less than 10 m were taken into account. In particular, were considered PlanetScope (3.2 m, *https://earth.esa.int/eogateway/missions/planetscope*), Worldview3 (2 m, *https://earth.esa.int/eogateway/missions/worldview-3*), Sentinel-2 (10 m, *https://sentinels.copernicus.eu/web/sentinel/missions/sentinel-2*), and Pleiades (2 m for MS and 0.5 m for Pan bands, *https://earth.esa.int/eogateway/missions/pleiades*). Thus, the SAM values between the spectral signatures of the collected samples and that of the sand were computed by considering reflectance values at the centre wavelength of the bands of the mentioned sensors. As a result, a matrix of the SAM values of the various sand/sample combinations (in rows) for the different sensors (in columns) was computed.

Subsequently, some percentiles, p, of the SAM values were calculated for each sensor. The number, E, of the sand/sample combinations exceeded the i-th p value was computed. Thus, for each p, only the sensors characterised by E values higher than the 30% of the total sand/sample combinations were assumed as suitable for detection including the evaluation of the best bands. The p values computed are: 50th, 75th, 90th, 98th and the 99th.

All the analyses were performed using the MATLAB® software and the main results are reported in the dedicated results section.

4.2.2 Marine litter

4.2.2.1 TrackMPD and STM models: general overview

Macroplastics were tracked by applying two different models: TrackMPD and STM, written in MATLAB®.

Originally, TrackMPD gives as outcomes the intermediate and the final particles' position. Two additional outcomes were produced allowing a better description of the effects of the simulated pollution at the sea and at the coastal areas: the density and beaching maps. The former allow to detect the accumulation areas for each simulation step by counting on a grid basis (on the pixel's size of the CMSs' data) the number of particles felt inside each pixel. The latter enable to evaluate the impact of macroplastic litter on the coastline by counting (on a grid basis, as for the density map) the number of particles felt inside each pixel of a coastline buffer area. Both outcomes give important information regarding the areas most impacted by plastic pollution, considering a coastal release. Initially, TrackMPD simulated the movement of one/more particles released at a specific time instant. Assuming that rivers discharge particles debris continuously in time, the TrackMPD was implemented to allow a multiple particles' releases during a time interval. From a practical point of view, the model was modified to run in a loop were several particles from the indicated source points are continuously released for the entire simulation period. Additionally, it was modified to use the Copernicus Marine Service Sea currents data.

The TrackMPD model is composed by the following modules (Jalón-Rojas et al.,2019):

- Advection.
- Behaviour.
- Dispersion.

- TRAJstruct (outputs).
- TransformInputs.
- RunTrackMPD.

These modules are independent, and it is possible to work on each of them by specifying some parameters. The RunTrackMPD module allows setting the simulation general parameters. In particular, it is required to indicate the Hydrodynamic model's name (a label identifying the simulation), the domain, the physical processes to be included, the particles' behaviour and the trajectory setting. This latter regards the simulation mode (2D or 3D), the date of particle release, the trajectory duration (simulation temporal window), the time step and the direction of the tracking (forward or backward). It is also possible to simulate different phenomena such as beaching, washing off or refloating. These last two processes could be simulated only in 3D mode. Despite it is well known that wind action influences the transport of plastic debris cause of the force exerted on the surface above water (Tong et al. 2021; Critchell et al. 2019), the model does not allow to consider the wind influence on the simulations.

Regarding the particles' behaviour, it is possible to set the characteristics of the particles to which simulate the tracking:

1. Macro or microplastic, plastic density < 1 g/cm^3, no biofouling, no degradation.
2. Macroplastic or microplastic with a known velocity, plastic density >1 g/cm^3, no biofouling, no degradation.
3. Microplastic (defined by shape, size and density), plastic density >1 g/cm^3, no biofouling, no degradation.
4. Microplastic (defined by shape, size and density), biofouling (constant parameters over time), no degradation.

5. Microplastic (defined by shape, size and density), biofouling (no constant parameters over time), no degradation.

6. Microplastic (shape, size, density), no biofouling, degradation.

For the 2D simulation mode, the particles' sinking, the washing off and refloating cannot be simulated. So, in this case is not useful to load the depth data as input. However, the beaching phenomena can be analysed also in the 2D mode, with the possibly to exclude the biofouling and the degradation factor.

The model can work in forward mode, allowing individuating the final particles position once known the initial discharge points, or *vice versa* in backward.

In the following the main equations of the phenomena taken into account during the simulations are reported.

The general equations of TrackMPD are the following:

$$dX(t) = dX_{adv}(t) + dX_{diff}(t) = U(x, y, z, t)dt + dX'(t) \qquad \text{Eq. 4.3}$$

$$dY(t) = dY_{adv}(t) + dY_{diff}(t) = V(x, y, z, t)dt + dY'(t) \qquad \text{Eq. 4.4}$$

$$dZ(t) = dZ_{adv}(t) + dZ_{diff}(t) + dZ_{sink}(t) =$$

$$= W(x, y, z, t)dt + dZ'(t) - w_s(t)dt \qquad \text{Eq. 4.5}$$

These equations rule the shifts, dX, dY, dZ of a particle at time, t, along the x, y, z axes as the consequence of the sea current velocities U, V, W measured in the time interval, dt. Where the first terms are the advective components (dX_{adv}, dY_{adv}, dZ_{adv}), the second ones (dX_{diff}, dY_{diff}, dZ_{diff}) are the diffusive ones; the term "sink" in Eq. 4.5 refers to the sinking phenomena (only in the 3D mode) and w_s is the settling velocity (m/s).

Moving to a finite form (where Δt is the finite time-step) the advection's component is evaluated as:

$$x_{n+1} = x_n + U\Delta t_i \qquad \text{Eq. 4.6}$$

$$y_{n+1} = y_n + V\Delta t_i \qquad \text{Eq. 4.7}$$

$$z_{n+1} = z_n + W\Delta t_i \qquad \text{Eq. 4.8}$$

In Eq. 4.6, 4.7, 4.8 the subscript $n + 1$ relates to the future position of the plastics' particles obtained by the original n position plus the sea current velocities (U, V, W) multiply by the time step Δt_i. The sea current velocities acting on particles are provided by processing the sea current field data using the Runge-Kutta assimilation scheme (Schlegel et al. 2009) of order 4/5 working in both space and time. Using this assimilation scheme, the sea current velocities at the particle location are evaluated using an iterative process, at each temporal step, by considering the velocities at previous and future time steps to estimate the trajectory of the particles.

The turbulence is computed through a random-walk model in the horizontal direction. The equation used is the following:

$$x_{n+1} = x_n + U + R[2r^{-1}k_h\Delta t_i]^{1/2} \qquad \text{Eq. 4.9}$$

Where k_h is the constant horizontal diffusivity (equal to 1 m^2/s), and R is a random number with mean equal to zero and standard deviation equal to 1.

In case of 3D model, it is also possible to evaluate the turbulence in the vertical direction.
The particles' characteristics influence their movement at sea and, particularly, their density, shape and size play an important role (Chubarenko et al. 2016). Noticeably that these characteristics are strongly connected each other. For example, the density is highly variable depending

on the particles' shape; the latter relates to the kind of particles realised which have also impacts on their degradation. Commonly the plastic debris are fibres, pellets and fragments characterised by different geometry (spherically, irregular etc.). The particles shape influences their velocity at sea. Different studies were conducted to study the parametrization of plastic particles. In the TrackMPD model the spherical particles are simulated accordingly to Zhiyao et al. 2008; whereas, the cylindrical particles are simulated accordingly to Khatmullina and Isachenko (2017).

For the spheres particles is used:

$$w_s = \frac{v}{2R} d_*^3 (38.1 + 0.93 d_*^{12/7})^{-7/8}$$ Eq. 4.10

Where d_* is the dimensionless particle diameter computable considering the particle density ρ_p, the water density ρ_w, the water kinematic viscosity $v \ (m^2/s)$ and the gravity acceleration $g \ (m/s^2)$. R (m) is the radius of the particles.

The cylinders particles are simulated with:

$$w_s = \frac{\pi}{2} \frac{1}{v} g \frac{\rho_p - \rho_w}{\rho_w} \frac{2RL}{55.238L + 12.691}$$ Eq. 4.11

Where, L is the length of the particles; whereas ρ_p, ρ_w, v, g, R are the same variables involved in Eq. 4.10.

Equations 4.10 and 4.11 can be used indiscriminately for short cylinders.

Other shapes of the particles could be considered, and the specific density can be calculated accordingly to Chubarenko et al. (2016).

The STM model, is a simplified Lagrangian model based only on the advection phenomenon (Eq. 4.3, 4.4). Beaching and density maps are also computed.

The main difference with the TrackMPD model lies in the calculation of the velocity acting on the particles. In fact, it was evaluated applying the

Inverse Distance Weighted (IDW) method without applying any space-temporal assimilation scheme (i.e. the Runge-Kutta used in TrackMPD). The IDW allows to evaluate the velocities, v' with the following:

$$v' = \frac{\sum_{i=1}^{N} w_i(r) u_i}{\sum_{i=1}^{N} w_i(r)}$$ Eq. 4.12

In which v is the weighted-mean-distance-based velocity, u_i the velocities falling within a search radius, r, and w_i the weighting factors computed according to:

$$w_i(r) = \frac{1}{d(r,r_i)^p}$$ Eq. 4.13

where $d(r,ri)$ is the distance between the point r and the r_i, and p is a coefficient chosen by the user $p = 0, 1, 2 \dots n$. Regarding the simulation time, the model is set to discharge every day a fixed number of particles. The time resolution is the same of the input sea current used as input by the model.

For both TrackMPD and STM models the coastline is a closed boundary, whereas at open sea open boundaries were set. Both models employ a regular grid calculation mesh characterised by the same spatial resolution of the sea current data.

4.2.2.1.1 TrackMPD and STM applications: Mediterranean basin – Liberia/Gulf of Guinea

The Liberia/Gulf of Guinea case study was analysed using only the TrackMPD. Instead, the Mediterranean basin was studied through the application of TrackMPD, for the application on the Tyrrhenian Sea, and using both TrackMPD and STM models for the Strait of Sicily area.

The application of the two models allows to evaluate the main differences, in terms of outcomes, determined using hydrodynamic models with different complexity degree. Furthermore, the necessity to compute a simulation with several discharging points for the Strait of Sicily case study, to compered models' results with the *in-situ* data, led to apply the STM model. Indeed, the less complexity of this model, allows to compute the outcomes in a reasonable time.

In this section the methodologies applied for each area are reported.

South Tyrrhenian Sea

The TrackMPD model was applied in the Tyrrhenian Sea considering a realistic discharging scenario. In particular, the number of particles to be released was determined by applying a proportion with the quantities of macroplastics sampled during the *in-situ* sampling activities (Table 4.1). It was hypnotized that 0.4 plastic-item/m^2 (the higher quantity sampled) corresponds to 500 particles; thus, the release quantities for all the other beaches (Table 4.4) were determined.

Table 4.4 – Quantity of particles discharged from each sampled beach.

Beach - code	Macroplastics discharged
M-D1	6
M-D2	5
M-D3	8
M-S1	6
M-S2	8
M-S3	7
M-L1	4
M-L2	4
I-1	500
I-2	358
I-3	199

Figure 4.13 shows the discharging points; particles were released only on the 1st November 2021 from all the sampled beaches. The discharging points were shifted of ~ 20 km from the coastline (according to the spatial resolution of CMS data) allowing the particles to be moved by the sea current. The transport of the macroplastics (< 1 g/cm^3) was studied until the 31st May 2022 (before the start of the new summer season) with daily temporal resolution. The main hypothesis is that the plastic debris accumulation is generated during the summer season and these debris are considered source of pollution also in the winter period (once the raining season started, factor known to facilitate the runoff of particle from coasts to offshore).
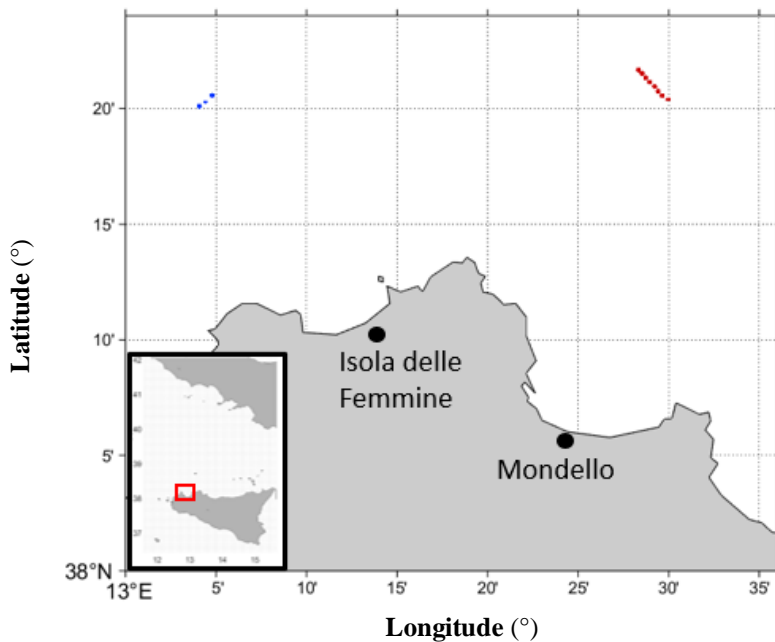
Figure 4.13 – TrackMPD application in the Tyrrhenian Sea. Discharge points: red dots represent the particles released from Mondello, instead the blue dots the ones from Isola delle Femmine.

Strait of Sicily

As mentioned in the Section 4.1.2.1.1, for the coastal release application the discharge points were chosen considering the information available in the Ocean Cleanup website. However, the data available in it are in terms of kilograms of microplastic/year discharged from the rivers instead both TrackMPD and STM models need daily/hourly input data in terms of number of particles. Therefore, after some tests of computational time, it was assumed that 100 kg of plastic debris discharged from rivers are equivalent to 2 particles per day. Totally, 144 macroplastics (< 1 g/cm^3) were released every day and tracked with a daily temporal resolution. The particles were deployed perpendicular to the rivers considering a distance from the coastline ~ 20 km; this offset from the estuaries was imposed to ensure the particles fall into the Copernicus Sea current field. The discharge points used to run both models are reported in Figure 4.14.
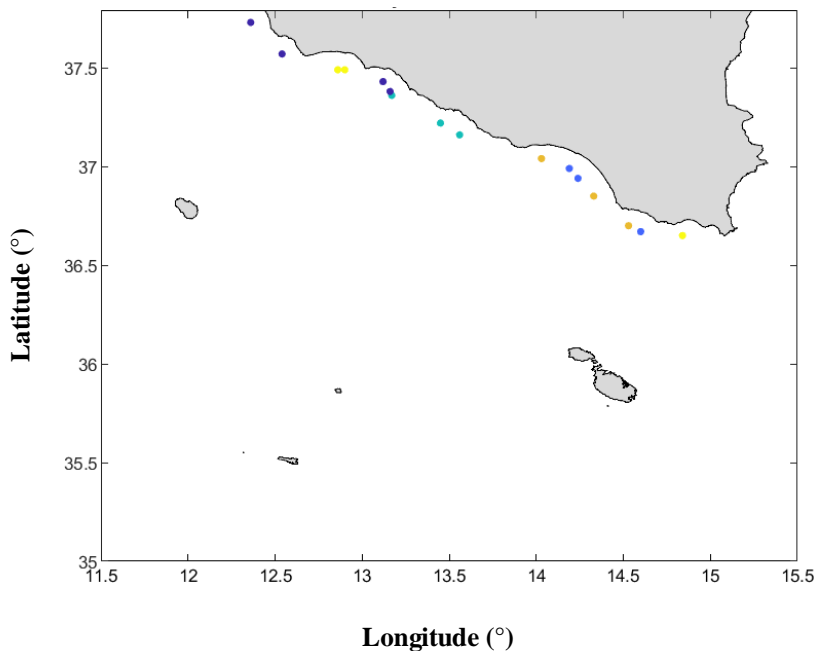
Figure 4.14 – STM and TrackMPD – coastal release application. Study area: the dots are the discharge points.

The results of the STM and TrackMPD − coastal release application were compared to test the effects on the particles' tracking due to the use of models characterised by two different complexity degree.

For both models, the simulations were realised releasing every day the same quantity of particles and tracking their position over the time. For the two models and for the two case studies, the simulations were performed in 2D mode with daily temporal resolution. The trajectory direction considered is *forward* mode.

In the following, the specific parameters set for the TrackMPD are described. The particles simulated were macroplastics with density lower than 1 g/cm^3. The k_h horizontal dispersion coefficient was set at 1 m^2/s. Considering that the model was not set to run in 3D mode, the k_v vertical dispersion coefficient was not considered as well as the parameters controlling the refloating effect. The beaching, biofouling and degradation phenomena were considered.

The parameters set for STM model regarded the search radius R that was chosen 2 times the grid resolution of the CMS data and coefficient p equal to 2.

The applications on the Strait of Sicily were compared with *in-situ* data by quantifying the particles modelled by both the hydrodynamic models within a buffer from each *in-situ* transect performed by ARPA - CNR during a monitoring campaign in 2018 and 2019. Both the TrackMPD and the STM were applied in the periods between 1st May - 30th September 2018 and between 1st May - 30th September 2019. Both simulations start in May as it is supposed that it is the period in which the anthropic pressure on the beaches starts. The comparison was performed in terms of coefficient of determination R^2 evaluated between the models' outcomes and sampling (for the whole period, 2018 - 2019). As shown in Table 4.2, the sampling

campaigns were conducted at different days for each transect. The models' outputs were filtered considering only the particles located in the buffer area between the day before and after the sampling campaign.

In addition, as it is unknown the actual discharging period of the debris recorded by ARPA-CNR the comparison was performed by considering 105 scenarios each one characterised by a different start of the daily releasing of particles. The longest daily discharge temporal windows are from 1st May - 14th August 2018 and from 1st May - 14th August 2019. For all the other scenarios the discharging temporal windows decrease as the start of the particles' discharging is moved forward by one day. The last scenario includes only 2 days, the first in which the particles are released and the second one in which it is possible to analyse their movement.

The impossibility to infer the actual sources of discharging, required to apply Lagrangian hydrodynamic model to the whole sea current fields allowing assessing the tendency of the sea surface currents to accumulate floating plastic debris. To this aim there were considered as discharging points the centre of a regular grid covering the whole study area. Even if it is not a realistic scenario, in terms of number of items and their deployed, the application is useful to study the domain area. 336 particles in total were released every day (Figure 4.15). This simulation was realised only with STM model, excluding the TrackMPD for the high computation time.
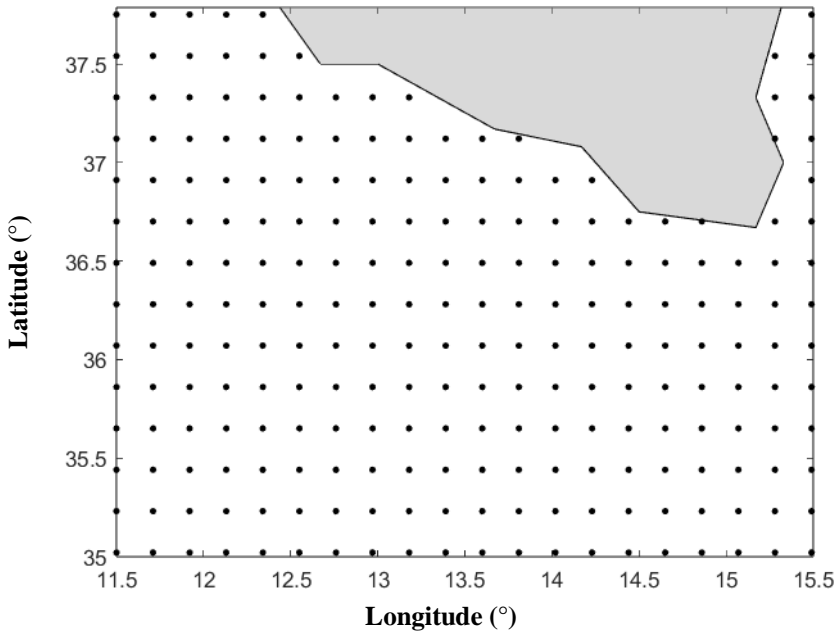
Figure 4.15 – STM - grid release application. Study area: the dots are the discharge points.

For the Strait of Sicily case study, the beaching maps were not realised because the main goal is the comparison of the models using the *in-situ* data. However, the density maps were produced to individuate the accumulation areas at sea.

The Results section reports the main models' outcomes.

Liberia/Gulf of Guinea

For the Liberia/Gulf of Guinea case study, it was assumed that five macroplastics particles (< 1 g/cm^3) were discharge daily from each river (Figure 4.16), approximating that the quantities of pollutants from each one was constant. The total number of macroplastics daily discharged (25) for the whole 2021 allowed limiting the computation time needed to track these particles over the very huge study area (210000 km^2 c.a.). Noticeably that, within the GDA AID Marine Environment & Blue Economy project (on

going) *in-situ* information will be provided from the local institutions (still not available nowadays) and the quantities of plastics to be discharged will be changed accordingly. The particles were realised ~20 km far away from the coastline.
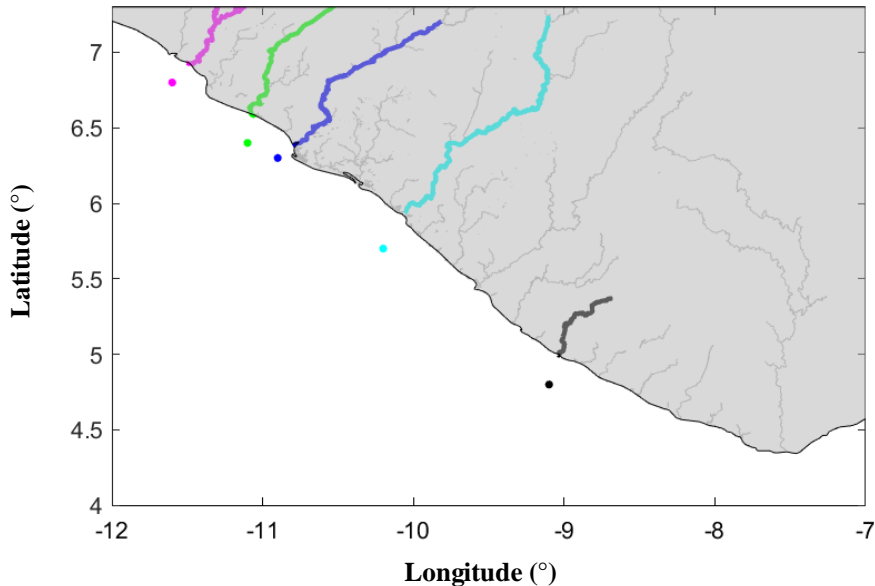
Figure 4.16 – Liberia/Gulf of Guinea TrackMPD Application. Study area: the main rivers from which the particles were realised are represented. The dots are the discharge points.

4.2.2.2 Aegean Gulf: detection of floating target on sea surface

The detection of the floating plastic target was achieved using PRISMA hyperspectral data, characterised by 30 m of spatial resolution. The size of the target (diameter of 28 meters) was not sufficient to have pure pixels over it (i.e. 100% covered by the target). As the consequence, several issues needed to be addressed to achieve a sub-pixel detection. The first challenge concerned the reliability of the geometric correction of the satellite data. Indeed, the identification of sub-pixel target positions in data with low

spatial resolution is particularly susceptible to errors, increasing the likelihood of misjudging the precise target location. The second issue regarded the selection of a proper atmospheric correction to be applied in marine environment. Indeed, the differences between the spectra of pure water and of mixed water-target pixel could be of the same magnitude of the atmospheric contribution; thus, the use of the most accurate atmospheric processor was considered mandatory in this research activity. In this framework the ACOLITE method was chosen as further explained.

The methodologies applied in this work have been structured to address the following scientific questions:

i)   Exploring the benefits and disadvantages associated with the use of hyperspectral data.

ii)   Evaluating the detection feasibility of different band-sets (subsets of spectral bands).

iii) Finally, to determine if it is possible to reduce computational costs without compromising detection performance using a specific band-set.

In this framework, the methodologies adopted, encompassing pre-processing and processing analyses, were focused on the aim to identify the most reliable target position in the PRISMA images and target fraction coverage pixelwise; all the steps realised are following explained.

Pre-processing

Pre-processing analyses involved the atmospheric correction of the PRISMA level 1A images and their geometric correction. Although PRISMA atmospherically corrected images (level 2D) are available, the MODTRAN6 radiative-transfer model is applied; several studies (e.g. Alevizos, Le Bas, and Alexakis 2022 and Valdivieso-Ros, Alonso-Sarria, and Gomariz-Castillo 2021) have shown that MODTRAN6 outcomes are reliable for land applications and one of the best atmospheric correction

algorithm for the aquatic environments is ACOLITE (Basu et al. 2021; Valdivieso-Ros, Alonso-Sarria, and Gomariz-Castillo 2021). In this framework, the level 1A PRISMA images were atmospherically corrected applying the ACOLITE atmospheric correction algorithm.

As level 1A are not georeferenced, the geometric correction was done using the software ENVI® (by L3HARRIS™) applying the *Geographic Lookup Table* (GLT) to obtain the standard georeferenced images (geoTIFF), which were used for all subsequent procedures. Furthermore, a fine georeferencing was done using the following higher spatial resolution data, closest (in terms of acquisition time) to each PRISMA data: UAV orthophoto map and PlanetScope's image (3 m pixel size). The use of the latter image also allowed the digitalization and the identification of the targets. At end of the above-described procedures, it was possible to geolocate the targets in the PRISMA grid and identify a set of possible pixels covered by the floating plastic target.

Processing

The processing analyses included the application of the nonlinear spectral unmixing, the SAM index and the linear spectral unmixing techniques (workflow reported in Figure 4.17). These algorithms chain allowed for the acquisition of the spectral signature of the plastic target and the computation of the fraction covered by the target pixel wise.
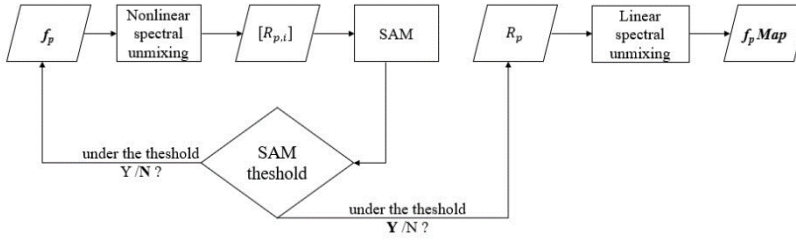
Figure 4.17 – PRISMA processing analyses: workflow.

To assess whether some bands combinations (band-set) were more suitable for the target detection, the workflow was applied to the following band-sets:

- All the bands of the VIS-NIR range, B_{VNIR}.

- All the bands of the SWIR range, B_{SWIR}.

- All the bands selected on the basis of a Principal Component Analysis (PCA), B_{PCA}.

- The bands at the centre wavelength of PlanetScope bands B_{pl}.

With regard to the B_{PCA} this band-set is composed by all the bands provided a correlation with the first PCA higher than a threshold, T.

The not known of the target spectral signature represented an issue. This was addressed by combining the nonlinear spectral unmixing (Dobigeon et al. 2014) technique with the Spectral Angle Mapper (SAM) (Kruse et al. 1993). In particular, the spectral signatures of the plastic target, R_p, was iteratively determined and then considered as the endmember of the unmixing procedure applied to retrieve the fraction covered by the plastic target pixel wise.

In particular, with varying the plastic fractional cover, $f_{p,i}$, it was possible to evaluate a set of possible spectral signatures of the plastic target, $R_{p,i}(\lambda)$, for each pixel i by inverting the Eq. 4.14.

$$R_{mix,i}(\lambda) = f_{p,i} \times R_{p,i}(\lambda) + f_{w,i} \times R_{w,i}(\lambda) \qquad \text{Eq. 4.14}$$

where $R_{mix,i}(\lambda)$ and $R_{w,i}(\lambda)$ are the reflectances of mixed i-th pixel (composed by plastic and water) and of pure seawater at the wavelengths (λ), respectively; $f_{w,i}$ is the seawater fraction cover value at the i-th pixel (with $f_{w,i}$ the complement to one for each $f_{p,i}$). The set of $R_{p,i}(\lambda)$, $[R_{p,i}]$, is thus composed of a number C of f_p-f_w couples selected within the iterative process. The Eq. 4.14 was applied to all the pixels which on the basis of the UAV data were occupied by the target, even with a small percentage. Having obtained a set of possible $R_{p,i}(\lambda)$, the SAM value was calculated among these i-th signatures. Taking into account that the SAM allows to quantify the differences between two spectra (Kruse et al. 1993) and that low SAM values are evidence of great similarity between spectra. The final R_p was chosen if the SAM computed among all $R_{p,i}(\lambda)$ was under a given threshold, S. The resulting R_p was used as the endmember of the linear spectral unmixing (Dobigeon et al. 2014) allowing to determine the plastic fraction within each PRISMA pixel.

A comparative analysis was conducted by applying the linear unmixing method to the PlanetScope image at its original spatial resolution (3 m) and at the PRISMA resolution (30 m, resulted from the application of a pixels-aggregation technique). For this comparative analysis the spectral signature of the plastic target acquired by the 3 m image was employed. This comparison allowed the evaluation of the feasibility of a sensor with few bands but with high (3 m) or low (30 m) spatial resolutions to detect the floating plastic target.

Chapter 5

Results

5.1 Beach litter

The results reported in this section focus on the macroplastics quantification and characterisation in terms of materials and size (according with the "Joint List of Litter Categories for Marine Macrolitter Monitoring") and the spectroradiometric analysis realised in the Remote Sensing Laboratory at the University of Palermo.

5.1.1 Surveys results

The first results, shown in Figure 5.1, report the different quantities of debris in all beach portions of Mondello (reported as M) and Isola delle Femmine (reported as I) beaches. In this analysis, the beach portions sampled in both sites were considered together, without any distinction in terms of access options (then management measures) this in order to visualize the main hypothesis difference, or rather difference in the amount of marine litter between a managed and a free-access unmanaged beach.
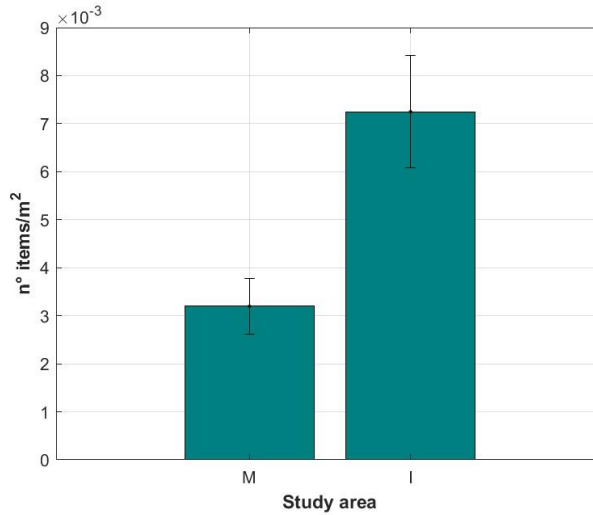
Figure 5.1 – Average number of items/m^2 (mean number items/m^2 $\pm$ se) in Mondello (M) and Isola delle Femmine (I) beaches.

By taking advantage by the subscription options available in Mondello beach, that reflected into different time of permanence offered to citizen (in a range of seasonal, daily, and hourly options) the differences in terms of quantity and typology of debris collected at the various sites were investigated. This analysis, reported in Figure 5.2, showed the average per square meter of debris found out in the seasonal beaches (indicated with S, including M-S1, M-S2, M-S3), in daily (indicated with D, including M-D1, M-D2, M-D3) and low-cost access (indicated with L, including M-L1, M-L2).
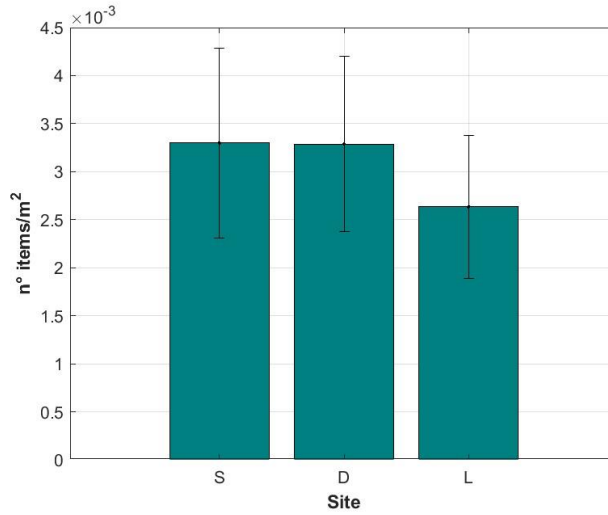
Figure 5.2 – Mean of N° items/m² with standard error for all material in all sites of Mondello.

The mean of items per square meters shows comparable values between seasonal and daily beaches. Instead, lower values were found on the low-cost beaches.

While the management of all beaches in Isola delle Femmine was uniform (no ongoing cleaning), a comparative analysis of debris quantities was conducted to assess potential variations between the area within the MPA (I-1) and the others two Figure 5.3. The quantities of litter in I-1 are higher than the other sites.
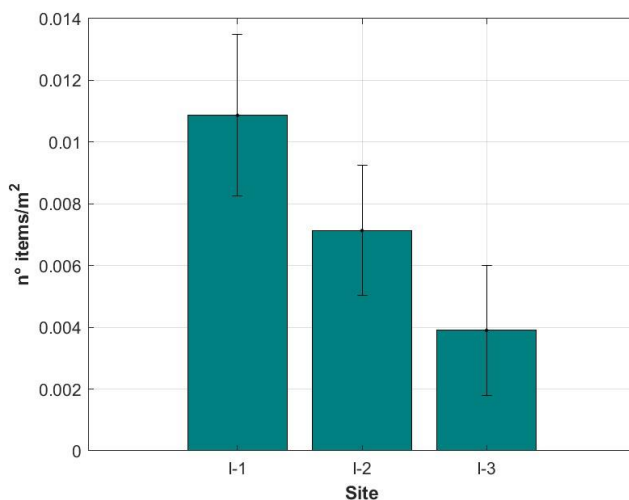
Figure 5.3 – Mean of n° items/m^2 with standard error for all material in all sites of Isola delle Femmine.

In Figure 5.4 and Figure 5.5 the quantities of beach litter are reported, classified into the main categories (artificial polymers plastic, chemicals, clothes textile, glass ceramics, metal, paper cardboard processed worked wood and rubber) for the sites of Mondello and Isola delle Femmine respectively.
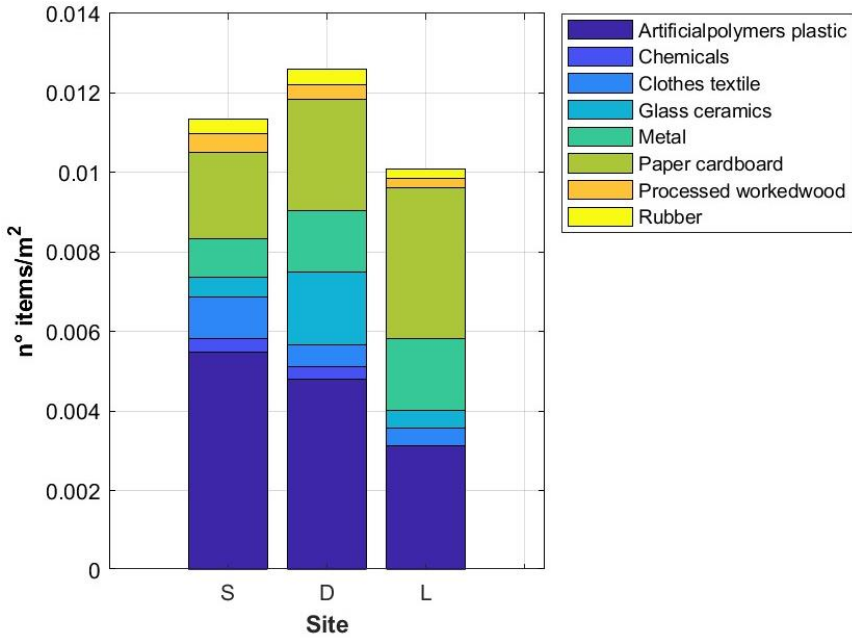
Figure 5.4 – Mean of n° items/m^2 for each material in all sites of Mondello.

In the seasonal and daily sites, the quantity of the "artificial polymers plastic" category is higher compared with the others. Instead, in the low-cost sites the most frequent category is the "paper cardboard". All the others quantities are comparable between all sites, with an exception for "glass ceramics" category that is higher in the daily beaches.
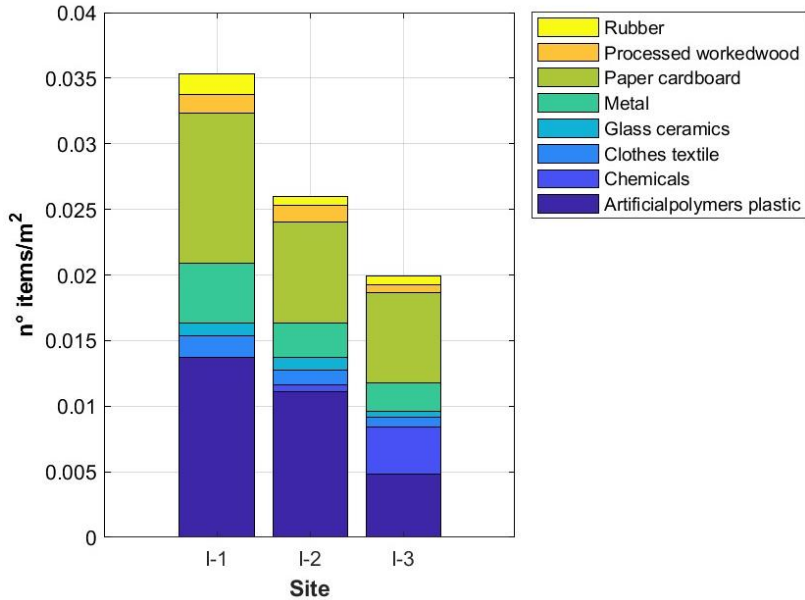
Figure 5.5 – Mean of n° items/m^2 for each material in all sites of Isola delle Femmine.

The "artificial polymers plastic" category was found with higher frequency than the other litter in the sites I-1 and I-2. Instead, the "paper cardboard" fraction is the most frequent in I-3. All the other quantities are comparable between the all sites except for the "metal" fraction that is higher in I-1. Moreover, the "rubber" category presents higher value in I-1 comparing it with the other sites.

A more detailed analysis was carried out with the aim of identifying the five most frequent categories on each site. These results are shown in Figure 5.6 and Figure 5.7 and the description of each category is shown in Table 5.1.
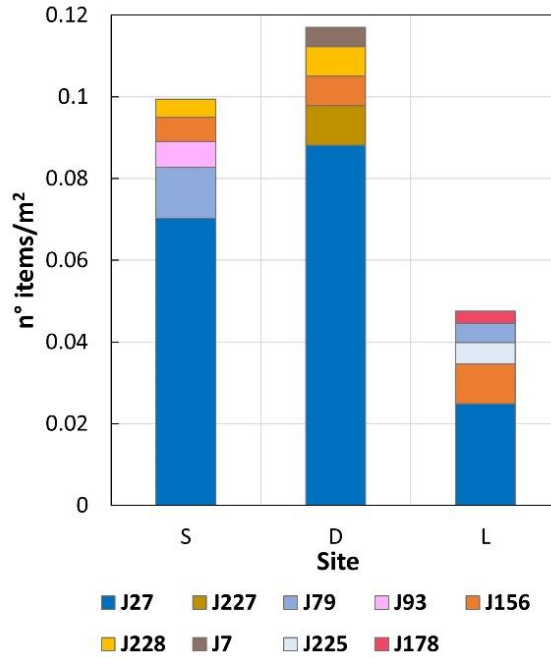
Figure 5.6 – Five categories of litter most frequent in each site of Mondello.

The categories of litter most frequently sampled in all sites of Mondello is the J27 "tobacco products with filters - cigarette butts with filters". A common item found out with high frequency in all sites is the J156 "paper fragments".
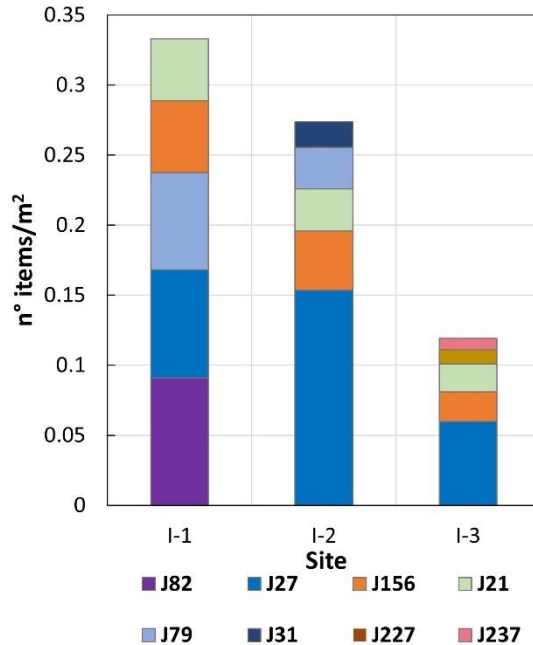
Figure 5.7 – Five categories of litter most frequent in each site of Isola delle Femmine.

The site I-1 at Isola delle Femmine beach is characterised by a high presence of the J79 "fragments of Non-Foamed Plastic 2.5cm $\geq$ $\leq$ 50cm". Moreover, all sites are characterised by a high presence of the J156 (Paper fragments").

The materials and the J-name corresponding to the five categories most frequently in the two study areas are reported in Table 5.1.

Focusing on the plastic category, the five most common items were figure out. The results are reported in Figure 5.8 and Figure 5.9 with the relatives J-code and J-names in Table 5.1.
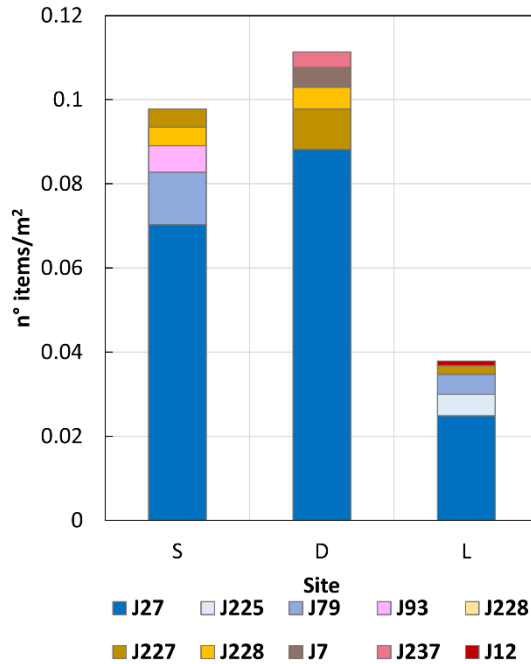
Figure 5.8 – Five plastic materials most frequent in each site of Mondello.

The plastic item most frequent in the all sites of Mondello is the J27 "tobacco products with filters - cigarette butts with filters". The sites S and L, present high quantity of J79 "fragments of non-foamed plastic 2.5 cm $\geq$ $\leq$ 50 cm" instead the J12 "plastic non-beach use related body care and cosmetic bottles and containers" is present in high quantity only in the D sites.
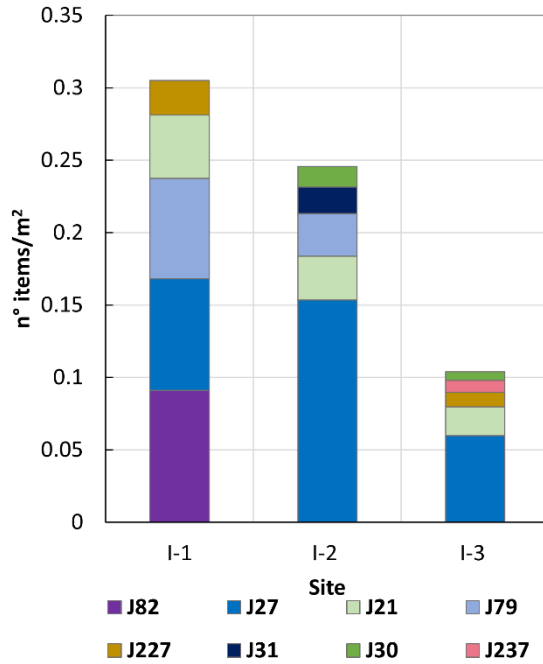
Figure 5.9 – Five plastic materials most frequent in each site of Isola delle Femmine.

All sampling sites of Isola delle Femmine present high quantities of J27 "tobacco products with filters - cigarette butts with filters". In the I-1 sites there is a high presence of J82 "fragments of foamed polystyrene 2.5 cm $\geq$ $\leq$ 50 cm".

Table 5.1 – Description (in terms of Material, J-code and J-name) of the most frequent materials and plastic items.

Materials	J-code	J-name
P.A.	J7	Plastic drink bottles ≤ 0.5 l
P.A.	J12	Plastic non-beach use related body care and cosmetic bottles and containers
P.A.	J21	Plastic caps/lids drinks
P.A.	J27	Tobacco products with filters (cigarette butts with filters)
P.A.	J30	Plastic crisps packets/sweets wrappers
P.A.	J31	Plastic lolly & ice-cream sticks
P.A.	J79	Fragments Of Non-Foamed Plastic 2.5 cm ≥ ≤ 50 cm
P.A.	J82	Fragments of foamed polystyrene 2.5 cm ≥ ≤ 50 cm
P.A.	J93	Plastic cable ties
Paper/Cardboard	J156	Paper fragments
Metal	J178	Metal bottle caps, lids & pull tabs from cans
P.A.	J225	Plastic food containers made of hard non-foamed plastic
P.A.	J227	Cups and lids of hard plastic
P.A.	J228	Plastic cutlery
P.A.	J237	Plastic wet wipes

5.1.2 Laboratory Experiments

Analysis of the spectra and role played by the illumination geometry

As anticipated, the spectra of litter were acquired considering two different illumination conditions. Figure 5.10 reports the spectra acquired within the white box (diffuse illumination) related to the samples in Figure 4.3.

λ **(nm)**
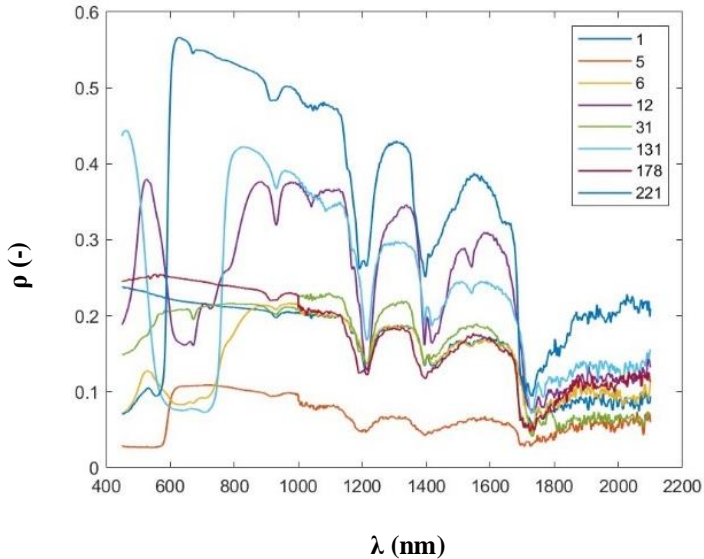
Figure 5.10 – Spectral signatures of some harvested marine debris, reported in Figure 4.3, acquired within the white box.

Noticeably several spectra quietly differ in the visible region, instead have similar behaviour in some wavelengths such as 930, 1200, 1400, and 1700 nm.

The comparison between the average of the spectra acquired inside the white and the black box, $\rho\mu_{s,white}$ and $\rho\mu_{s,black}$ reveals a coefficient of determination R^2 equal to 0.43 (Figure 5.11).
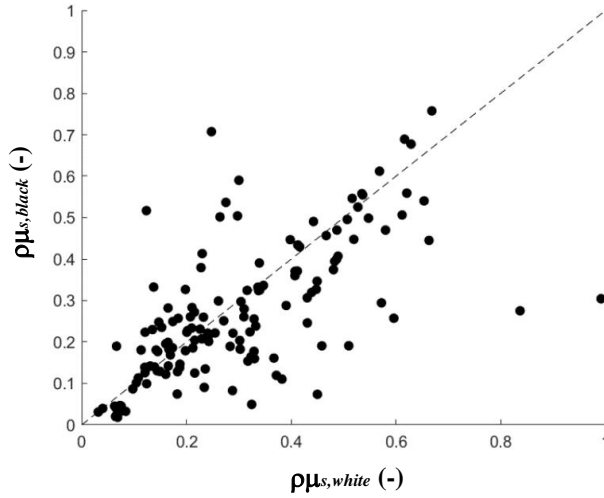
Figure 5.11 – Comparison between the mean of spectral signatures of all samples acquired inside the white box (x-axis) and the black box (y-axis).

About 70% of the data is within a buffer area of ± 0.1 (10% of the reflectance) from the 1:1 line (Figure 5.12) and exhibits an R^2 equal to 0.92.
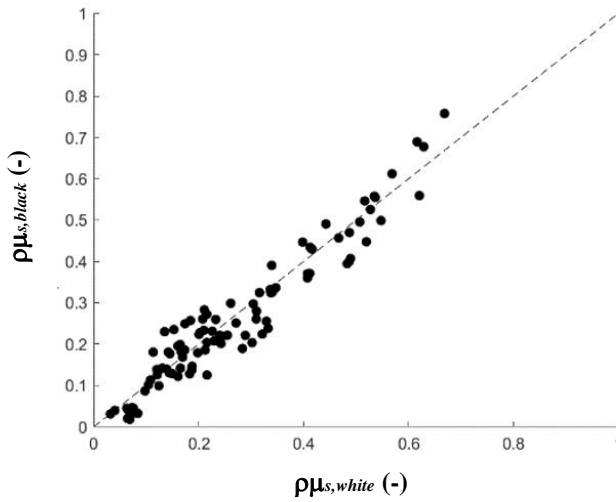
Figure 5.12 – Mean of spectral signatures of samples within the buffer aera. In x-axis are represented the measures acquired inside the white box and in y-axis the ones acquired in the black one.

The remaining 30% of the samples are those for which the illumination geometry played an important role (Figure 5.13). In particular, for some of

the samples the higher reflectance values were measured in the black box and *vice versa*.
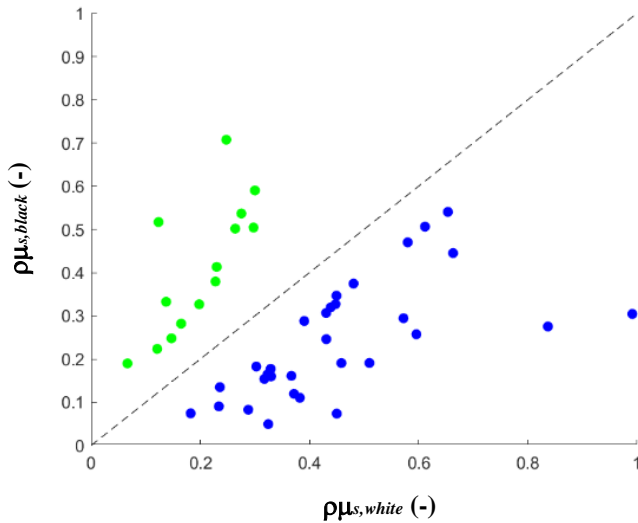
Figure 5.13 – Identification of the samples outside the buffer area. In the x-axis are reported the measures within the white box instead in the y-axis the measures within the black box. The green dots represent the samples with higher reflectance when measured in the black box. The blue dots are the samples with higher reflectance when measured in the white box.

The samples clearly influenced by the different illumination conditions were further investigated. As an example, the spectra of the sample n. 75 acquired in the white box are shifted upwards compared to the one collected in the black box. However, both the spectra are characterised by similar peaks of reflectance (Figure 5.14).

Instead, Figure 5.15 shows the spectral signatures of the sample n. 12 which was inside the buffer area of the 45° line of the scatterplot of Figure 5.12 (less influence of the illumination conditions).
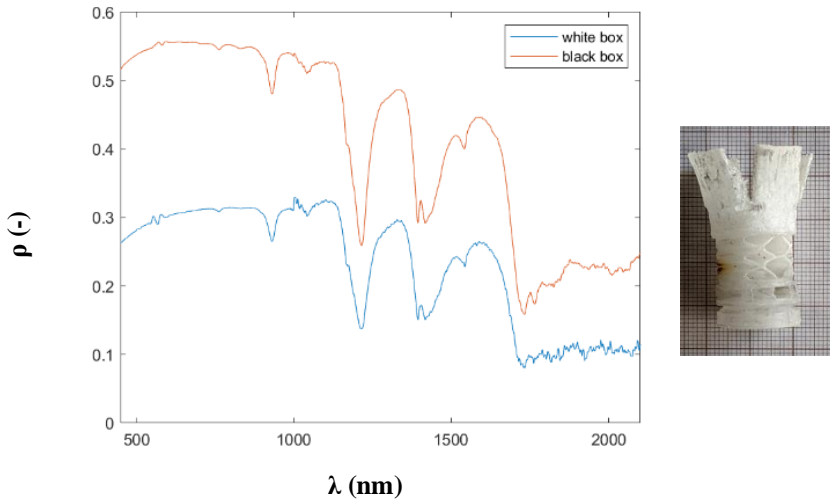
Figure 5.14 – Spectral signatures of the sample n. 75 acquired in white and black box.
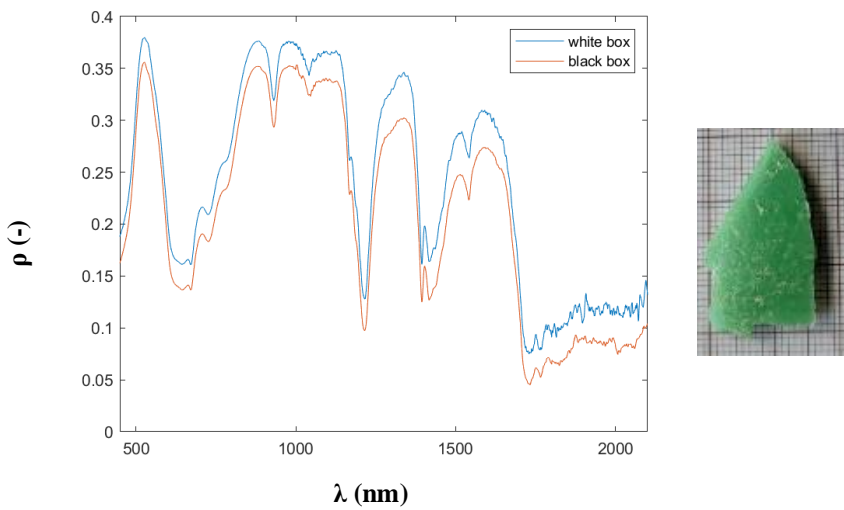
Figure 5.15 – Spectral signatures of the samples n. 12 acquired in white and black box.

Litter on sand detectability using SAM and role played by the illumination geometry

The values of the SAM index calculated considering the whole spectral signatures (whole wavelength range) are reported in Figure 5.16.

Samples

(a)   *(b)*
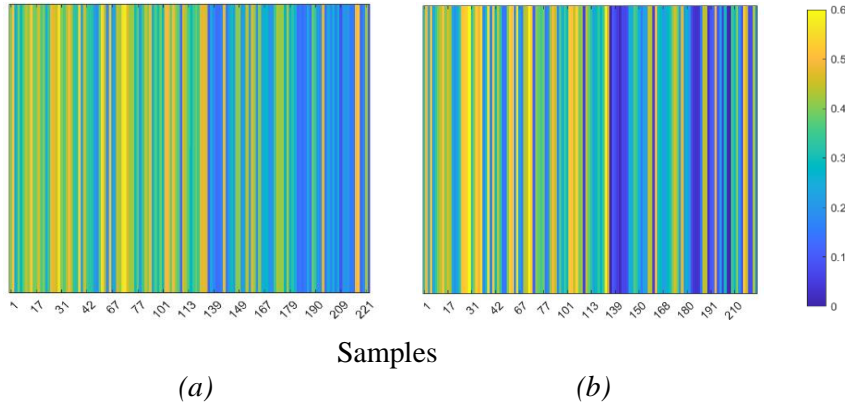
Figure 5.16 – SAM index values (evaluated between samples *vs* sand) using all wavelengths of the spectral signatures acquired inside the white *(a)* and the black *(b)* box. In the x-axis are reported the samples. The vertical lines represent the SAM values for the different samples.

The SAM values of the samples collected both in the white and black box (in different illumination conditions) are quite similar. Some samples (18% and 15% of the total, for the white and black box cases respectively) are scarcely detectable from the sand as they exhibit SAM values lower than 0.2; whereas other samples (21% and 37% of the total, for the white and black box cases respectively) are moderately-highly distinguishable from sand as characterised by the highest SAM values (~> 0.5). To determine the role played by the two illumination geometries the SAM values between sand and samples for the white and black box were compared in a scatterplot (Figure 5.17).
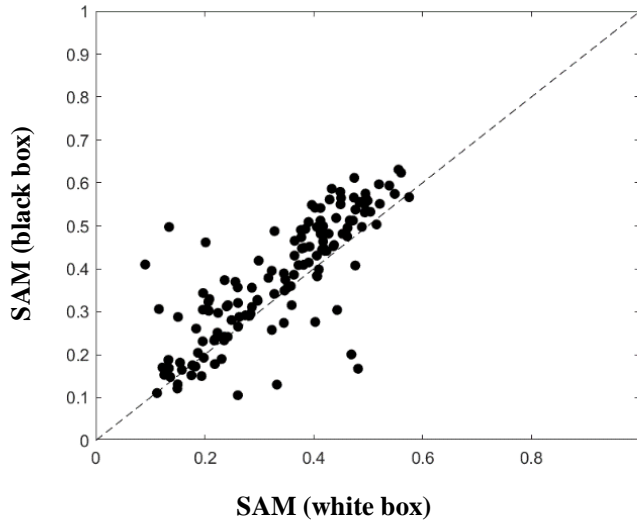
Figure 5.17 – Scatterplot reporting the SAM index values (evaluated between samples *vs* sand) collected inside the white box (x-axis) and the black box (y-axis).

Figure 5.17 suggests that SAM values are in general slightly higher if signatures are acquired inside the black box. Some samples are represented by points far from the 1:1 line whereas around 20% of them exhibit very similar SAM values.

Best spectral bands suitable for litter detection on sandy beaches

The SAM matrix computed using a moving window of 21 nm (Figure 5.18) reveals that bands more suitable for beach litter detection are similar for the white and the black box cases.
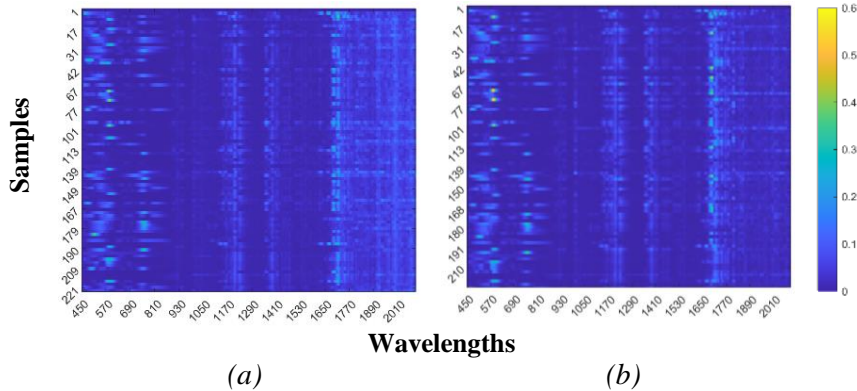
Figure 5.18 – SAM index values (samples *vs* sand) evaluated considering a moving window of 21 nm. The analyses were performed considering the data acquired within the white *(a)* and the black *(b)* box. In the x-axis are reported the wavelengths and in the y-axis the samples.

Although some litter samples need specific bands for their detection, for the majority of the samples the most suitable bands for the detection (i.e. those with higher values of SAM) are positioned: *i*) in the visible (450-630 nm) range; *ii*) around the red-edge (700-770 nm); and, in some infrared bands around 1230 nm, 1400 nm 1720nm. It is to point out that the bands around 1400 nm could not be used operatively as in overlap with one of the two main atmosphere water absorption bands (1350-1450 nm). On the opposite, different wavelengths are not useful for detection, like as the ones between 800-1000 nm, 1250-1300 nm and around 1450-1650 nm. By sorting the samples for decreasing global SAM (i.e. the SAM computed using the whole spectral signature) it is noticed that the samples which have less probability to be detected on sand are those characterised by low or null SAM in the visible and red-edge bands.

Assessment of the polymers composition of plastic litter through analysis of the spectral signature

The evaluation of SAM values between spectra of the virgin polymers and those of the samples did not reveal a clear identification of the composition of the plastic debris collected.

Detectability performance of different virgin polymers from sand

The SAM values between the spectra of the virgin plastic polymers (EVA, HPDE, PET, PP, and PS) and that of the sand (Figure 5.19) revealed that EVA polymer (used to make beach shoes especially) is the one exhibiting the higher SAM values (higher detectability) followed by HDPE, PP, PS, and PET. The same behaviour is found using spectra collected within the white and black boxes.
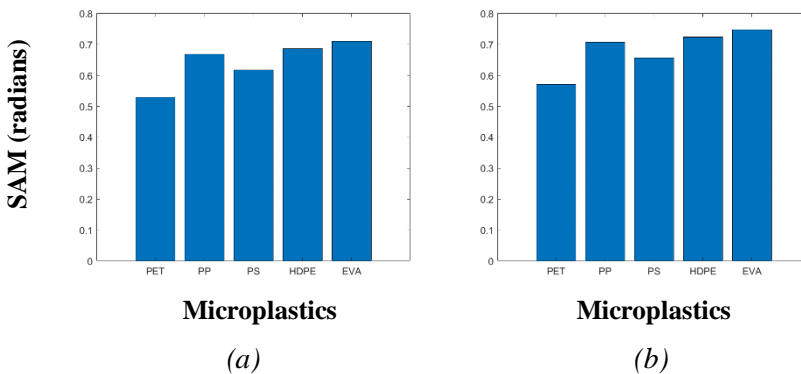
Figure 5.19 – SAM values evaluated between the spectral signatures of microplastics and the sand. Measurement realised in the white *(a)* and in the black *(b)* box.

Best currently operating satellite sensors to detect litter on sandy beaches

The SAM index between spectra of the samples and that of the sand computed for the bands of the currently operating high spatial resolution

satellite sensors (Figure 5.20 and Table 5.2) pointed out that the sensors providing the higher SAM values is the Worldview-3.
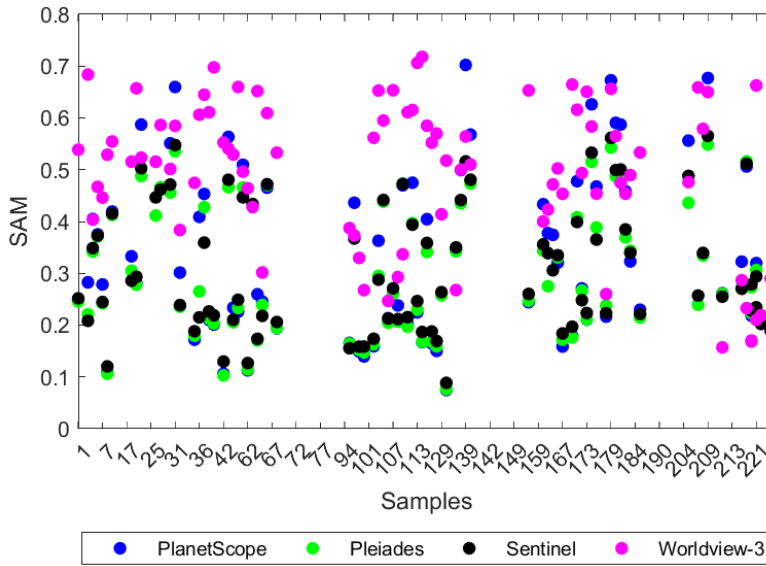
Figure 5.20 – SAM values between the spectral signatures of sand and samples considering the wavelengths at the canter bands of the various sensors take into account. White box.

Mode and median values between all sand-sample pairs are reported for each sensor in Table 5.2.

Table 5.2 – Mode and Median between all sand-samples pairs for each sensor.

	PlanetScope	Pleiades	Sentinel-2	Worldview-3
Mode	0.026	0.010	0.024	0.119
Median	0.262	0.246	0.250	0.475

The number, E, of the sand/sample combinations exceeded the i-th p value is reported in Table 5.3. The values E higher than the 30% of the total sand/sample combinations are in bold highlighted.

Table 5.3 – E values (in %) for the different percentiles (white box experiment).

Percentile	PlanetScope	Pleiades	Sentinel-2	Worldview-3
50	**44**	40	39	**77**
75	20	13	13	**53**
90	10	1	2	27
98	3	1	1	4
99	1	1	1	1

These results are reported in terms of percentage of distinct combinations with the percentile in Figure 5.21.
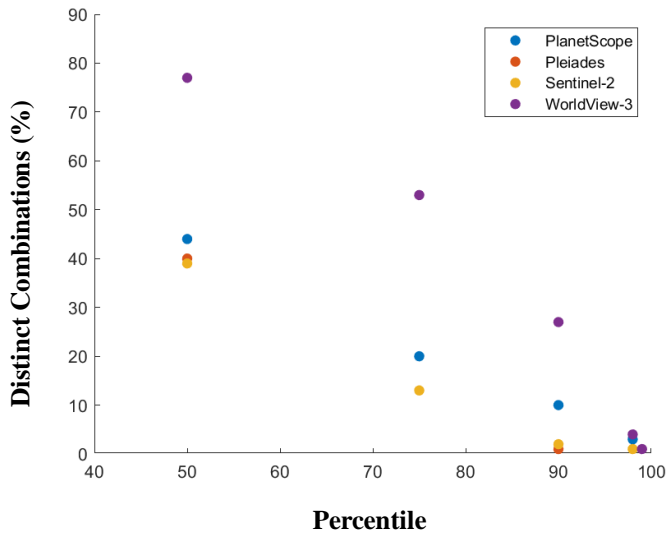
Figure 5.21 – Distinct combinations (%) for each percentile - White box.

From this analysis is evident that PlanetScope allows to identify for the $p = 50$, the 44% of the samples. Instead, with Worldview-3 it is possible to potentially individuate 77% and 53% of the samples, for $p=50$ and $p=75$ respectively.

The same analysis was done considering the black box (Table 5.4 and Figure 5.22).

Table 5.4 – *E* values (in %) for the different percentiles (black box experiment).

Percentile	PlanetScope	Pleiades	Sentinel-2	Worldview-3
50	**45**	37	37	**81**
75	19	11	12	**58**
90	7	1	1	32
98	1	1	0	6
99	1	0	0	3

Also using as input spectra collected in the black box PlanetScope (for p=50 only) and Worldview-3 (for *p*=50 and *p*=75) are to be considered the only sensors suitable for the detection of litter on sandy beaches.
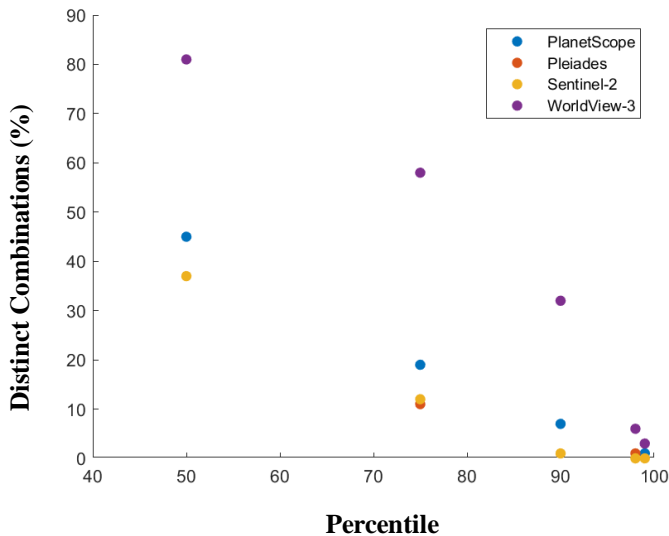
Figure 5.22 – Distinct combinations (%) for each percentile - Black box.

Once clearly evidenced that the Worldview-3 is the best sensor for the collected samples detection, a further analysis regarded which of the spectral bands of this sensor allow achieving the best detectability. This analysis was carried out for all the percentiles previously mentioned and considering the centre bands of all Worldview-3 bands. The values *E* higher than the 30% of the total sand/sample combinations, for the different percentiles and

centre bands, are reported in Table 5.5 (considering both white and black box).

Table 5.5 – *E* values for the different percentiles and the Worldview-3 bands - White and black box.

Wavelengths (nm)	Percentile					
	50th		75th		90th	
	White box	Black box	White box	Black box	White box	Black box
425	99	61	-	-	-	-
480	41	58	-	-	-	-
545	100	99	98	96	-	51
1570	78	89	65	70	-	51
1660		44	-	-	-	-
1730	48	63	-	-	-	-
2165	53	-	-	-	-	-
2205	60	-	-	-	-	-
2260	98	86	69	54	-	-
2330	100	-	82	-	62	-

5.2 Marine litter

5.2.1   Hydrodynamics modelling outcomes

In this section, results of the hydrodynamic models applied to the study areas are shown with a particular focus on the density and the beaching maps. Furthermore, results regarding the comparison done for the Sicilian area employing the *in-situ* data collected during the ARPA-CNR monitoring campaign is presented.

5.2.1.1 TrackMPD model results

5.2.1.1.1   TrackMPD model application: Mediterranean basin

South Tyrrhenian Sea

The model setup and the calculation time are summarised in Table 5.6.

Table 5.6 – Setup of the simulation in the South Tyrrhenian Sea.

Domain area	10.8°W, 16°E; 35.8°S, 43°N
CMS data	MEDSEA_ANALYSISFORECAST_PHY_006_013
Particles number	1105
Spatial resolution	4- 5 km c.a.
Temporal resolution	1 Days
Simulation period	1st November 2021 - 31st May 2022
Discharging time	1st November 2021
Source	Beaches sampled in the *in-situ* campaigns
Calculation time	7 h

As output of the Tyrrhenian Sea area is reported the position of macroplastics all over the simulated period (Figure 5.23). From it is evident that several particles remain close to the Sicily as trapped by an eddy structure.
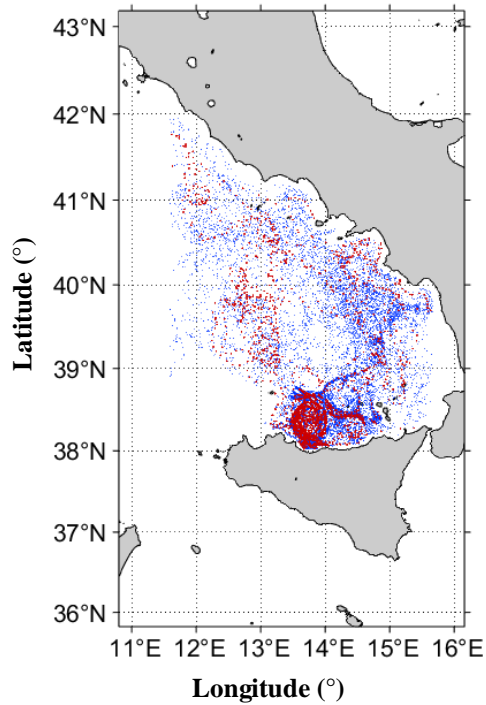
Figure 5.23 – Particles' map for the simulated period in the Tyrrhenian Sea. Red dots represent the particles released from Mondello, instead the blue dots the ones from Isola delle Femmine.

Density maps have been computed for each day of the simulation period. The most significant ones are shown in Figure 5.24. The trapping by the eddy structure cause the formation of particles accumulation areas.
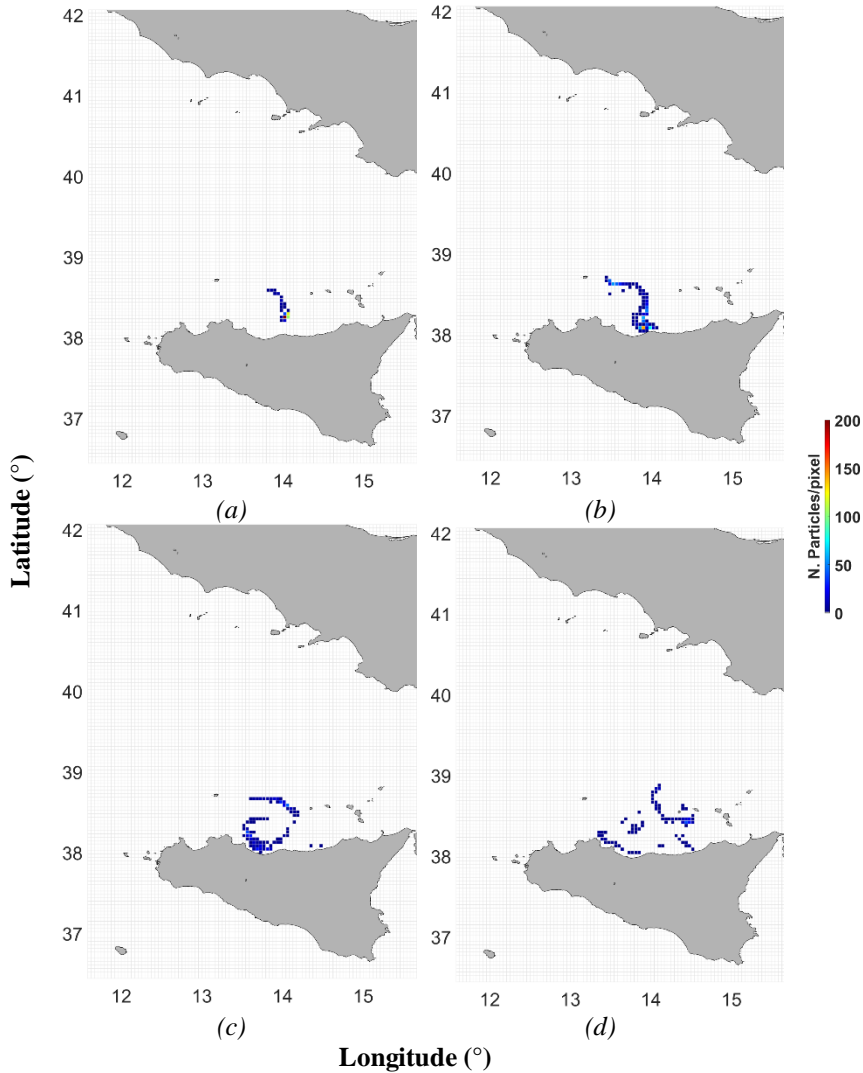
Figure 5.24 – TrackMPD, Tyrrhenian Sea application. Density maps for four representative days (year 2018): 7th November 2021 *(a)*, 19th November 2021 *(b)*, 23rd November 2021 *(c)*, 01st December 2021 *(d)*.

Strait of Sicily

The TrackMPD model was applied in the Strait of Sicily by simulating the particles' releasing in two periods: from 1st May - 30th September 2018

and between 1st May - 30th September 2019 (Application – 1, releasing from the coast).

The model setup and the calculation time are summarised in Table 5.7.

Table 5.7 – Setup of the simulation in the Strait of Sicily.

Domain area	11.5° W, 16.5° E; 35° S, 37.8°N
CMS data	MEDSEA_ANALYSISFORECAST_PHY_006_013
Particles number	144
Spatial resolution	4- 5 km c.a.
Temporal resolution	1 Days
Simulation period	1st May - 30th September 2018 1st May - 30th September 2019
Discharging time	Daily
Source	Main rivers (Ocean Cleanup source)
Calculation time	1 Day

As the final focus of the application in the Strait of Sicily was the comparison with *in-situ* measurements performed in the same area, only the density maps were analysed. In Figure 5.25 the simulation domain is reported.
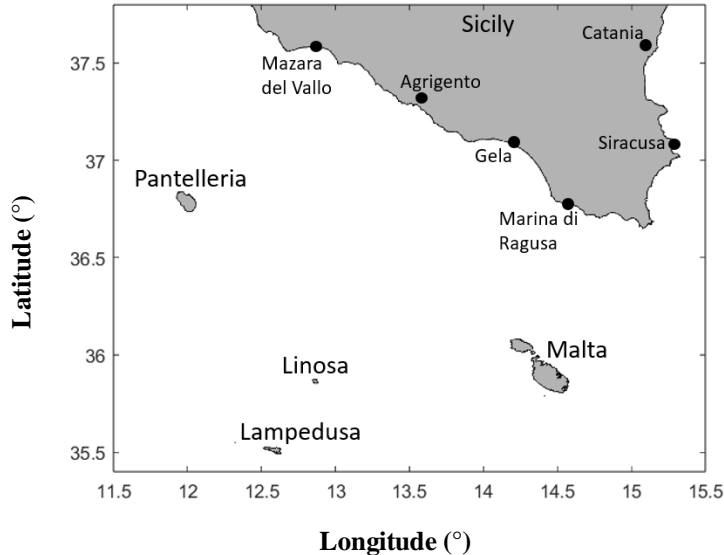
Figure 5.25 – Domain of the simulations done in the Strait of Sicily.

The accumulation maps concerning some of the most representative days for the simulation of 2018 are reported in Figure 5.26.
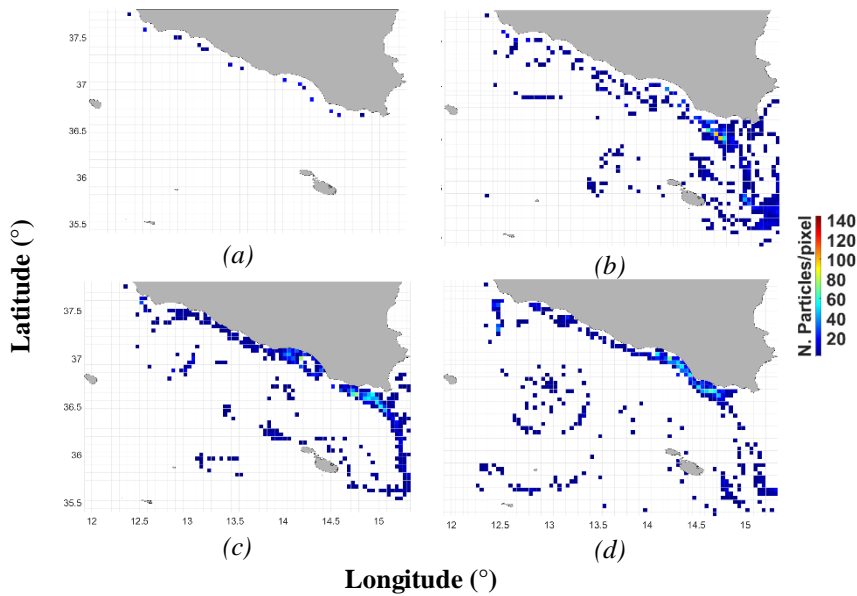
Figure 5.26 – TrackMPD, year 2018. Density maps for four representative days (year 2018): 01st May *(a)*, 26th May *(b)*, 03rd June *(c)*, 12th September *(d)*.

From Figure 5.26 is evident how the particles are accumulated in the central part of the domain in the middle period of the simulation. Also, the trapping of particles by the ABV eddy is observable. Moreover, it is noticeable the role played by the Atlantic Ionian Stream which move initially the most part of the particles in the north-west to south-east direction (parallel to the coast); in May an accumulation in the eastern Sicily-Malta channel is observable; in June and September the particles, drifted by the AIS, finally are moved out from the domain.

Concerning the simulations of 2019, the accumulation maps regarding some of the most representative days are reported in Figure 5.27.
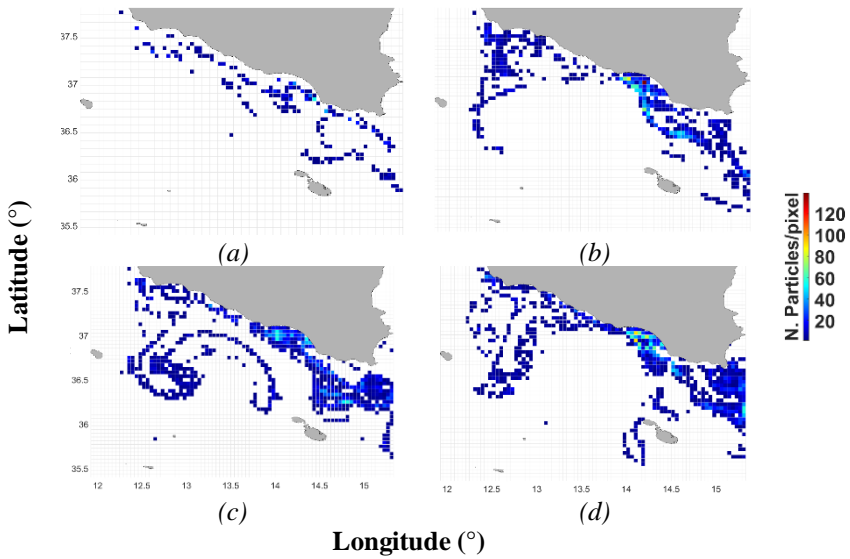
Figure 5.27 – TrackMPD, year 2019. Density maps for four representative days: 13th May *(a)*, 31th August *(b)*, 16th September *(c)*, 21th September *(d)*.

Similar considerations of the 2018 case study can be done analysing the density maps computed for the 2019 period (Figure 5.27). From May to September, two main accumulation areas are found: the first in the north-western part (Trapani province area, close to Mazara del Vallo); the second one in the eastern area (Gela-Ragusa-Siracusa areas). Moreover, from Figure 5.27, panel *c*, it is evident the formation of a vortex that disperses the particles few days later (panel *d*).

5.2.1.1.2 TrackMPD model application: Liberia/Gulf of Guinea

The model setup and the calculation time are summarised in Table 5.8.

Table 5.8 – Setup of the simulation in the Strait of Sicily.

Domain area	17°W, 12°E; -5°S, 7° N
CMS data	GLOBAL_ANALYSISFORECAST_PHY_001_024
Particles number	25
Spatial resolution	10 km c.a.
Temporal resolution	1 Days
Simulation period	1st January - 31st December 2021
Discharging time	Daily
Source	Main rivers (Liberian Hydrological service)
Calculation time	6 Day

The results regard the area represented with the dashed black box in Figure 3.10 because it is where the particles have mostly accumulated and beached. This area is reported in Figure 5.28 also indicating the name of the Regions and of the Island impacted by the plastic particles.
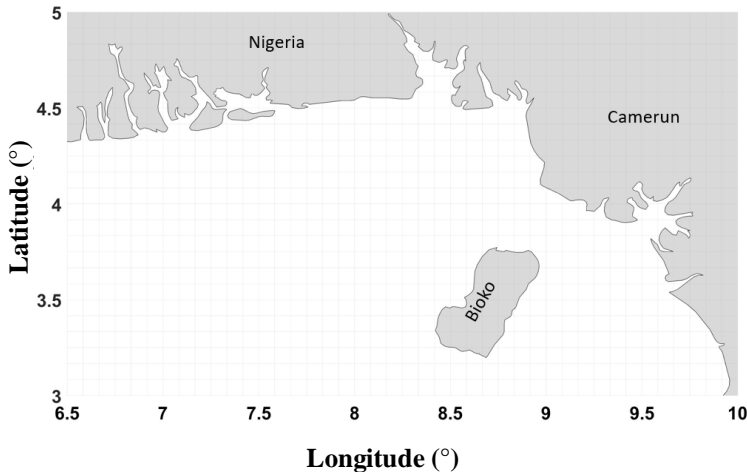
Figure 5.28 – Regions interested by plastic particles accumulation and beaching.

The density maps were realised for all the simulation period with the main goal to quantify the presence of macroplastics in the study area.

Figure 5.29 reports maps of the most significant days in which is possible to recognise some particles' displacement patterns and the formation of accumulation areas.
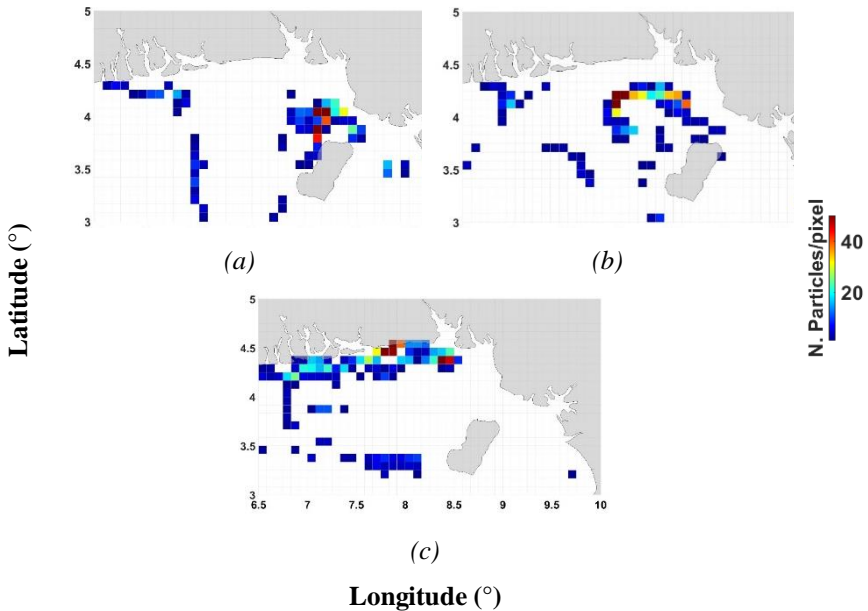
Figure 5.29 – TrackMPD. Application in the Liberia/Gulf of Guinea area, year 2021. Density maps for three representative days: 30th   July *(a)*, 03nd August *(b)*, 13th August *(c)*.

Density maps show an accumulation of particles in the Guinea Gulf probably caused by the coastal geomorphology and the sea surface current patterns. The formation of a buildup area is evident as early as a few days after the start of the simulation. Furthermore, the accumulation area increases with the simulation time.

Figure 5.30 shows the most significant beaching maps.
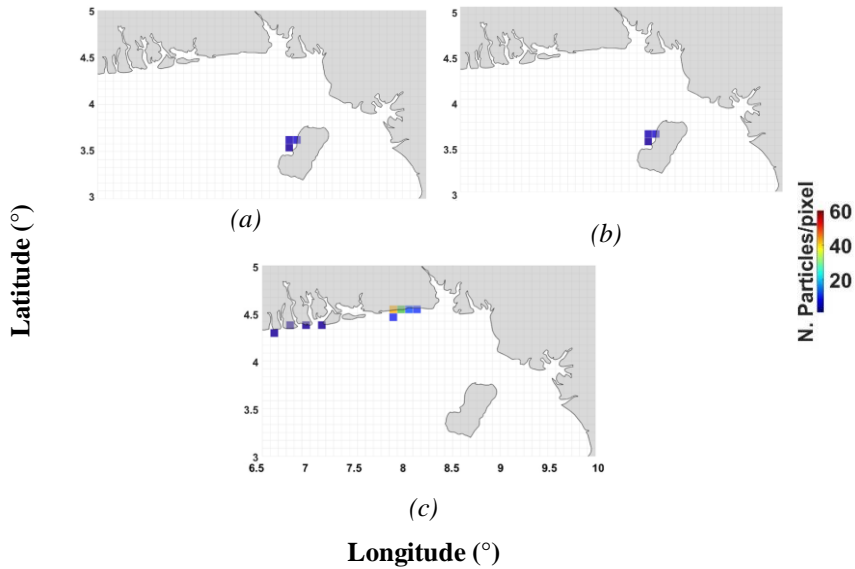
Figure 5.30 – TrackMPD. Application in the Liberia/Gulf of Guinea area, year 2021. Beaching maps for three representative days: 30th July *(a)*, 03rd August *(b)*, 13th August *(c)*.

Figure 5.30 confirms that differ particles impact the coastal area; indeed, a moderate number of particles are found in the west coast of Bioko Island and at the coast of Nigeria region. Noticeably that beaching and density maps highlight that the plastic released from the Liberian rivers involved the all-domain area (boundless problem).

5.2.1.2   STM model results

This section summarises the results (in terms of density maps) concerning the STM model run for the coastal and grid release applications.

5.2.1.2.1   STM model application: Strait of Sicily

The model setup and the calculation time are summarised in Table 5.9.

Table 5.9 – Setup of the simulation in the Strait of Sicily.

Domain area	11.5° W, 16.5° E; 35° S, 37.8°N
CMS data	MEDSEA_ANALYSISFORECAST_PHY_006_013
Particles number	336
Spatial resolution	4-5 km c.a.
Temporal resolution	1 Days
Simulation period	1st January - 31st September 2018 1st May - 30th September 2019
Discharging time	Daily
Source	Centre of the pixel
Calculation time	10 h

The density maps relative to STM – coastal release application (144 points discharged from the main Sicilian rivers), referred to 2018 and 2019 are reported in Figure 5.31 and Figure 5.32 respectively.
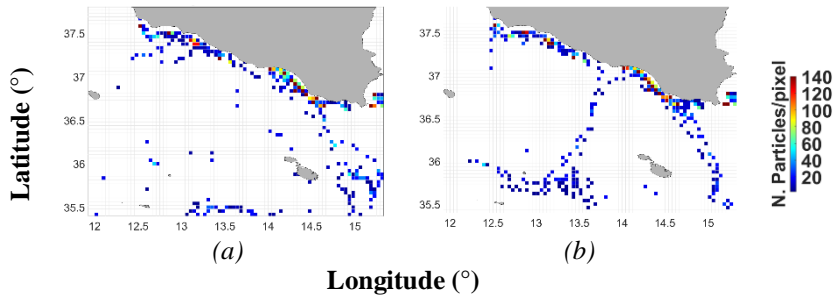
Figure 5.31 – STM – coastal release application, year 2018. Density maps for two representative days: 21th August *(a)*, 12th September *(b)*.
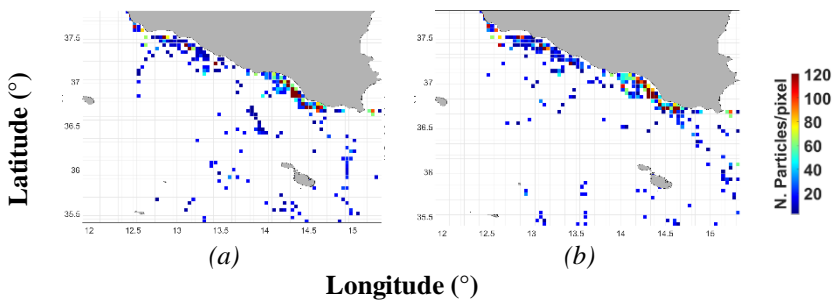
Figure 5.32 – STM – coastal release application, year 2019. Density maps for two representative days: 31th July *(a)*, 22th August *(b)*.

The figures highlight the general tendency of the particles to be accumulated along the south coast of Sicily. In the south-eastern the particles follow the AIS jet; noticeably in September 2018 (Figure 5.31, panel *b*) the presence of an accumulation patch in the north-south direction.

Regarding the STM - grid release application (336 points discharged on a regular grid basis) Figure 5.33 and Figure 5.34 show the density maps for the 2018 and 2019 periods respectively.
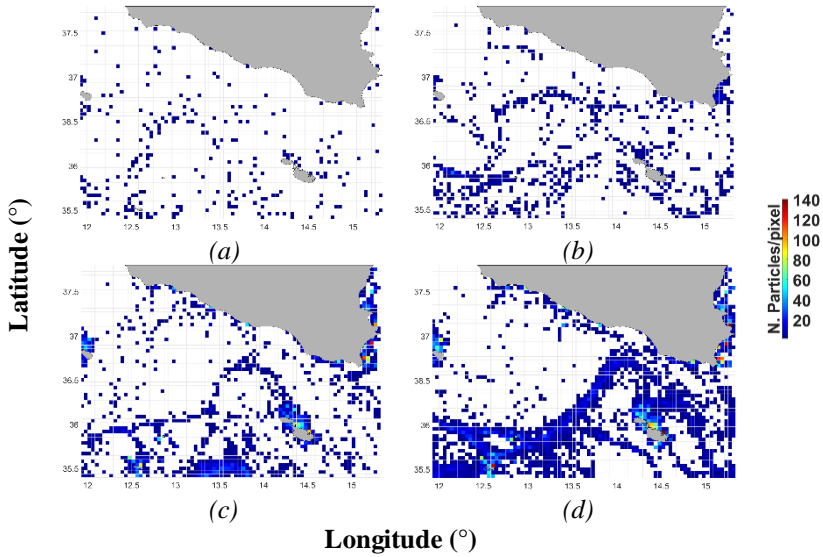
Figure 5.33 – STM – grid release application, year 2018. Density maps for four representative days: 12th May *(a)*, 23th May *(b)*, 23th August *(c)*, 22nd September *(d)*.
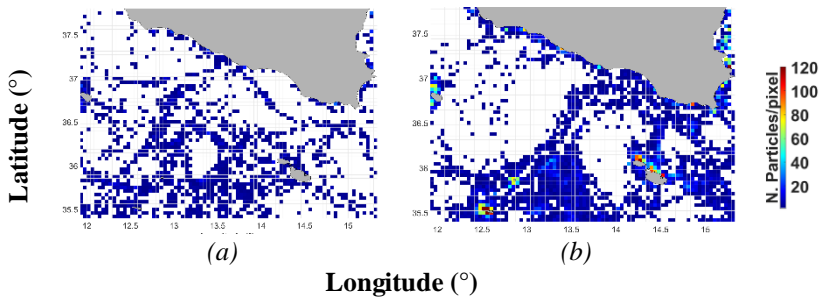
Figure 5.34 – STM - grid release application, year 2019. Density maps for two representative days: 14th June *(a)*, 25th September *(b)*.

It is evident from Figure 5.33 the formation of a stretched accumulation area from north-east to south-west (in the direction of the Tunisia). Very strong accumulations are found at coast especially in the Malta islands and in the east and south-east Sicilian coasts. Similar consideration can be done for the 2019 (Figure 5.34).

5.2.1.3   Comparison between the hydrodynamic models and sampling: Strait of Sicily

The comparison between the number of simulated particles within the *in-situ* transect (Figure 4.6) and the number of microplastics collected during the *in-situ* campaigns was done considering a total of 105 discharging scenarios (please refer to Section 4.2.2.1.1). The results concerning this analysis are reported for two representative days: 01st May 2018, 2019 (following named as "Scenario 1") and 31st July 2018, 2019 (following named as "Scenario 92").

The Scenario 1 is characterised by a daily discharge from 01st May to 14th August 2018 and 2019; instead, the Scenario 92 by a daily discharge from 31st July to 14th August 2018 and 2019.

Figure 5.35 and Figure 5.36 report the particles' position resulting at the sampling date under two different scenarios for the TrackMPD for 2018 and 2019 respectively. The buffers around the *in-situ* transect are also over imposed.
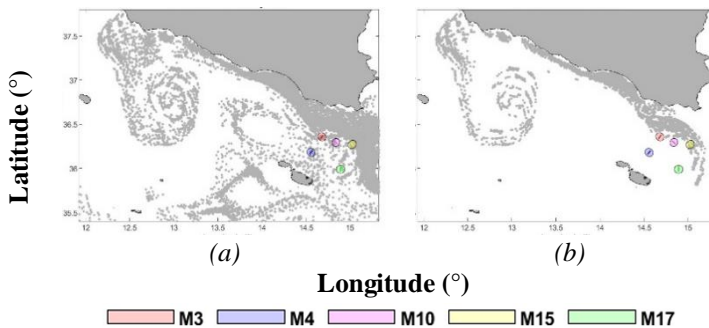
Figure 5.35 – TrackMPD, year 2018. Particles' maps for different scenarios. – Scenario 1: release 01st May– end of simulation 14th August *(a)*. Scenario 92: release 31st July– end of simulation 14th August *(b)*.
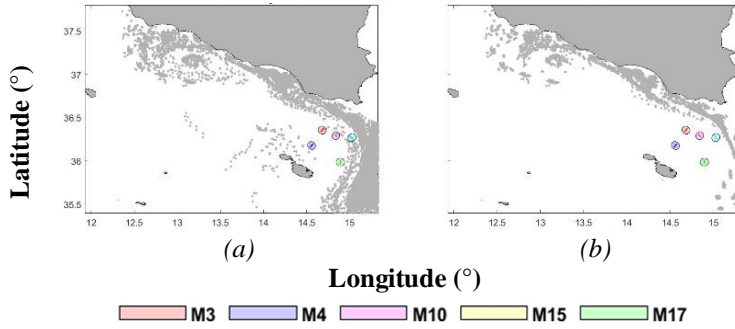
Figure 5.36 – TrackMPD, year 2019. Particles' maps for different scenarios. – Scenario 1: release 01st May – end of simulation 14th August *(a)*. Scenario 92: release 31st July – end of simulation 14th August *(b)*.

As expected, the particles' number decreases as the scenario's number increases. Indeed, the start of the releasing increase by a day from scenario 1 to the last one. Moreover, comparing Figure 5.35 with Figure 5.36, it is evident that patterns of the particles position are for the same day totally different as the start of the deployment change. It is also noticed that particles deployed in the early August 2019 do not fall within the buffers.

Figure 5.37 and Figure 5.38 report the particles' position for two different scenarios using the STM model (coastal release application).
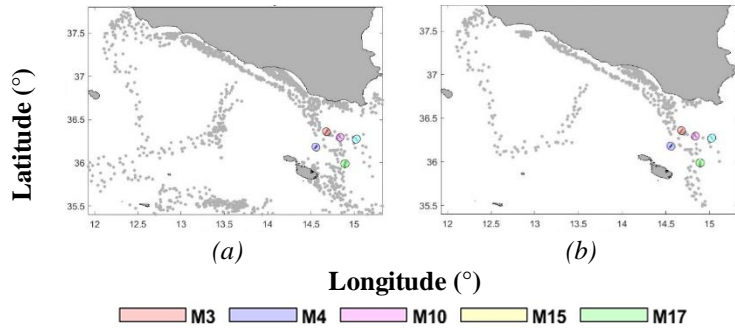
Figure 5.37 – STM - coastal release application, year 2018. Particles' maps for different scenarios. – Scenario 1, release from 01st May *(a)*. Scenario 92, release from 31st July *(b)*.
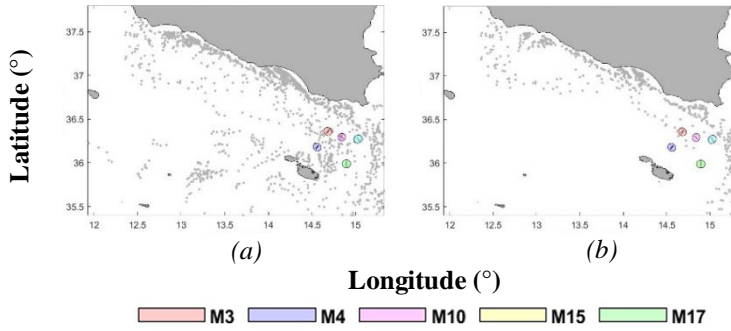
Figure 5.38 – STM - coastal release application, year 2019. Particles' maps for different scenarios. – Scenario 1, release from 01st May *(a)*. Scenario 92, release from 31st July *(b)*.

With the STM model the particles' number within the buffer area is greater than those found using TrackMPD.

The comparison between the models was realised considering the simulations performed using TrackMPD and STM (coastal release application). The sum of the simulated particles within each buffer area was calculated, for each scenario. The regression between these latter and the number of particles found during the *in-situ* campaigns (Table 4.3) was estimated through the R^2 (evaluated considering jointly 2018 and 2019 data). Figure 5.39 reports the R^2 evaluated for each scenario for TrackMPD and STM (coastal release application) respectively.

(a)   *(b)*
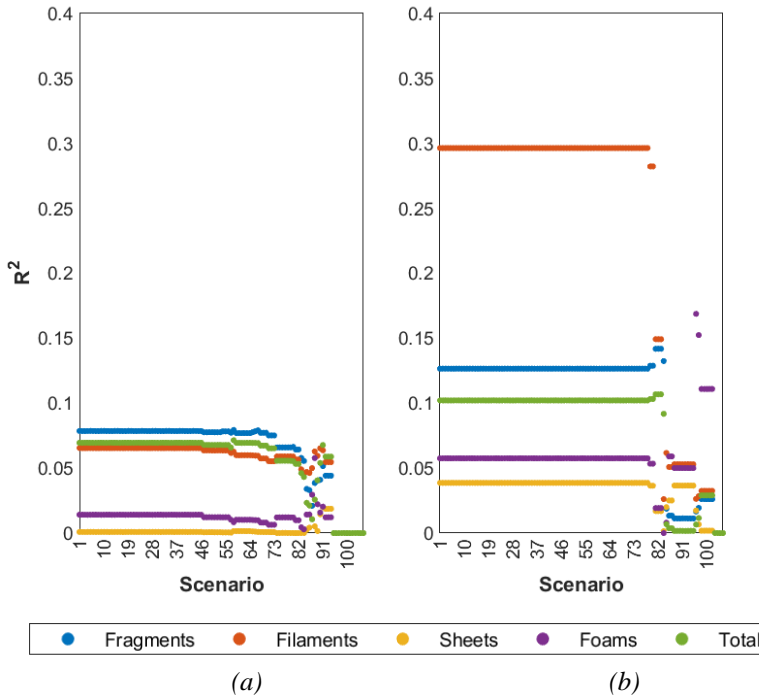
Figure 5.39 – R^2 coefficient evaluated between models' output and sampling for different scenarios. R^2 computed for TrackMPD / samples *(a)*; R^2 computed for STM – coastal release application / samples *(b)*.

The coefficient R^2 is almost constant all over the simulations, for both models. The higher R^2 values were found in the TrackMPD simulations for the filaments, whereas the lower was found for the sheets. The maximum values of R^2 for the different kind of plastic debris is reported in Table 5.10 and Table 5.11. The corresponding scenarios are also reported to determine if there is some scenario which fit better the *in-situ* observations.

Table 5.10 – Maximum R^2 coefficient, for relative scenarios, evaluated between TrackMPD model and sampling data (reported days refer to both years 2018 and 2019).

Samples	Fragments	Filaments	Sheets	Foams	Total
Scenario	58	1 - 46	91	88	58
Days	27/06	01/05-14/08	30/07	27/07	27/06
R^2	0.079	0.065	0.020	0.058	0.071

Table 5.11 – Maximum R^2 coefficient, for relative scenarios, evaluated between STM – coastal release application and sampling data (reported days refer to both years 2018 and 2019).

Samples	Fragments	Filaments	Sheets	Foams	Total
Scenario	81-83	1 - 78	1 - 78	96	81 - 83
Days	20/07-22/07	01/05-17/07	01/05-17/07	04/08	20/07-22/07
R^2	**0.142**	**0.296**	**0.039**	**0.169**	**0.107**

Noticeably that the unrepresentative R^2 values found for both STM and TrackMPD (coastal release application) highlight that the distribution of the debris found *in-situ* not match with the releasing mode of coastal release application.

The failure of the comparison procedure, considering as discharging points the coastal area, led to analyse the attitude of the sea surface current to accumulate particles. The amount of discharging points considered, led to apply the STM model (less complex than the TrackMPD). For this application, the particles' position maps were not reported because no significant information are deductible. Indeed, as expected, the deployment on the basis of a regular grid produced an increasing of the number of particles within the whole domain and also within the buffer areas. Furthermore, no significant patterns could be highlighted. The comparison with the *in-situ* data reveals some matching in terms of R^2 values (Figure 5.40) especially for filaments and foams, with maximum R^2 values found considering the start of releasing in July (2018 and 2019).
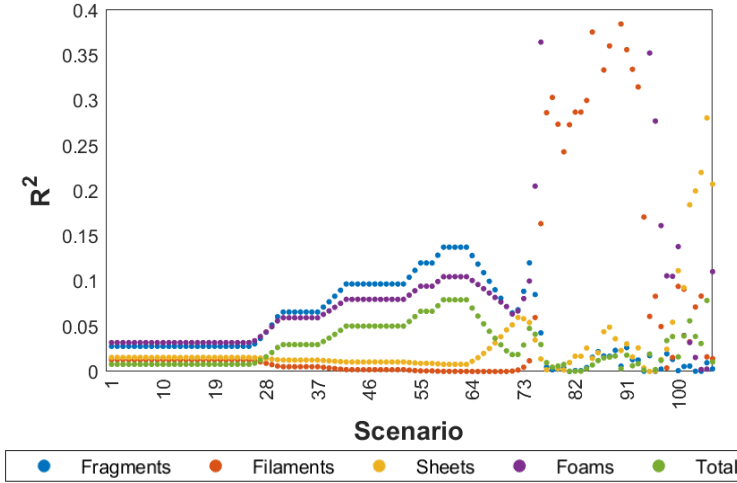
Figure 5.40 – R^2 coefficient evaluated between STM – grid release application models' output and sampling for different scenarios.

The variability of R^2 with the scenario is shown in Figure 5.40. The maximum R^2 values and the corresponding scenario are reported in Table 5.12.

Table 5.12 – Maximum R^2 coefficient, for relative scenarios, evaluated between STM – grid release application model and sampling data (reported days refer to both years 2018 and 2019).

Samples	Fragments	Filaments	Sheets	Foams	Total
Scenarios	59-63	86	105	87	59-63
Days	28/06-02/07	25/07	13/08	26/07	28/06-02/07
R^2	0.138	0.412	0.281	0.595	0.079

5.2.2 Results of floating target detection: an application on Aegean Sea surface

The workflow described in Section 4.2.2.2 allowed achieving the spectral signatures of the floating plastic target and the target fractional cover for all the pixels overlapping the target itself. By over imposing, for all different acquisition times, UAV data with the satellite images it was possible to identify a number N ($i = 1,2…N$) of pixels, probably occupied

by the plastic target (Figure 5.41). Note that the maximum number of pixels that could be involved is equal to 4.
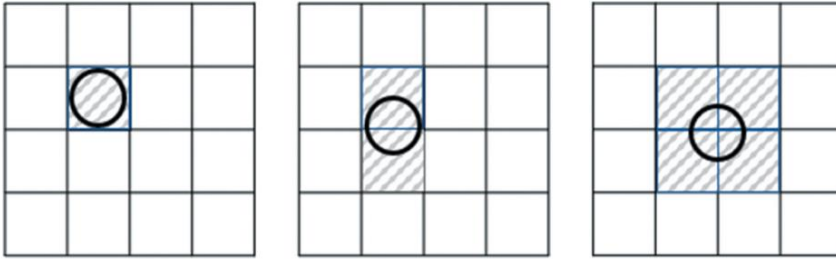
Figure 5.41 – Possible target's position in PRISMA's pixels.

Figure 5.42 shows the spectral signatures of the floating target by considering the B_{VNIR}, B_{SWIR} and B_{PCA} band-sets.

(a)

(b)

(c)
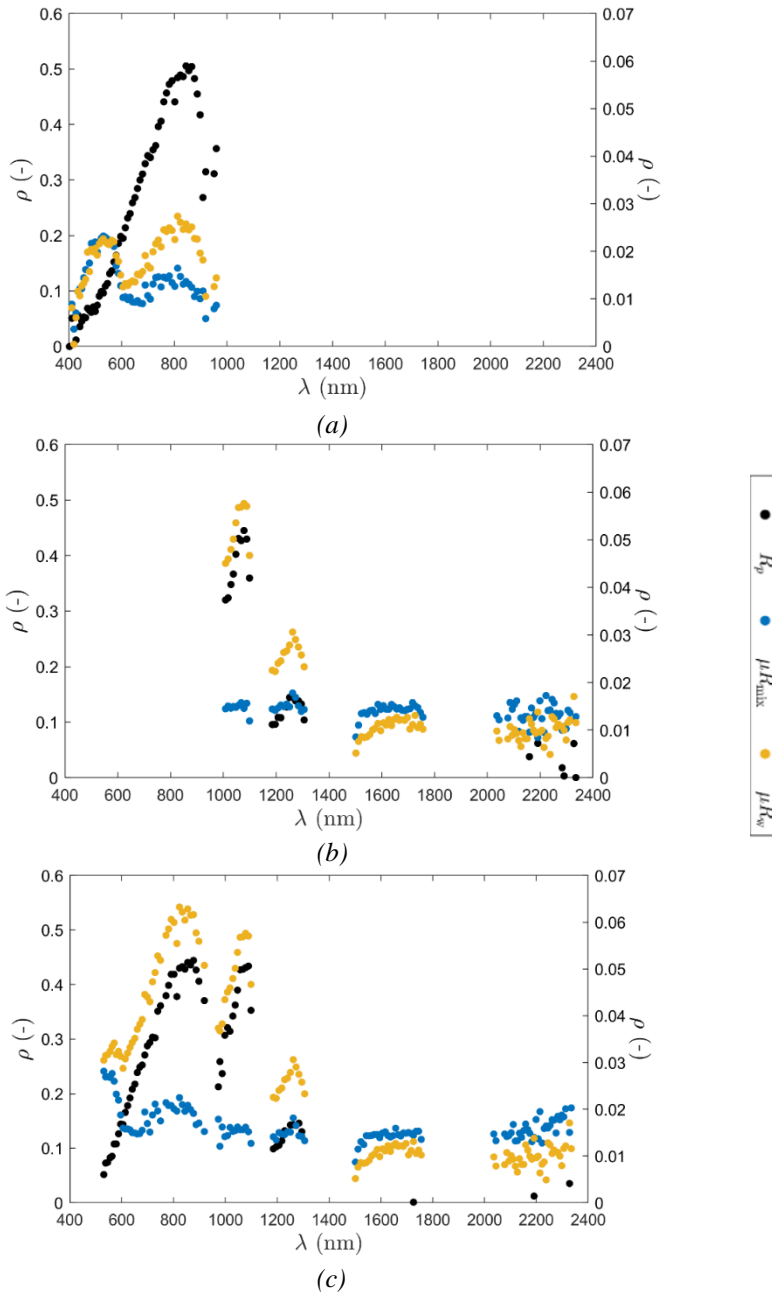
Figure 5.42 – Spectral signatures of the plastic's target endmember, the pixels occupied by plastic and seawater and water. The signatures are calculated for each band combinations: B_{VNIR} *(a)*, B_{SWIR} *(b)*, B_{PCA} *(c)*.

In particular, in Figure 5.42 R_p is the resulting spectral signature of plastic target (chosen as the endmember), μR_w is the mean spectral signature of pixels of water close to the target and μR_{mix} is that of the mixed pixels (μR_w and μR_{mix} are reported in the secondary ordinate axis). The trend of μR_{mix} is the same as R_p confirming the good results obtained by applying the non-linear spectral unmixing method.

The fractional cover maps were obtained by evaluating the spectral signatures of the plastic target using the Eq. 4.14 for the different band-set. A number C of ten f_p - f_w couples was considered. Starting from the first value $f_p = 0$ (which implies a $f_w = 1$) ten steps were applied until the value $f_p = 1$ (which corresponds to $f_w = 0$) was reached.

The B_{PCA} were selected considering the first PCA characterised by an explained variance of 97%. 126 bands composed this band-set (between 531 – 2335 nm) and were characterised by a correlation with the first PCA higher than the threshold, $T = 0.9$.

Figure 5.43 shows the fractional cover maps obtained for the different band-sets.

(a)   *(b)*

(c)   *(d)*
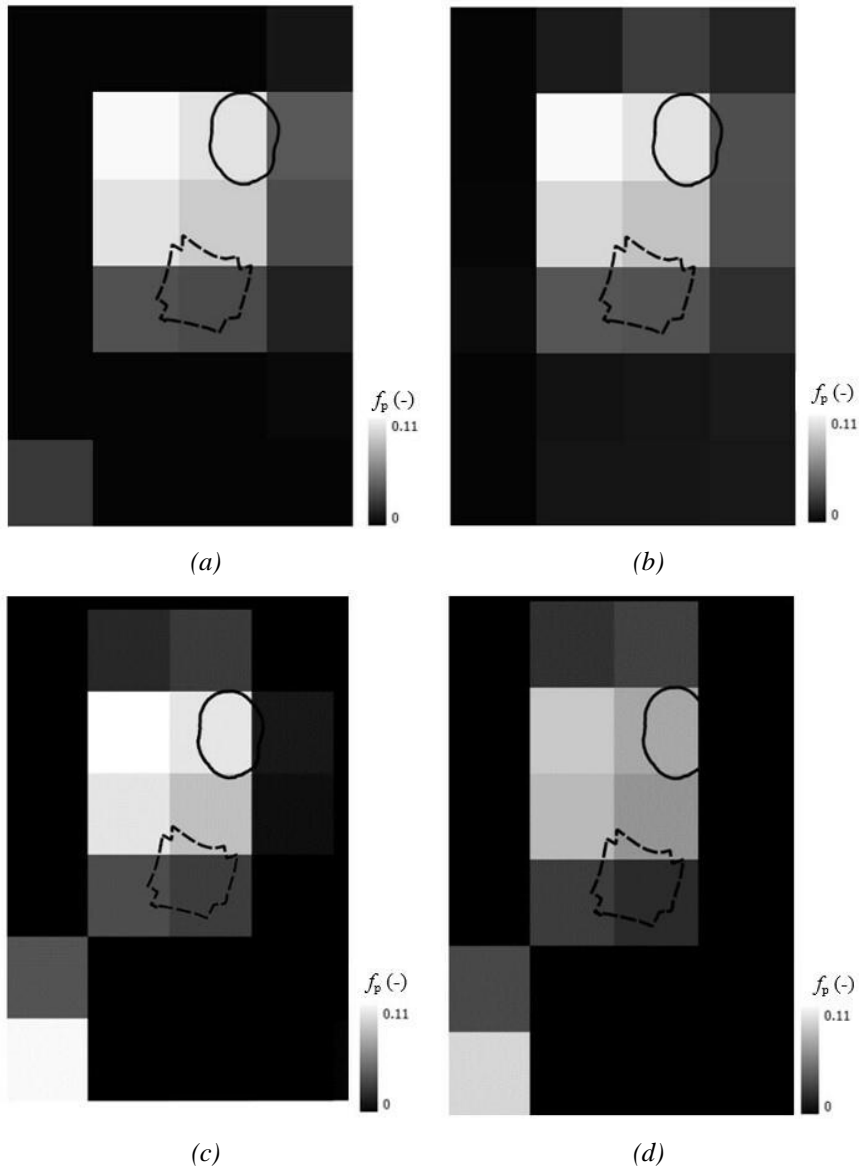
Figure 5.43 – Fractional cover occupied by plastic's target (16/07/2021) calculated for each band combinations: B_{VNIR} *(a)*, B_{SWIR} *(a)*, B_{PCA} *(c)*, B_{Pl} *(d)*.

The f_p maps obtained from PRISMA image by considering the band-set B_{VNIR}, B_{SWIR}, and B_{PCA} appear quite similar. Indeed, it is possible to identify four brighter pixels with an average f_p of ~10%. Whereas, by using the

PlanetScope bands, B_{Pl} there is an underestimation of the plastic present in the scene because (the avarege f_p is ~7%). By analysing Figure 5.43 it is also possible to quantify the geolocation error. A sub-pixel error is noticeable by comparing the f_p maps with the plastic target position digitalized using the UAV data. The resulting f_p maps are in agreement with the dimension of the plastic target (~28 m of diameter) which thus could occupy two or four contiguous PRISMA pixels. Finally, there is a good match of the f_p values with the actual setup.

For the comparative analysis, the linear unmixing techniques was applied on the PlanetScope image by taking into account the endmember spectral signature directly retrieved from a pure pixel of the image (100% covered by the target due to the enough spatial resolution of PlanetScope data). This signature is shown in Figure 5.44 where the mean of the water spectral signature, μR_w, and the mean of the pixels covered, also partially, by the plastic target, μR_{mix}, are also reported.
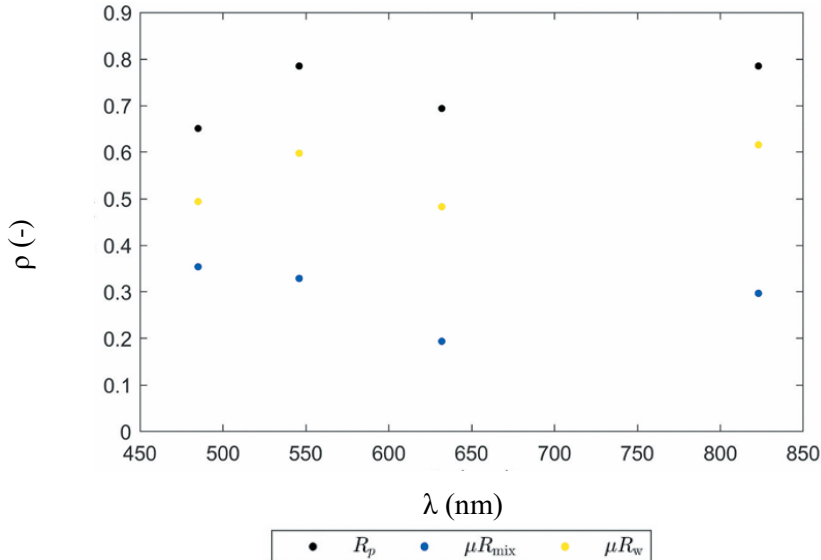
Figure 5.44 – Spectral signatures of plastic target R_p, the mean of water μR_w and of the mixed pixel μR_{mix}.

Using the endmember signature the fractional cover maps for the PlanetScope image at the original (3m) and the PRISMA spatial resolution (pixel aggregated) were retrieved (Figure 5.45).

<div style="text-align:center">(a)   (b)</div>
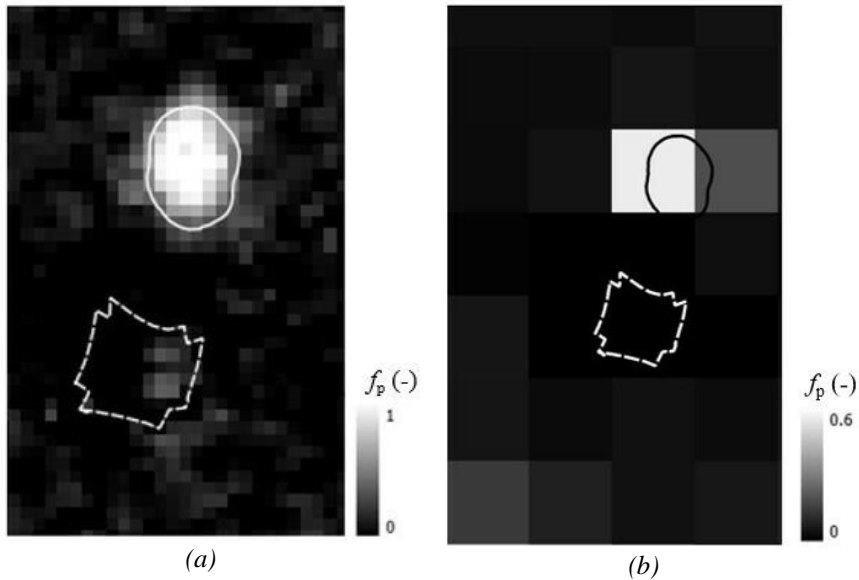
Figure 5.45 – Fractional cover occupied by plastic's target in Planetscope's image (17th June 2021) calculated on Planetscope's resolution (3m) *(a)* and PRISMA's resolution *(b)*.

As expected, the f_p retrieved using the PlanetScope image at 3 m of spatial resolution perfectly allows to detect the plastic target (Figure 5.45, *a*). However, at the PRISMA spatial resolution, the f_p map shows one brighter pixel characterised by a $f_p \sim 60\%$ (Figure 5.45, *b*). This test allowed to demonstrate that the target detection with few spectral bands is possible only by benefitting from a very high spatial resolution (if compared to the target dimension).

Chapter 6

Discussion

6.1 Beach litter

6.1.1 *In-situ* sampling

The present thesis moves from a direct collection of plastic litter from beach environment, to assess the possibility to detect marine litter through different monitoring tools. The individuation of source and sinks areas of marine litter, will allow to address future mitigation/remediation strategies.

The high quantity of debris collected in both the surveyed beaches confirm the urgency to mitigate the marine plastics pollution. The modelling efforts of this thesis confirms the cross-border and transnational nature of the problem (Mæland and Staupe-Delgado 2020; Derraik 2002).

The collated database allows to fill the knowledge gaps about the socio-economic drivers of the marine plastic pollution reflecting a still existing lack of social perception of this problem, as well a lack of active governance action in place (both confirmed at the free-access beach).

It is important to point out how the variety of litter items found highlight that the beach pollution not only concerns plastic but also paper, metal, and glass even if with plastic being the most frequent items found out in both areas. The depicted patterns of marine litter across the studied beaches follow a trend highlighted also by other monitoring campaign conducted, along the coast of Alicante Province, Spain (Asensio-Montesinos, Anfuso, and Williams 2019). Plastic remains among the pollutants cause greater concern due to its high degradation times, negative impacts on the ecosystem, and the enormous quantities in which it is dispersed (Gall and Thompson 2015; Genovese et al. 2023). It should also be emphasised that

its exposure to natural elements, such as sun, wind, and wave action, leads to material degradation, causing greater difficulty in identification and consequently in its removal from the environment and proper disposal resulting in higher environmental associated risk (Salerno et al. 2021; Berlino et al. 2021).

The comparison between Mondello and Isola delle Femmine study areas, underlines the importance to implement local management measures about disposable materials. The plastic generated in Europe amounts to 39.9% of packaging, and one of the primary sources is tourist and recreational activities (Chen et al. 2021). The presence of a private company managing the Mondello beaches may partially explain the lower rate of marine litter when compared with the unmanaged beaches. Therefore the quantity and quality of items, especially on areas characterised by highest permanence of users, underline the need for a higher effort in creating awareness around the issue of marine litter as well as the need for higher effort in mitigating the presence of item reinforcing cleaning up actions and support more initiatives to incentive local retailers and products to enhance models for the circular-life of Single Use Plastics and improve waste management.

Focusing on Mondello beach litter patterns, it is possible to note that in low-cost beaches, compared to seasonal and daily ones, there is a higher presence of paper and metal but a lower presence of glass and ceramic, which is more prevalent in daily beaches but less in seasonal ones. Low-cost beaches are the only ones where the "metal bottle caps, lids & pull tabs from cans" are represent among the top five found items. This may be explained by a higher presence of young people among users of the hourly entrance subscription who consume this type of beverages more and prefer daily and seasonal entrance subscription. Interestingly "daily" entrance beaches are the only ones showing the presence of "cups and lids of hard plastic" among

the identified top five items. This may be explained by the presence of users who spend the entire day at these beaches tending to bring food containers with them, which they may not dispose of properly but abandon on the sand.

Focusing on Isola delle Femmine beach, the beach portion belonging to the Marine Protected Area (MPA, zone C), has been characterised by the highest amounts of pollutants, as potentially resulting by the presence of services (e.g. bar, shops) and by the proximity to the port hosting a small touristic marina and a small-scale fishing fleet. However, all beaches' portions in Isola delle Femmine are characterised by the presence of fishing-related waste, confirming the presence of an active fishing fleet in the area. Beaches off commercial activities, such as ice cream shops, and cafeteria, shows a significant presence of "plastic caps/lids drinks" confirming the strong connection between the type of users and/or, in this case, how the presence of commercial activities influences the type of litter present.

Looking at the top five items of plastic waste found on the beaches of Mondello and Isola delle Femmine, it is important to note that the predominant category is "tobacco products with filters (cigarette butts with filters)" confirming data from others sampling campaigns like those carried out in the coast of Alicante Province, Spain (Asensio-Montesinos et al. 2019) and in the Romanian Black Sea coast (Golumbeanu et al. 2017).

Another category of waste present on in Mondello and on two over three sites at Isola delle Femmine is "fragments of Non-Foamed Plastic 2.5cm $\geq$ $\leq$ 50 cm" it is highly likely that these elements result from the fragmentation of larger plastic waste (so-called secondary waste). This category has a significant ecosystem impact due to the difficulty of detection and the ease with which they can bury themselves in the sand, remaining underground for years.

Lastly, it is important to note that among all the sites, the majority of plastic waste present is of the 'single-use' type, such as "plastic cutlery", "plastic crisps packets/sweets wrappers". This trend is, hopefully, expected to decrease in the coming years with the entry into force (in 2021) in Italy of Directive 2019/904/EU, which prohibits the production and market placement of single-use plastics, consequently reducing their abandonment in marine environments.

All these considerations, suggest how the demography of people and the uses of the beaches are strongly connected to the beach litter, influencing it in terms of quantity and quality (type of items). This reveals how the local policy to cope with the impact of marine litter is insufficient, underlining the need to involve more in a process of awareness both the local administration, the local manger, and the citizens to find common and specific approaches to mitigate and solve it. For example, the implementation of dedicated bins (currently absent on Italian beaches) for the proper disposal of cigarette butts could be considered. Capacity development is recognised as an approach to achieve stakeholders' relationship improvement, influencing the actors' attitudes, values and motivations involved in the process (Stojic and Salhofer 2022). Moreover, it is demonstrated that a trustworthy knowledge-in-action is a driver to achieving eco-sustainable transitions across stakeholders (Grodzińska-Jurczak et al. 2022).

6.1.2 Laboratory experiment

The quantification and characterisation of beach litter is not easy to obtain. The most common approach used are *in-situ* monitoring campaigns which need to be executed according to standardised protocols (Schernewski et al. 2018). However, this approach has several limitations:

it is time-demanding, requires a high number of operators, and is difficult to sample large areas in a reasonable time. To overcome these limits, the use of remote sensing techniques were recently proposed (e.g., Gonçalves et al. 2022) like the UAV to detect beach litter (e.g. Scarrica et al. 2022). These tools allow to monitor large area by involving a limited numbers of operators. Indeed, different researches demonstrated that these techniques could provide fast information regarding abundance and spatial distribution of beach litter (Escobar-Sánchez et al. 2021). Nevertheless, several limitations were underlined by different authors. For example it is hard to identify and characterise the plastic debris due their heterogeneity in terms of shapes and colours and due the lack of information regarding their spectral signatures (Andriolo et al. 2021; Taddia et al. 2021). In this framework, different projects were recently focused on the acquisition of the spectral signatures of marine debris; thus contributing to increase an online spectra library (Corbari et al. 2020; Garaba and Dierssen 2020). Unfortunately, different methodologies were applied to acquire the spectra and, sometime, a detailed description of the experiment phases is missing; thus not allowing replicability of the experiments.

In this framework, with the aim to contribute to the formalisation of a standardised protocol, in this work two different experimental setups were carried out allowing evaluating the role played by two opposite illumination conditions. In particular, some litter samples were spectral characterised implementing: *i*) a direct light inside a black box and, *ii*) a diffusive light in a white box.

The comparison between the spectral data acquired through these two experimental setups showed that for most of the samples the illumination geometry did not affect the spectral signatures, whereas it was crucial for some of them (~ 30% of the total). These latter are those characterised by

peculiar shapes and are those exhibiting a very smooth surface (not Lambertian surface samples). The laboratory experiment allowed also to detect some common absorption peaks in the following ranges: 900-950 nm, 1160-1300 nm, 1380-1430 nm, 1520-1560 nm and 1715-1750 nm. These results are in agreement with outcomes of other studies (e.g., Garaba and Dierssen 2018).

Through the laboratory experiments it was not possible to identify the polymer compositions of the plastic litter collected *in-situ* comparing them with the spectral signatures of some virgin polymers. This is probably due to the fact that the samples collected, as often happens, are not made with only one polymer but with a mix of them.

Analysis on the spectral signatures collected was performed with the aim to evaluate the possibility to detect beach litter samples on sandy beaches through the application of remote sensing techniques. This topic was addressed by computing a spectral separability index, SAM, between the spectra of each sample and that of the sand. For this analysis the comparison between the outcomes data, acquired using the white and black boxes evidenced that for some of the samples the illumination geometry played an important role. Indeed, it was evidenced that for some samples higher SAM were observed using the white box and *vice versa*. The evaluation of the SAM index over a moving wavelength window of ~20 nm allowed to select the most suitable wavelengths for the beach litter detection. It was evident that for several samples the most useful bands are positioned: *i*) in the visible (450-630 nm) range; *ii*) around the red-edge (700-770 nm) range; and, in some infrared bands around 1230 nm, 1400 nm 1720 nm. Nevertheless, the bands around 1400 nm could not be used operatively as in overlap with one of the two main water absorption bands (1350-1450 nm). Similar results are reported in Salgado-Hernanz et al. (2021). Finally, a test of detectability of

litter using the currently operating satellite sensors characterised by high spatial resolution (equal or less of 10 m) was done. The WorldView-3 resulted the one more promising sensor to detect litter on sandy beaches.

6.2 Marine litter

6.2.1 Hydrodynamical models

Hydrodynamic models are powerful tools for studying the fate and transport of marine litter in the ocean (Hardesty et al. 2017). The use of these models helps scientists to predict where debris can accumulate once discharged in the sea environment. Different models were developed in the past and most of them use a Lagrangian approach (Jalón-Rojas, Wang, and Fredj 2019; Mansui et al. 2020; Alosairi, Al-Salem, and Al Ragum 2020). There are various advantages to using a hydrodynamical model to track the marine litter on the sea environment. Firstly, most of the models allow to consider different kind of plastic particles in terms of size, material, shape and give the opportunity to simulate different scenarios of discharging in terms of particles quantities, point of source and discharge time-scheduling (Phan and Luscombe 2023). For the plastic debris specifically, some models consider different phenomena that influence the residence time and the fate of the plastic particles in the sea. For example, due to the biofouling, particles can increase their weight (Tsiaras et al. 2021) and sink in the water column, reaching the sea bottom. Degradation actions caused by waves, solar irradiation, and wind actions can change the shape and weight of the particles also causing their fragmentation in smaller sizes with different shapes.

The simulation of plastic particles transport in the sea environment represents a useful tool for marine litter monitoring. Indeed the *in-situ* monitoring campaigns are expensive and, also present difficulties for the

identification and quantification of the debris, that are not all floating at the sea surface. The use of the remote sensing, which has different benefits, does not allow to predict the particles movement exposed to the sea currents thus a combined approach, including hydrodynamic simulations, can provide a more comprehensive understanding of the marine litter problem. For example, detection through remote sensing can provide validation data for the hydrodynamic models (i.e., position and severity of the accumulation at the sea and/or beaching at the coast); *vice versa*, results of the hydrodynamic simulations can provide the positions of area which can be further examined by applying remote sensing techniques.

Hydrodynamic models, while powerful, do have certain limitations. The incorrect set of the parameters of the model have an important impact on the accuracy of the hydrodynamic model results (Karim et al. 2023). There is often a trade-off between spatial and temporal resolution in hydrodynamic models (Ganju et al. 2016): high spatial resolution models may lack temporal detail and *vice versa*. Also, the computational demand of the hydrodynamic models can be severe, especially when studying particularly extensive and complex domains (Vennell et al. 2021). It is often necessary to reduce the spatial and/or the temporal resolution of the input layers if a large domain is to be investigated thus leading to non-realistic input scenarios. Furthermore, the computation demand can limit the applicability in real-time or in near-real-time of scenarios where rapid results are needed. In this framework, two different hydrodynamic models were tested. The TrackMPD, a complex model which allows to take into account several phenomena, and the STM, a simplified approach that can rapidly (confirmed by the calculation time reported for each simulation) simulate different scenarios of discharged pollutants. For the Strait of Sicily study area, both models were applied considering the same initial conditions. A greater

number of particles persists during the simulated time using the STM compared to the TrackMPD model. This is probably caused by the absence of dispersion effects which increases the probability that particles stay longer inside of the pixels. Furthermore, in STM application the particles are not creating a specific vortex, as in TrackMPD.

The impossibility to known the sources of the microplastics collected thorough the *in-situ* monitor campaign, conducted by ARPA and CNR, prompt to use the STM model assessing the tendency of the sea surface currents to accumulate floating plastic debris. Higher correlations have been found for filaments and foams considering the start of releasing in July 2018 and 2019.

From the outcomes of this work emerges that the marine plastic pollution is a transboundary problem. Indeed, for all the case studies examined it is evident that the marine litter particles are accumulating and/or beaching in area which can be very far from the discharge points. Noticeably also that the use of the hydrodynamic models can play an important dissemination role providing to responsible government entities useful information to plan future strategies to fight with the marine litter problem.

6.2.2 Detection of floating target on sea surface

The detection of the marine litter using remote sensing is a challenging issue. Different research studies have been conducted to define the main limitations in marine plastic detection through remote sensing techniques and to figure out the methodologies useful for the identification and quantification of marine debris. One of the main problems relates to the spectral and spatial resolution of the sensors. The sensor with high spatial resolution have low spectral resolution and *vice versa*. Several researchers

underlined the need to explore the use of hyperspectral data for marine plastic detection (e.g. Martínez-Vicente et al. 2019).

The aim of this part of the research was to assess the capability to detect an artificial plastic target placed in a coastal region of Lesvos, Greece, using satellite remote sensing data. Detection activities were carried out using the satellite hyperspectral PRISMA (with a spatial resolution of 30 m) considering different band combinations to evaluate the most feasible one. Good results were achieved using VNIR and SWIR bands. PCA analysis was conducted with the aim to reduce the number of computational loads and use few bands. However, the results did not prove that there is an advantage using a band-set built on the basis of a PCA (which was time-consuming).

A comparative detection analysis using a PlanetScope at its original spatial resolution (very high if compared to the target dimension) and at the PRISMA spatial resolution (comparable to the target dimension) demonstrated that the detection with only few bands was possible only by exploiting the high spatial resolution.

The need to use hyperspectral data is confirmed by different applications. For example, in Papageorgiou et al. 2022, the same setup of this study was analysed using Sentinel-2. Despite this sensor a better spatial resolution than PRISMA, it is underlines the necessity to have a plastic fractional cover higher than 20% to be detected. Using PRISMA images, this limit seems to be overcome, as it was possible to identify the pixels covered by a plastic mesh covering the pixel only for the 30% of its total area.

Chapter 7

Conclusions and future developments

Marine litter pollution has recently become one of the major focus of global scientific research, as it is a growing issue that requires public engagement and behavioural changes for prevention/mitigation. To date, only localised efforts, in some areas, have quantified its extent and intensity. Given the urgent, widespread, complex and multifaceted nature of this challenge, an interdisciplinary approach is mandatory in the near future to inspire effective solutions. Scientific relevance and data collection must support decision makers; education must be as a tool to generate changes to behavioural psychology, consciousness, and responsibility; modelling must help tailoring management and policy processes; effective prevention should represent the long-term solution.

The interdisciplinary approach developed in this study highlights the importance of synergising scientific resources from multiple disciplines for a better understanding of marine litter pollution. The *in-situ* data collection along the coast, in addition to providing useful information about the quantities and kind of marine litter in different study areas, was useful to implement two indoor laboratory experiments. The use of two different experimental setups provided important information for developing future standard protocols for spectroradiometric acquisition. Additionally the comparison of the data acquired, allowed to investigate and to conclude that the illumination conditions play a role on the detectability of some samples with jagged shapes, particular colour or transparency conditions. These experiments, represent one of the first study focused on the detection of marine debris in a sandy background comparing different illumination conditions. The analyses highlighted that particular wavelengths the VNIR

and SWIR ranges could be useful for the litter detection and some are already used by the WorldView-3 which resulted the most promising nowadays operating sensor (confirming outcomes of other researches). Future works can include the analysis of images, in which the spectral signatures of the samples will be acquired jointly with the sand performing an *ad-hoc* outdoor experiment. The bottom-up approach adapted in this study will be useful to carry future UAV beach litter detection activities (more complex due to changing light conditions, wind action etc.) by acquiring images with multispectral/hyperspectral cameras. Also, the setup of a spectral characterisation of floating litter debris will be useful to extend gather useful information for the detection at the sea using remote sensing techniques.

The link between beach and marine litter was studied using two hydrodynamic Lagrangian models with the aim to individuate macroplastics accumulation area on the sea surface and on the coastal line. The results suggest the cross-border characteristic of the marine litter phenomena, considering that macroplastics could be accumulate in areas far away from the discharging points. Future development of this work will assess the sensitivity of the hydrodynamic models to different parameters. Additionally, as a possible future development, the implementation of the 3D Lagrangian models will allow to include different phenomena such as the biofouling, sinking, particle degradation etc. Also, the model outputs could be used to address new *in-situ* surveys and clean-up actions.

Satellite remote sensing techniques were applied to detect a large plastic target deployed on the sea surface evaluating the potentiality to use PRISMA hyperspectral data. The detection of this target was possible only exploiting the hyperspectral capability of the PRISMA sensor as confirmed by the comparative analysis carried out using the PlanetScope data. As a

future development, outdoor applications could be carried out by planning the *in-situ* spectral signature characterisation of the target through the employment of a spectroradiometer and/or of a UAV equipped with an hyperspectral sensor. Additionally to the PRISMA images, further analyses could be carried out by processing other satellite hyperspectral data such as those acquired by the new Indian HySIS (HyperSpectral Imaging Satellite) satellite (https://www.eoportal.org/satellitemissions/hysis#eop-quick-facts-section) and by the incoming "pixxel space hyperspectral constellation" (https://www.pixxel.space/) which promises the acquisition of 300 spectral bands at 5 m spatial resolution.

The different tools described in this research activity can be synergically adopted. Density and beaching maps derived by the hydrodynamic tracking models could drive *in-situ* and remote sensing monitoring campaigns at sea and coastal areas respectively. *Vice versa* remote sensing detection and/or *in-situ* sampling could be considered as discharging areas for hydrodynamic simulations. Further analysis will be focused on the use of indoor experimental data as endmember for satellite images classification in coastal environments.

References

Acuña-Ruz, Tomás, Diego Uribe, Richard Taylor, Lucas Amézquita, María Cristina Guzmán, Javier Merrill, Paula Martínez, Leandro Voisin, and Cristian Mattar B. 2018. 'Anthropogenic Marine Debris over Beaches: Spectral Characterization for Remote Sensing Applications'. *Remote Sensing of Environment* 217 (November): 309–22. doi:10.1016/j.rse.2018.08.008.

Alevizos, Evangelos, Tim Le Bas, and Dimitrios D. Alexakis. 2022. 'Assessment of PRISMA Level-2 Hyperspectral Imagery for Large Scale Satellite-Derived Bathymetry Retrieval'. *Marine Geodesy* 45 (3): 251–73. doi:10.1080/01490419.2022.2032497.

Allsopp, Michelle, Adam Walters, David Santillo, and Paul Johnston. 2016. 'Plastic Debris in the World's Oceans'.

Alosairi, Y., S. M. Al-Salem, and A. Al Ragum. 2020. 'Three-Dimensional Numerical Modelling of Transport, Fate and Distribution of Microplastics in the Northwestern Arabian/Persian Gulf'. *Marine Pollution Bulletin* 161 (December): 111723. doi:10.1016/j.marpolbul.2020.111723.

Andriolo, Umberto, Odei Garcia-Garin, Morgana Vighi, Asunción Borrell, and Gil Gonçalves. 2022. 'Beached and Floating Litter Surveys by Unmanned Aerial Vehicles: Operational Analogies and Differences'. *Remote Sensing* 14 (6): 1336. doi:10.3390/rs14061336.

Andriolo, Umberto, Gil Gonçalves, Paula Sobral, and Filipa Bessa. 2021. 'Spatial and Size Distribution of Macro-Litter on Coastal Dunes from Drone Images: A Case Study on the Atlantic Coast'. *Marine Pollution Bulletin* 169 (August): 112490. doi:10.1016/j.marpolbul.2021.112490.

Annan, Richard Fiifi, and Xiaoyun Wan. 2022. 'Recovering Bathymetry of the Gulf of Guinea Using Altimetry-Derived Gravity Field Products Combined via Convolutional Neural Network'. *Surveys in Geophysics* 43 (5): 1541–61. doi:10.1007/s10712-022-09720-5.

Asensio-Montesinos, F., G. Anfuso, P. Randerson, and A.T. Williams. 2019. 'Seasonal Comparison of Beach Litter on Mediterranean

Coastal Sites (Alicante, SE Spain)'. *Ocean & Coastal Management* 181 (November): 104914. doi:10.1016/j.ocecoaman.2019.104914.

Azarpira, Maryam, Amir Reza Zarrati, and Pouya Farrokhzad. 2021. 'Comparison between the Lagrangian and Eulerian Approach in Simulation of Free Surface Air-Core Vortices'. *Water* 13 (5). Multidisciplinary Digital Publishing Institute: 726. doi:10.3390/w13050726.

Balsi, Marco, Monica Moroni, Valter Chiarabini, and Giovanni Tanda. 2021. 'High-Resolution Aerial Detection of Marine Plastic Litter by Hyperspectral Sensing'. *Remote Sensing* 13 (8): 1557. doi:10.3390/rs13081557.

Banchani, John-Paul Safunu. 2016. 'The Relevance of the Gulf of Guinea in Global Energy Politics'. *African Security Review* 25 (4): 420–26. doi:10.1080/10246029.2016.1225585.

Basilone, G., A. Bonanno, B. Patti, S. Mazzola, M. Barra, A. Cuttitta, and R. McBride. 2013. 'Spawning Site Selection by European Anchovy (*Engraulis Encrasicolus*) in Relation to Oceanographic Conditions in the Strait of Sicily'. *Fisheries Oceanography* 22 (4): 309–23. doi:10.1111/fog.12024.

Basu, Bidroha, Srikanta Sannigrahi, Arunima Sarkar Basu, and Francesco Pilla. 2021. 'Development of Novel Classification Algorithms for Detection of Floating Plastic Debris in Coastal Waterbodies Using Multispectral Sentinel-2 Remote Sensing Imagery'. *Remote Sensing* 13 (8): 1598. doi:10.3390/rs13081598.

Batchelor, G. K. 2000. *An Introduction to Fluid Dynamics*. 1st ed. Cambridge University Press. doi:10.1017/CBO9780511800955.

Bennema, Floris P., and Adriaan D. Rijnsdorp. 2015. 'Fish Abundance, Fisheries, Fish Trade and Consumption in Sixteenth-Century Netherlands as Described by Adriaen Coenen'. *Fisheries Research* 161 (January): 384–99. doi:10.1016/j.fishres.2014.09.001.

Béranger, K, L Mortier, G. -P Gasparini, L Gervasio, M Astraldi, and M Crépon. 2004. 'The Dynamics of the Sicily Strait: A Comprehensive Study from Observations and Models'. *Deep Sea Research Part II: Topical Studies in Oceanography*, The Physical

Oceanography of Sea Straits, 51 (4): 411–40. doi:10.1016/j.dsr2.2003.08.004.

Bergmann, Melanie, Lars Gutow, Michael Klages, Alfred-Wegener-Institut, and Göteborgs universitet, eds. 2015. *Marine Anthropogenic Litter*. Springer Open. Cham Heidelberg New York Dordrecht London: Springer.

Berlino, M., M. C. Mangano, C. De Vittor, and G. Sarà. 2021. 'Effects of Microplastics on the Functional Traits of Aquatic Benthic Organisms: A Global-Scale Meta-Analysis'. *Environmental Pollution (Barking, Essex: 1987)* 285 (September): 117174. doi:10.1016/j.envpol.2021.117174.

Bianchi, C Nike, and Carla Morri. 2000. 'RMESUaLTrSine Biodiversity of the Mediterranean Sea: Situation, Problems and Prospects for Future Research'. *Marine Pollution Bulletin* 40 (5).

Biermann, Lauren, Daniel Clewley, Victor Martinez-Vicente, and Konstantinos Topouzelis. 2020. 'Finding Plastic Patches in Coastal Waters Using Optical Satellite Data'. *Scientific Reports* 10 (1): 5364. doi:10.1038/s41598-020-62298-z.

Bigdeli, Mostafa, Abdolmajid Mohammadian, Abolghasem Pilechi, and Mercedeh Taheri. 2022. 'Lagrangian Modeling of Marine Microplastics Fate and Transport: The State of the Science'. *Journal of Marine Science and Engineering* 10 (4): 481. doi:10.3390/jmse10040481.

Browne, Mark Anthony, Stewart J. Niven, Tamara S. Galloway, Steve J. Rowland, and Richard C. Thompson. 2013. 'Microplastic Moves Pollutants and Additives to Worms, Reducing Functions Linked to Health and Biodiversity'. *Current Biology* 23 (23): 2388–92. doi:10.1016/j.cub.2013.10.012.

Brownfield, M.E. and Charpentier, R.R. 2006. 'Geology and Total Petroleum Systems of the Gulf of Guinea Province of West Africa'. doi:10.3133/b2207C.

Capodici, Fulvio, Giuseppe Ciraolo, Simone Cosoli, Antonino Maltese, M. Cristina Mangano, and Gianluca Sarà. 2018. 'Downscaling Hydrodynamics Features to Depict Causes of Major Productivity of Sicilian-Maltese Area and Implications for Resource Management'.

Science of The Total Environment 628–629 (July): 815–25. doi:10.1016/j.scitotenv.2018.02.106.

Capodici, Fulvio, Simone Cosoli, Giuseppe Ciraolo, Carmelo Nasello, Antonino Maltese, Pierre-Marie Poulain, Aldo Drago, Joel Azzopardi, and Adam Gauci. 2019. 'Validation of HF Radar Sea Surface Currents in the Malta-Sicily Channel'. *Remote Sensing of Environment* 225 (May): 65–76. doi:10.1016/j.rse.2019.02.026.

Cesarano, Cinzia, Giuseppe Aulicino, Carlo Cerrano, Massimo Ponti, and Stefania Puce. 2023. 'Marine Beach Litter Monitoring Strategies along Mediterranean Coasts. A Methodological Review'. *Marine Pollution Bulletin* 186 (January): 114401. doi:10.1016/j.marpolbul.2022.114401.

Chen, Yuan, Abhishek Kumar Awasthi, Fan Wei, Quanyin Tan, and Jinhui Li. 2021. 'Single-Use Plastics: Production, Usage, Disposal, and Adverse Impacts'. *The Science of the Total Environment* 752 (January): 141772. doi:10.1016/j.scitotenv.2020.141772.

Chubarenko, I., A. Bagaev, M. Zobkov, and E. Esiukova. 2016. 'On Some Physical and Dynamical Properties of Microplastic Particles in Marine Environment'. *Marine Pollution Bulletin* 108 (1–2): 105–12. doi:10.1016/j.marpolbul.2016.04.048.

COBSEA & CSIRO. 2022. 'Marine Litter Monitoring Methods Handbook. Part 1'.

Corbari, L., A. Maltese, F. Capodici, M. C. Mangano, G. Sarà, and G. Ciraolo. 2020. 'Indoor Spectroradiometric Characterization of Plastic Litters Commonly Polluting the Mediterranean Sea: Toward the Application of Multispectral Imagery'. *Scientific Reports* 10 (1): 19850. doi:10.1038/s41598-020-74543-6.

Cosoli, Simone, Aldo Drago, Giuseppe Ciraolo, and Fulvio Capodici. 2015. 'Tidal Currents in the Malta – Sicily Channel from High-Frequency Radar Observations'. *Continental Shelf Research* 109 (October): 10–23. doi:10.1016/j.csr.2015.08.030.

Cózar, Andrés, Marina Sanz-Martín, Elisa Martí, J. Ignacio González-Gordillo, Bárbara Ubeda, José Á. Gálvez, Xabier Irigoien, and Carlos M. Duarte. 2015. 'Plastic Accumulation in the

Mediterranean Sea'. Edited by Erik V. Thuesen. *PLOS ONE* 10 (4): e0121762. doi:10.1371/journal.pone.0121762.

Critchell, K., M. Hamann, N. Wildermann, and A. Grech. 2019. 'Predicting the Exposure of Coastal Species to Plastic Pollution in a Complex Island Archipelago'. *Environmental Pollution* 252: 982–91. doi:10.1016/j.envpol.2019.06.031.

Crosti, Roberto, Antonella Arcangeli, Silvana Campagnuolo, Luca Castriota, Manuela Falautano, Teresa Maggio, and Franco Andaloro. 2020. 'Assessing Worth of Marine Protected Areas for the Protection of Threatened Biodiversity Using IUCN Red List and Red List Index. A Pilot Study in Six Mediterranean Areas'. *Ecological Indicators* 119 (December): 106765. doi:10.1016/j.ecolind.2020.106765.

Delandmeter, Philippe, and Erik van Sebille. 2019. 'The Parcels v2.0 Lagrangian Framework: New Field Interpolation Schemes'. *Geoscientific Model Development* 12 (8). Copernicus GmbH: 3571–84. doi:10.5194/gmd-12-3571-2019.

Derraik, José G. B. 2002. 'The Pollution of the Marine Environment by Plastic Debris: A Review'. *Marine Pollution Bulletin* 44 (9): 842–52. doi:10.1016/S0025-326X(02)00220-5.

Djakouré, Sandrine, Pierrick Penven, Bernard Bourlès, Jennifer Veitch, and Vamara Koné. 2014. 'Coastally Trapped Eddies in the North of the Gulf of Guinea'. *Journal of Geophysical Research: Oceans* 119 (10): 6805–19. doi:10.1002/2014JC010243.

Dobigeon, Nicolas, Jean-Yves Tourneret, Cédric Richard, José C. M. Bermudez, Stephen McLaughlin, and Alfred O. Hero. 2014. 'Nonlinear Unmixing of Hyperspectral Images: Models and Algorithms'. *IEEE Signal Processing Magazine* 31 (1): 82–94. doi:10.1109/MSP.2013.2279274.

Doyle, Miriam J., William Watson, Noelle M. Bowlin, and Seba B. Sheavly. 2011. 'Plastic Particles in Coastal Pelagic Ecosystems of the Northeast Pacific Ocean'. *Marine Environmental Research* 71 (1): 41–52. doi:10.1016/j.marenvres.2010.10.001.

Drago, A, G Ciraolo, F Capodici, S Cosoli, M Gacic, R Tarasova, J Azzopardi, et al. n.d. 'An Operational Network of HF Radars for the Malta-Sicily Channel'.

Kershaw P.J., Turra A. and Galgani F. 2019. 'Guidelines for the Monitoring and Assessment of Plastic Litter and Microplastics in the Ocean.' 130pp. GESAMP Joint Group of Experts on the Scientific Aspects of Marine Environmental Protection. doi:10.25607/OBP-435.

Egorov, A. V., M. C. Hansen, D. P. Roy, A. Kommareddy, and P. V. Potapov. 2015. 'Image Interpretation-Guided Supervised Classification Using Nested Segmentation'. *Remote Sensing of Environment* 165 (August): 135–47. doi:10.1016/j.rse.2015.04.022.

Eriksen, Marcus, Max Liboiron, Tim Kiessling, Louis Charron, Abigail Alling, Laurent Lebreton, Heather Richards, et al. 2018. 'Microplastic Sampling with the AVANI Trawl Compared to Two Neuston Trawls in the Bay of Bengal and South Pacific'. *Environmental Pollution* 232 (January): 430–39. doi:10.1016/j.envpol.2017.09.058.

Escobar-Sánchez, Gabriela, Mirco Haseler, Natascha Oppelt, and Gerald Schernewski. 2021. 'Efficiency of Aerial Drones for Macrolitter Monitoring on Baltic Sea Beaches'. *Frontiers in Environmental Science* 8. https://www.frontiersin.org/articles/10.3389/fenvs.2020.560237.

European Commission, Joint Research Centre. 2015. *Review of the Commission Decision 2010/477/EU Concerning MSFD Criteria for Assessing Good Environmental Status – Descriptor 10 Properties and Quantities of Marine Litter Do Not Cause Harm to the Coastal and Marine Environment*. LU: Publications Office. https://data.europa.eu/doi/10.2788/037925.

Fallati, L., A. Polidori, C. Salvatore, L. Saponari, A. Savini, and P. Galli. 2019. 'Anthropogenic Marine Debris Assessment with Unmanned Aerial Vehicle Imagery and Deep Learning: A Case Study along the Beaches of the Republic of Maldives'. *Science of The Total Environment* 693: 133581. doi:https://doi.org/10.1016/j.scitotenv.2019.133581.

Fazey, Francesca M.C., and Peter G. Ryan. 2016. 'Debris Size and Buoyancy Influence the Dispersal Distance of Stranded Litter'.

Marine Pollution Bulletin 110 (1): 371–77. doi:10.1016/j.marpolbul.2016.06.039.

Fredj, Erick, Daniel F. Carlson, Yael Amitai, Avi Gozolchiani, and Hezi Gildor. 2016. 'The Particle Tracking and Analysis Toolbox (PaTATO) for Matlab: PaTATO for Matlab'. *Limnology and Oceanography: Methods* 14 (9): 586–99. doi:10.1002/lom3.10114.

Freitas, Sara, Hugo Silva, and Eduardo Silva. 2021. 'Remote Hyperspectral Imaging Acquisition and Characterization for Marine Litter Detection'. *Remote Sensing* 13 (13): 2536. doi:10.3390/rs13132536.

Fuente, Rebeca de la, Gábor Drótos, Emilio Hernández-García, Cristóbal López, and Erik van Sebille. 2021. 'Sinking Microplastics in the Water Column: Simulations in the Mediterranean Sea'. *Ocean Science* 17 (2). Copernicus GmbH: 431–53. doi:10.5194/os-17-431-2021.

Galgani, F., G. Hanke, S. Werner, and L. De Vrees. 2013. 'Marine Litter within the European Marine Strategy Framework Directive'. *ICES Journal of Marine Science* 70 (6): 1055–64. doi:10.1093/icesjms/fst122.

Gall, S. C., and R. C. Thompson. 2015. 'The Impact of Debris on Marine Life'. *Marine Pollution Bulletin* 92 (1): 170–79. doi:10.1016/j.marpolbul.2014.12.041.

Ganju, Neil K., Mark J. Brush, Brenda Rashleigh, Alfredo L. Aretxabaleta, Pilar del Barrio, Jason S. Grear, Lora A. Harris, et al. 2016. 'Progress and Challenges in Coupled Hydrodynamic-Ecological Estuarine Modeling'. *Estuaries and Coasts* 39 (2): 311–32. doi:10.1007/s12237-015-0011-y.

Garaba, Shungudzemwoyo P., Tomás Acuña-Ruz, and Cristian B. Mattar. 2020. 'Hyperspectral Longwave Infrared Reflectance Spectra of Naturally Dried Algae, Anthropogenic Plastics, Sands and Shells'. *Earth System Science Data* 12 (4). Copernicus GmbH: 2665–78. doi:10.5194/essd-12-2665-2020.

Garaba, Shungudzemwoyo P., and Heidi M. Dierssen. 2018. 'An Airborne Remote Sensing Case Study of Synthetic Hydrocarbon Detection Using Short Wave Infrared Absorption Features Identified from

Marine-Harvested Macro- and Microplastics'. *Remote Sensing of Environment* 205 (February): 224–35. doi:10.1016/j.rse.2017.11.023.

———. 2020. 'Hyperspectral Ultraviolet to Shortwave Infrared Characteristics of Marine-Harvested, Washed-Ashore and Virgin Plastics'. *Earth System Science Data* 12 (1). Copernicus GmbH: 77–86. doi:10.5194/essd-12-77-2020.

Genovese, Martina, Maria Cristina Mangano, Federica Papa, Teresa Romeo, and Silvestro Greco. 2023. 'Local Businesses' Consumption and Perception of Single-Use Plastics: A Preliminary Assessment for Conservation and Mitigation Plans in the Egadi Islands Marine Protected Area'. *Marine Pollution Bulletin* 194 (Pt A): 115252. doi:10.1016/j.marpolbul.2023.115252.

Gola, Deepak, Pankaj Kumar Tyagi, Arvind Arya, Nitin Chauhan, Meenu Agarwal, S. K. Singh, and Sunil Gola. 2021. 'The Impact of Microplastics on Marine Environment: A Review'. *Environmental Nanotechnology, Monitoring & Management* 16 (December): 100552. doi:10.1016/j.enmm.2021.100552.

Golumbeanu, M, M Nenciu, M Galatchi, V Nita, E Anton, A Oros, C Ioakeimidis, and C Belchior. 2017. 'MARINE LITTER WATCH APP AS A TOOL FOR ECOLOGICAL EDUCATION AND AWARENESS RAISING ALONG THE ROMANIAN BLACK SEA COAST'.

Gonçalves, Gil, Umberto Andriolo, Luísa M. S. Gonçalves, Paula Sobral, and Filipa Bessa. 2022. 'Beach Litter Survey by Drones: Mini-Review and Discussion of a Potential Standardization'. *Environmental Pollution* 315 (December): 120370. doi:10.1016/j.envpol.2022.120370.

Grodzińska-Jurczak, Małgorzata, Aleksandra Krawczyk, Arash Akhshik, Zuzanna Dedyk, and Marianna Strzelecka. 2022. 'Contradictory or Complementary? Stakeholders' Perceptions of a Circular Economy for Single-Use Plastics'. *Waste Management (New York, N.Y.)* 142 (April): 1–8. doi:10.1016/j.wasman.2022.01.036.

Gruber, Elisabeth S., Vanessa Stadlbauer, Verena Pichler, Katharina Resch-Fauster, Andrea Todorovic, Thomas C. Meisel, Sibylle Trawoeger, et al. 2023. 'To Waste or Not to Waste: Questioning Potential

Health Risks of Micro- and Nanoplastics with a Focus on Their Ingestion and Potential Carcinogenicity'. *Exposure and Health* 15 (1): 33–51. doi:10.1007/s12403-022-00470-8.

Guerrini, Federica, Lorenzo Mari, and Renato Casagrandi. 2021. 'The Dynamics of Microplastics and Associated Contaminants: Data-Driven Lagrangian and Eulerian Modelling Approaches in the Mediterranean Sea'. *Science of The Total Environment* 777 (July): 145944. doi:10.1016/j.scitotenv.2021.145944.

Hanke, Georg, Francois Galgani, Stefanie Werner, Lex Oosterbaan, Per Nilsson, David Fleet, Sue Kinsey, et al. 2014. 'Guidance on Monitoring of Marine Litter in European Seas'. *JRC Publications Repository*. February 4. doi:10.2788/99816.

Hardesty, Britta D., Joseph Harari, Atsuhiko Isobe, Laurent Lebreton, Nikolai Maximenko, Jim Potemra, Erik van Sebille, A. Dick Vethaak, and Chris Wilcox. 2017. 'Using Numerical Model Simulations to Improve the Understanding of Micro-Plastic Distribution and Pathways in the Marine Environment'. *Frontiers in Marine Science* 4. https://www.frontiersin.org/articles/10.3389/fmars.2017.00030.

Jalón-Rojas, Isabel, Xiao Hua Wang, and Erick Fredj. 2019. 'A 3D Numerical Model to Track Marine Plastic Debris (TrackMPD): Sensitivity of Microplastic Trajectories and Fates to Particle Dynamical Properties and Physical Processes'. *Marine Pollution Bulletin* 141: 256–72. doi:10.1016/j.marpolbul.2019.02.052.

Jones, B., B. C. O'Neill, and J. Gao. 2020. 'Global 1-Km Downscaled Population Base Year and Projection Grids for the Shared Socioeconomic Pathways (SSPs), Revision 01'. Palisades, NY: NASA Socioeconomic Data and Applications Center (SEDAC). doi:10.7927/Q7Z9-9R69.

Karim, Fazlul, Mohammed Ali Armin, David Ahmedt-Aristizabal, Lachlan Tychsen-Smith, and Lars Petersson. 2023. 'A Review of Hydrodynamic and Machine Learning Approaches for Flood Inundation Modeling'. *Water* 15 (3). Multidisciplinary Digital Publishing Institute: 566. doi:10.3390/w15030566.

Kershaw, P. J., Turra, A., & Galgani, F. 2019. 'Guidelines for the Monitoring and Assessment of Plastic Litter and Microplastics in

the Ocean.', (IMO/FAO/UNESCO-IOC/UNIDO/WMO/IAEA/UN/UNEP/UNDP/ISA Joint Group of Experts on the Scientific Aspects of Marine Environmental Protection). Rep. Stud. GESAMP No. 99, 130p.

Khatmullina, Liliya, and Igor Isachenko. 2017. 'Settling Velocity of Microplastic Particles of Regular Shapes'. *Marine Pollution Bulletin* 114 (2): 871–80. doi:10.1016/j.marpolbul.2016.11.024.

Knaeps, Els, Sindy Sterckx, Gert Strackx, Johan Mijnendonckx, Mehrdad Moshtaghi, Shungudzemwoyo P. Garaba, and Dieter Meire. 2021. 'Hyperspectral-Reflectance Dataset of Dry, Wet and Submerged Marine Litter'. *Earth System Science Data* 13 (2): 713–30. doi:10.5194/essd-13-713-2021.

Kremezi, Maria, Viktoria Kristollari, Vassilia Karathanassi, Konstantinos Topouzelis, Pol Kolokoussis, Nicolo Taggio, Antonello Aiello, Giulio Ceriola, Enrico Barbone, and Paolo Corradi. 2021. 'Pansharpening PRISMA Data for Marine Plastic Litter Detection Using Plastic Indexes'. *IEEE Access* 9: 61955–71. doi:10.1109/ACCESS.2021.3073903.

Kroon, Frederieke J., Cherie E. Motti, Lene H. Jensen, and Kathryn L. E. Berry. 2018. 'Classification of Marine Microdebris: A Review and Case Study on Fish from the Great Barrier Reef, Australia'. *Scientific Reports* 8 (1). Nature Publishing Group: 16422. doi:10.1038/s41598-018-34590-6.

Kruse, F A, K B Heidebrecht, A T Shapiro, P J Barloon, and A F H Goetz. 1993. 'The Spectral Image Processing System (SIPS) Interactive Visualization and Analysis of Imaging Spectrometer Data'.

Kühn, Susanne, Elisa L. Bravo Rebolledo, and Jan A. van Franeker. 2015. 'Deleterious Effects of Litter on Marine Life'. In *Marine Anthropogenic Litter*, edited by Melanie Bergmann, Lars Gutow, and Michael Klages, 75–116. Cham: Springer International Publishing. doi:10.1007/978-3-319-16510-3_4.

La Loggia, Goffredo La, Fulvio Capodici, Giuseppe Ciraolo, Aldo Drago, and Antonino Maltese. 2011. 'Monitoring Mediterranean Marine Pollution Using Remote Sensing and Hydrodynamic Modelling'. In *Remote Sensing for Agriculture, Ecosystems, and Hydrology XIII*, 8174:373–81. SPIE. doi:10.1117/12.903761.

Lacombe H, Gascard JC, Gonella J, Bethoux JP. n.d. 'Response of the Mediterranean to the Water and Energy Fluxes across Its Surface, on Seasonal and Interannual Scales.'

Lebreton, Laurent C. M., Joost van der Zwet, Jan-Willem Damsteeg, Boyan Slat, Anthony Andrady, and Julia Reisser. 2017. 'River Plastic Emissions to the World's Oceans'. *Nature Communications* 8 (1). Nature Publishing Group: 15611. doi:10.1038/ncomms15611.

Li, Yanfang, Hua Zhang, and Cheng Tang. 2020. 'A Review of Possible Pathways of Marine Microplastics Transport in the Ocean'. *Anthropocene Coasts* 3 (1). NRC Research Press: 6–13. doi:10.1139/anc-2018-0030.

Lippiatt, S.; Opfer, S. and Arthur, C. (201). Marine Debris Monitoring and Assessment: Recommendations for Monitoring Debris Trends in the Marine Environment. Silver Spring, MD, NOAA Marine Debris Division, 82pp. (NOAA Technical Memorandum NOS-OR&R-46). DOI: http://dx.doi.org/10.25607/OBP-727

Liubartseva, S., G. Coppini, R. Lecci, and E. Clementi. 2018. 'Tracking Plastics in the Mediterranean: 2D Lagrangian Model'. *Marine Pollution Bulletin* 129 (1): 151–62. doi:10.1016/j.marpolbul.2018.02.019.

Mæland, Carmen E., and Reidar Staupe-Delgado. 2020. 'Can the Global Problem of Marine Litter Be Considered a Crisis?' *Risk, Hazards & Crisis in Public Policy* 11 (1): 87–104. doi:10.1002/rhc3.12180.

Manfreda, Salvatore, Matthew F. McCabe, Pauline E. Miller, Richard Lucas, Victor Pajuelo Madrigal, Giorgos Mallinis, Eyal Ben Dor, et al. 2018. 'On the Use of Unmanned Aerial Systems for Environmental Monitoring'. *Remote Sensing* 10 (4). Multidisciplinary Digital Publishing Institute: 641. doi:10.3390/rs10040641.

Mangano, M. C., and G. Sarà. 2017. 'Collating Science-Based Evidence to Inform Public Opinion on the Environmental Effects of Marine Drilling Platforms in the Mediterranean Sea'. *Journal of Environmental Management* 188 (March): 195–202. doi:10.1016/j.jenvman.2016.12.013.

Mansui, J., G. Darmon, T. Ballerini, O. van Canneyt, Y. Ourmieres, and C. Miaud. 2020. 'Predicting Marine Litter Accumulation Patterns in the Mediterranean Basin: Spatio-Temporal Variability and Comparison with Empirical Data'. *Progress in Oceanography* 182 (March): 102268. doi:10.1016/j.pocean.2020.102268.

Martínez-Vicente, Víctor, James R. Clark, Paolo Corradi, Stefano Aliani, Manuel Arias, Mathias Bochow, Guillaume Bonnery, et al. 2019. 'Measuring Marine Plastic Debris from Space: Initial Assessment of Observation Requirements.' doi:10.3390/rs11202443.

Masoumi, Hamed, Seyed Mohsen Safavi, and Z. Khani. 2012. 'Identification and Classification of Plastic Resins Using near Infrared Reflectance Spectroscopy'. *International Journal of Mechanical and Industrial Engineering* 6 (January): 213–20.

Meijer, Lourens J. J., Tim Van Emmerik, Ruud Van Der Ent, Christian Schmidt, and Laurent Lebreton. 2021. 'More than 1000 Rivers Account for 80% of Global Riverine Plastic Emissions into the Ocean'. *Science Advances* 7 (18): eaaz5803. doi:10.1126/sciadv.aaz5803.

Menna, Milena, Pierre-Marie Poulain, Daniele Ciani, Andrea Doglioli, Giulio Notarstefano, Riccardo Gerin, Marie-Helene Rio, Rosalia Santoleri, Adam Gauci, and Aldo Drago. 2019. 'New Insights of the Sicily Channel and Southern Tyrrhenian Sea Variability'. *Water* 11 (7). Multidisciplinary Digital Publishing Institute: 1355. doi:10.3390/w11071355.

Merlino, Silvia, Marco Paterni, Andrea Berton, and Luciano Massetti. 2020. 'Unmanned Aerial Vehicles for Debris Survey in Coastal Areas: Long-Term Monitoring Programme to Study Spatial and Temporal Accumulation of the Dynamics of Beached Marine Litter'. *Remote Sensing* 12 (8): 1260. doi:10.3390/rs12081260.

Monique, Mancuso, Panarello Giuseppe, Falco Francesca, Di Paola Davide, Serena Savoca, Capillo Gioele, Romeo Teresa, et al. 2022. 'Investigating the Effects of Microplastic Ingestion in Scyliorhinus Canicula from the South of Sicily'. *Science of The Total Environment* 850 (December): 157875. doi:10.1016/j.scitotenv.2022.157875.

Mountford, A. S., and M. A. Morales Maqueda. 2019. 'Eulerian Modeling of the Three-Dimensional Distribution of Seven Popular Microplastic Types in the Global Ocean'. *Journal of Geophysical Research: Oceans* 124 (12): 8558–73. doi:10.1029/2019JC015050.

Nachite, Driss, Faiçal Maziane, Giorgio Anfuso, and Allan T. Williams. 2019. 'Spatial and Temporal Variations of Litter at the Mediterranean Beaches of Morocco Mainly Due to Beach Users'. *Ocean & Coastal Management* 179 (September): 104846. doi:10.1016/j.ocecoaman.2019.104846.

'NEMO Ocean Engine'. 2024. Accessed January 7. https://zenodo.org/records/6334656.

Nordam, Tor, Ruben Kristiansen, Raymond Nepstad, Erik van Sebille, and Andy M. Booth. 2023. 'A Comparison of Eulerian and Lagrangian Methods for Vertical Particle Transport in the Water Column'. *Geoscientific Model Development* 16 (18). Copernicus GmbH: 5339–63. doi:10.5194/gmd-16-5339-2023.

Osaretin, Idahosa. 2011. 'Energy Security in the Gulf of Guinea and the Challenges of the Great Powers'. *Journal of Social Sciences* 27 (3): 187–91. doi:10.1080/09718923.2011.11892919.

Papageorgiou, Dimitris, Konstantinos Topouzelis, Giuseppe Suaria, Stefano Aliani, and Paolo Corradi. 2022. 'Sentinel-2 Detection of Floating Marine Litter Targets with Partial Spectral Unmixing and Spectral Comparison with Other Floating Materials (Plastic Litter Project 2021)'. *Remote Sensing* 14 (23): 5997. doi:10.3390/rs14235997.

Papakonstantinou, Apostolos, Marios Batsaris, Spyros Spondylidis, and Konstantinos Topouzelis. 2021. 'A Citizen Science Unmanned Aerial System Data Acquisition Protocol and Deep Learning Techniques for the Automatic Detection and Mapping of Marine Litter Concentrations in the Coastal Zone'. *Drones* 5 (1): 6. doi:10.3390/drones5010006.

Papatheodorou, G. 2012. 'Floating and Benthic Marine Litter in the Mediterranean Sea: Typology, Abundance, Sources, Survey Methods and Impacts on Marine Biota'. In *Life in the Mediterranean Sea: A Look at Habitat Changes*, 557–93.

Phan, Samantha, and Christine K. Luscombe. 2023. 'Recent Trends in Marine Microplastic Modeling and Machine Learning Tools: Potential for Long-Term Microplastic Monitoring'. *Journal of Applied Physics* 133 (2): 020701. doi:10.1063/5.0126358.

Portman, Michelle E., and Ruth E. Brennan. 2017. 'Marine Litter from Beach-Based Sources: Case Study of an Eastern Mediterranean Coastal Town'. *Waste Management* 69 (November): 535–44. doi:10.1016/j.wasman.2017.07.040.

United Nations Environment Programme, & Intergovernmental Oceanographic Commission (2009). UNEP/IOC Guidelines on Survey and Monitoring of Marine Litter. https://wedocs.unep.org/20.500.11822/13604.

Ribic, Christine A. 1992. 'Marine Debris Survey Manual'.

Ryan, Peter G. 2015. 'A Brief History of Marine Litter Research'. In *Marine Anthropogenic Litter*, edited by Melanie Bergmann, Lars Gutow, and Michael Klages, 1–25. Cham: Springer International Publishing. doi:10.1007/978-3-319-16510-3_1.

Saharia, Angshuman M., Zhenduo Zhu, Nirupam Aich, Mohammed Baalousha, and Joseph F. Atkinson. 2019. 'Modeling the Transport of Titanium Dioxide Nanomaterials from Combined Sewer Overflows in an Urban River'. *Science of The Total Environment* 696 (December): 133904. doi:10.1016/j.scitotenv.2019.133904.

Salerno, Martina, Manuel Berlino, M. Cristina Mangano, and Gianluca Sarà. 2021. 'Microplastics and the Functional Traits of Fishes: A Global Meta-Analysis'. *Global Change Biology* 27 (12): 2645–55. doi:10.1111/gcb.15570.

Salgado-Hernanz, Paula M., Joan Bauzà, Carme Alomar, Montserrat Compa, Laia Romero, and Salud Deudero. 2021. 'Assessment of Marine Litter through Remote Sensing: Recent Approaches and Future Goals'. *Marine Pollution Bulletin* 168 (July): 112347. doi:10.1016/j.marpolbul.2021.112347.

Samokhin, Andrey, Ksenia Sotnezova, Vitaly Lashin, and Igor Revelsky. 2015. 'Evaluation of Mass Spectral Library Search Algorithms Implemented in Commercial Software'. *Journal of Mass Spectrometry* 50 (6): 820–25. doi:10.1002/jms.3591.

Scarrica, Vincenzo M., Pietro P. C. Aucelli, Cosimo Cagnazzo, Angelo Casolaro, Pierpaolo Fiore, Marco La Salandra, Angela Rizzo, Giovanni Scardino, Giovanni Scicchitano, and Antonino Staiano. 2022. 'A Novel Beach Litter Analysis System Based on UAV Images and Convolutional Neural Networks'. *Ecological Informatics* 72 (December): 101875. doi:10.1016/j.ecoinf.2022.101875.

Schernewski, Gerald, Arunas Balciunas, Dennis Gräwe, Ulf Gräwe, Kristina Klesse, Marcus Schulz, Sylvie Wesnigk, et al. 2018. 'Beach Macro-Litter Monitoring on Southern Baltic Beaches: Results, Experiences and Recommendations'. *Journal of Coastal Conservation* 22 (1): 5–25. doi:10.1007/s11852-016-0489-x.

Schlegel, Martin, Oswald Knoth, Martin Arnold, and Ralf Wolke. 2009. 'Multirate Runge–Kutta Schemes for Advection Equations'. *Journal of Computational and Applied Mathematics* 226 (2): 345–57. doi:10.1016/j.cam.2008.08.009.

Sebille, Erik van, Stephen M. Griffies, Ryan Abernathey, Thomas P. Adams, Pavel Berloff, Arne Biastoch, Bruno Blanke, et al. 2018. 'Lagrangian Ocean Analysis: Fundamentals and Practices'. *Ocean Modelling* 121 (January): 49–75. doi:10.1016/j.ocemod.2017.11.008.

Serranti, Silvia, and Giuseppe Bonifazi. 2019. 'Techniques for Separation of Plastic Wastes - ScienceDirect'. https://www.sciencedirect.com/science/article/abs/pii/B978008102 6762000025?via%3Dihub.

Shchepetkin, Alexander F., and James C. McWilliams. 2005. 'The Regional Oceanic Modeling System (ROMS): A Split-Explicit, Free-Surface, Topography-Following-Coordinate Oceanic Model'. *Ocean Modelling* 9 (4): 347–404. doi:10.1016/j.ocemod.2004.08.002.

Solbakken, V.S., S. Kleiven, and M.L. Haarr. 2022. 'Deposition Rates and Residence Time of Litter Varies among Beaches in the Lofoten Archipelago, Norway'. *Marine Pollution Bulletin* 177 (April): 113533. doi:10.1016/j.marpolbul.2022.113533.

Stojic, Slobodan, and Stefan Salhofer. 2022. 'Capacity Development for Plastic Waste Management—A Critical Evaluation of Training

Materials'. *Sustainability* 14 (4). Multidisciplinary Digital Publishing Institute: 2118. doi:10.3390/su14042118.

Taddia, Yuri, Corinne Corbau, Joana Buoninsegni, Umberto Simeoni, and Alberto Pellegrinelli. 2021. 'UAV Approach for Detecting Plastic Marine Debris on the Beach: A Case Study in the Po River Delta (Italy)'. *Drones* 5 (4). Multidisciplinary Digital Publishing Institute: 140. doi:10.3390/drones5040140.

Tamvaki, Niki, and George Tsirtsis. 2005. 'INTEGRATED MODELLING IN COASTAL LAGOONS WATERSHED MODELLING GULF OF GERA CASE STUDY'.

Thompson, Richard C., Ylva Olsen, Richard P. Mitchell, Anthony Davis, Steven J. Rowland, Anthony W. G. John, Daniel McGonigle, and Andrea E. Russell. 2004. 'Lost at Sea: Where Is All the Plastic?' *Science* 304 (5672). American Association for the Advancement of Science: 838–838. doi:10.1126/science.1094559.

Tong, Xuneng, Mui-Choo Jong, Jingjie Zhang, Luhua You, and Karina Yew-Hoong Gin. 2021. 'Modelling the Spatial and Seasonal Distribution, Fate and Transport of Floating Plastics in Tropical Coastal Waters'. *Journal of Hazardous Materials* 414 (July): 125502. doi:10.1016/j.jhazmat.2021.125502.

Topouzelis, Konstantinos, Dimitris Papageorgiou, Alexandros Karagaitanakis, Apostolos Papakonstantinou, and Manuel Arias Ballesteros. 2020. 'Remote Sensing of Sea Surface Artificial Floating Plastic Targets with Sentinel-2 and Unmanned Aerial Systems (Plastic Litter Project 2019)'. *Remote Sensing* 12 (12): 2013. doi:10.3390/rs12122013.

Tsiaras, Kostas, Yannis Hatzonikolakis, Sofia Kalaroni, Annika Pollani, and George Triantafyllou. 2021. 'Modeling the Pathways and Accumulation Patterns of Micro- and Macro-Plastics in the Mediterranean'. *Frontiers in Marine Science* 8. https://www.frontiersin.org/articles/10.3389/fmars.2021.743117.

Unger, Bianca, Helena Herr, Sacha Viquerat, Anita Gilles, Patricia Burkhardt-Holm, and Ursula Siebert. 2021. 'Opportunistically Collected Data from Aerial Surveys Reveal Spatio-Temporal Distribution Patterns of Marine Debris in German Waters'.

Environmental Science and Pollution Research 28 (3): 2893–2903. doi:10.1007/s11356-020-10610-9.

Valdivieso-Ros, Carmen, Francisco Alonso-Sarria, and Francisco Gomariz-Castillo. 2021. 'Effect of Different Atmospheric Correction Algorithms on Sentinel-2 Imagery Classification Accuracy in a Semiarid Mediterranean Area'. *Remote Sensing* 13 (9): 1770. doi:10.3390/rs13091770.

Van Der Meer, Freek. 2006. 'The Effectiveness of Spectral Similarity Measures for the Analysis of Hyperspectral Imagery'. *International Journal of Applied Earth Observation and Geoinformation* 8 (1): 3–17. doi:10.1016/j.jag.2005.06.001.

Van Emmerik, Tim, Yvette Mellink, Rahel Hauk, Kryss Waldschläger, and Louise Schreyers. 2022. 'Rivers as Plastic Reservoirs'. *Frontiers in Water* 3 (January): 786936. doi:10.3389/frwa.2021.786936.

Van Utenhove, E.J.F. 2019. 'Modelling the Transport and Fate of Buoyant Macroplastics in Coastal Waters'.

Vennell, Ross, Max Scheel, Simon Weppe, Ben Knight, and Malcolm Smeaton. 2021. 'Fast Lagrangian Particle Tracking in Unstructured Ocean Model Grids'. *Ocean Dynamics* 71 (4): 423–37. doi:10.1007/s10236-020-01436-7.

Wan, Katty X., Ilan Vidavsky, and Michael L. Gross. 2002. 'Comparing Similar Spectra: From Similarity Index to Spectral Contrast Angle'. *Journal of the American Society for Mass Spectrometry* 13 (1): 85–88. doi:10.1016/S1044-0305(01)00327-0.

Wenneker, B.; Oosterbaan, L. and Intersessional Correspondence Group on Marine Litter (ICGML) (2010) Guideline for Monitoring Marine Litter on the Beaches in the OSPAR Maritime Area. Edition 1.0. London, UK, OSPAR Commission, 15pp. & Annexes. DOI: http://dx.doi.org/10.25607/OBP-968

Werner, Stefanie, Ania Budziak, Jan van Franeker, François Galgani, Georg Hanke, Thomas Maes, Marco Matiddi, et al. 2016. *Harm Caused by Marine Litter: MSFD GES TG Marine Litter - Thematic Report*. Luxembourg: Publications Office of the European Union.

Wimalaratne, Malinda R., Poojitha D. Yapa, Kisaburo Nakata, and Lakshitha T. Premathilake. 2015. 'Transport of Dissolved Gas and Its Ecological Impact after a Gas Release from Deepwater'. *Marine Pollution Bulletin* 100 (1): 279–88. doi:10.1016/j.marpolbul.2015.08.039.

Xia, Wulai, Qingyang Rao, Xuwei Deng, Jun Chen, and Ping Xie. 2020. 'Rainfall Is a Significant Environmental Factor of Microplastic Pollution in Inland Waters'. *Science of The Total Environment* 732 (August): 139065. doi:10.1016/j.scitotenv.2020.139065.

Zhang, Z., and Q. Chen. 2007. 'Comparison of the Eulerian and Lagrangian Methods for Predicting Particle Transport in Enclosed Spaces'. *Atmospheric Environment* 41 (25): 5236–48. doi:10.1016/j.atmosenv.2006.05.086.

Zhiyao, Song, Wu Tingting, Xu Fumin, and Li Ruijie. 2008. 'A Simple Formula for Predicting Settling Velocity of Sediment Particles'. *Water Science and Engineering* 1 (1): 37–43. doi:10.1016/S1674-2370(15)30017-X.

Cited websites

Asi.it, website.
https://www.asi.it/en/earth-science/prisma/

City Facts. (2020). Mondello (Palermo), website.
https://www.city-facts.com/mondello-palermo

City Facts. (2022). Isola delle Femmine (Palermo), website.
https://www.cityfacts.com/search?s=isola+delle+femmine&auto=

Copernicus Marine Service, website – "Copernicus Marine Data Store" section.
https://data.marine.copernicus.eu/products

Copernicus Marine Service, website – "Global Ocean Physics Analysis and Forecast" section.
https://doi.org/10.48670/moi-00016

The university of British Columbia, website.
https://www.eoas.ubc.ca/~rich/map.html

Liberian Hydrological Services Open Database, website.
https://lhsliberia.com/water-data/

The OeanCleanUp, website
https://theoceancleanup.com/

The OeanCleanUp, website – "Data sources" section.
https://theoceancleanup.com/sources/

Ministero dell'ambiente e della Sicurezza Energetica, website. "Area marina protetta Capo Gallo - Isola delle Femmine" section.
https://www.mase.gov.it/pagina/area-marina-protetta-capo-gallo-isola-delle-femmine

Natural Earth, website.
https://www.naturalearthdata.com

PlanetScope website,
https://earth.esa.int/eogateway/missions/planetscope

Plastic Litter Project, website.
https://plp.aegean.gr/

Pleiades, website
https://earth.esa.int/eogateway/missions/pleiades)

Sentinel-2, website
https://sentinels.copernicus.eu/web/sentinel/missions/sentinel-2

Worldview3, website
https://earth.esa.int/eogateway/missions/worldview-3

Annex
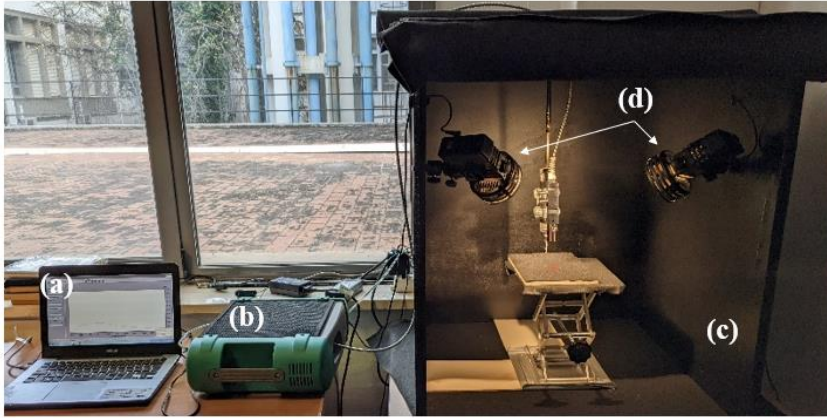
Figure A1 – Experimental setup: (a) Personal computer, (b) Spectroradiometer, (c) box (white and black), (d) lamps.
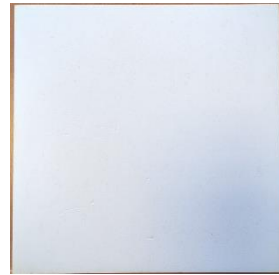
(a)   *(b)*

Figure A2 – Black *(a)* and white *(b)* panel used to place the samples to acquire the reflectance.
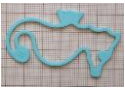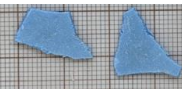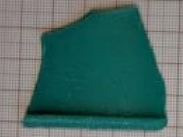
(a) *(b)*

Figure A3 –Black *(a)* and white *(b)* box used for the experiments.

Sample				
Id	1	3	4	5
Samples				
Id	6	7	8	12
Samples				
Id	13	14	17	18
Samples				
Id	20	21	22	25
Samples				
Id	26	27	28	29
Samples				
Id	31	32	33	34
Samples				
Id	35	36	37	38

Samples				
Id	39	40	42	57
Samples				
Id	58	59	60	62
Samples				
Id	63	64	65	66
Samples				
Id	67	68	69	70
Samples				
Id	71	72	73	74
Samples				
Id	75	76	77	79
Samples				
Id	80	81	82	94

Samples				
Id	97	98	99	100
Samples				
Id	101	103	104	105
Samples				
Id	106	107	108	110
Samples				
Id	111	112	113	11
Samples				
Id	115	117	127	129
Samples				
Id	130	131	134	138
Samples				
Id	139	140	141	142

Samples				
Id	144	145	146	148
Samples				
Id	149	150	151	152
Samples				
Id	156	159	160	161
Samples				
Id	165	166	167	168
Samples				
Id	169	170	173	174
Samples				
Id	176	177	178	179

Samples				
I	180	181	183	184
Samples				
Id	185	187	189	190
Samples				
Id	191	192	200	204
Sample				
Id	205	206	207	208
Sample				
Id	209	210	211	212
Sample				
Id	213	214	215	216
Samples				
Id	220	221	222	

Figure A4 – Samples spectrally characterized.